Binary Mixtures of Rod–like Colloids:

Mesoscopic Equilibrium Theory

and

Shear Induced Instabilities

vorgelegt von:
Master of Science (Physics)
Rodrigo Lugo-Frías
aus
Pachuca, Hidalgo, Mexiko

Von der Fakultät II – Mathematik und Naturwissenschaften
der Technischen Universität Berlin
zur Erlangung des akademischen Grades

Doktor der Naturwissenschaften
Dr. rer. nat.

genehmigte Dissertation

Promotionsausschuss:

Vorsitzender:	Prof. Dr. Michael Lehmann
1. Gutachterin:	Prof. Dr. Sabine H. L. Klapp
2. Gutachter:	PD Dr. Andreas Menzel

Tag der wissenschaftlichen Aussprache: 28. Juli 2016

Berlin 2016

Declaration of Authorship

Hiermit erkläre ich, dass ich die vorliegende Arbeit selbstständig und eigenhändig sowie ohne unerlaubte fremde Hilfe und ausschliesslich unter Verwendung der aufgeführten Quellen und Hilfsmittel angefertigt habe.

Berlin, den

Rodrigo Lugo-Frías

Publications

Most of this work is based on the publications listed below. Texts are partially rewritten and some extensions are introduced. Contributions from co-authors presented in this work are indicated in the text.

Binary mixtures of rod-like colloids under shear: microscopically-based equilibrium theory and order-parameter dynamics, R. Lugo-Frias and S. H. L. Klapp, *J. Phys.: Condens. Matter*, **28**, 244022, (2016)

This paper is concerned with the dynamics of a binary mixture of rod-like, repulsive colloidal particles driven out of equilibrium by means of a steady shear flow (Couette geometry). To this end we first derive, starting from a microscopic density functional in ParsonsLee approximation, a mesoscopic free energy functional whose main variables are the orientational order parameter tensors. Based on this mesoscopic functional we then explore the stability of isotropic and nematic equilibrium phases in terms of composition and rod lengths. Second, by combining the equilibrium theory with the DoiHess approach for the order parameter dynamics under shear, we investigate the orientational dynamics of binary mixtures for a range of shear rates and coupling parameters. We find a variety of dynamical states, including synchronized oscillatory states of the two components, but also symmetry breaking behavior where the components display different in-plane oscillatory states.

Shear banding in nematogenic fluids with oscillating orientational dynamics, R. Lugo-Frias, H. Reinken and S. H. L. Klapp, *submitted European Physical Journal E*. (2016)

We investigate the occurrence of shear banding in nematogenic fluids under planar Couette flow, based on mesoscopic dynamical equations for the orientational order parameter and the shear stress. We focus on parameter values where the sheared homogeneous system exhibits regular oscillatory orientational dynamics, whereas the equilibrium system is either isotropic (albeit close to the isotropic–nematic transition) or deep in its nematic phase. The numerical calculations are restricted to spatial variations in shear gradient direction. We find several new types of shear banded states characterized by regions with regular oscillatory orientational dynamics. In all cases shear banding is accompanied by a non–monotonicity of the flow curve of the homogeneous system; however, only in the case of the initially isotropic system this curve has the typical S–like shape. We also analyze the influence of different orientational boundary conditions and of the spatial correlation length.

Abstract

In this work we investigate the shear induced instabilities occurring in colloidal binary mixtures of rigid anisotropic particles. To this end, we derive a theoretical framework including equilibrium and non–equilibrium methods.

The equilibrium description is derived on the basis of microscopic density functionals in the Parsons–Lee and Ramakrishnan–Youssuf approximations. The result is a mesoscopic free energy given in terms of a set of orientational order parameter tensors (one for each component of the mixture) and their gradients. In this regard, our theory may be seen as an extension of the Landau–de Gennes theory to mixtures. However, our theory incorporates microscopic information, particularly the aspect ratios and number densities characterizing the components of the mixture. Specializing to binary mixtures of rod–like particles, these functionals are then used to explore the stability of isotropic and nematic equilibrium phases in terms of composition and rod lengths.

We extend the description to consider non-equilibrium phenomena by combining our equilibrium theory with the theory of irreversible processes. Thus, extending the Doi–Hess approach to the study of binary mixtures under shear. As a result, we obtain a set of hydrodynamic equations which take into account the competition between flow–induced effects on the alignment and the relaxation of the entire system towards equilibrium.

Based on these hydrodynamic equations we turn to the study of shear induced phenomena under planar Couette flow geometry. These investigations are divided in two parts. First, we focus on a one–component system and study the underlying relation existing between shear and stress. We observed that disregarding the equilibrium (un–sheared) state of the system (close to the isotropic–nematic transition or deep in its nematic phase), we find several new types of shear banded states characterized by regions with regular oscillatory orientational dynamics.

Finally we concentrate on binary mixtures. Here, after exploring a vast range of parameters, we observe several dynamical states appearing in the system. These dynamical states include the synchronization of of in– and out–of–the shear plane oscillatory states of the two components. Interestingly, for a specific set of parameters, we observe the appearance of symmetry breaking behavior where both components of the mixture display different in–phase oscillatory states.

Zusammenfassung

In dieser Arbeit untersuchen wir scherinduzierte Instabilitäten, welche in binären Mischung von starren anisotropen Teilchen auftreten. Hierzu leiten wir eine theoretische Beschreibung mit Gleichgewichts- und Nichtgleichgewichtsmethoden her.

Die Gleichgewichtsbeschreibung wird auf der Basis von einer mikroskopische Dichtefunktionaltheorie mit Hilfe von den Näherungen von Parsons–Lee und Ramakrishnan–Youssuf hergeleitet. Dieser Ansatz führt zu einem Ausdruck für die mesoskopischen freien Energie als Funktion von tensoriellen Ordnungsparametern (einer für jede Mischungskomponente) sowie deren Gradienten. Hierdurch kann unsere Arbeit als Erweiterung der Landau-de GennesTheorie zur Beschreibung von Mischungen angesehen werden. Allerdings berücksichtigt unsere Theorie die Abhängigkeit von mikroskopische Grössen, insbesondere dem Verhältnis von Teilchenlängen und -durchmesseren, sowie die Teilchendichten, welche die Mischungskomponenten charakterisieren. Für den Spezialfall von binäre Mischungen von stäbchenförmigen Teilchen verwenden wir das resultierende freie Energiefunktional, um die Stabilität von isotropen und nematischen Gleichgewichtsphasen in Bezug auf ihre Zusammensetzung und Stäbchenlängen zu untersuchen.

Zur Beschreibung von Nichtgleichgewichtsprozessen verbinden wir die Gleichgewichtstheorie mit der Theorie irreversibler Prozesse. Dies entspricht einer Erweiterung der Doi–Hess–Theorie zur Beschreibung von binären Mischungen unter Scherung. Wir erhalten ein System aus hydrodynamischen Gleichungen, welche den Wettstreit zwischen strömungsinduzierten Effekten und der Relaxation des gesamten Systems hin zum Gleichgewicht beschreibt.

Auf Basis dieser hydrodynamischen Gleichungen widmen wir uns der Untersuchung von scherinduzierten Phänomenen in einer ebenen Couette-Geometrie. Diese Untersuchungen bestehen aus zwei Teilen. Zuerst betrachten wir ein einkomponentiges System und die zugrundeliegende Beziehung zwischen Scherrate und Spannung. Ausgehend von unterschiedlichen Gleichgewichtszuständen (nahe des isotrop–nematischen Phasenübergangs und tief in der nematischen Phase) finden wir in den gescherten Systemen räumlich inhomogene Strukturen, sogenannte "*shear bands*". Diese sind durch Bereiche mit regulären oszillatorischen Ausrichtungsdynamiken charakterisiert.

Anschliessend konzentrieren wir uns auf gescherte binäre Mischungen. Hierbei identifizieren wir nach der Untersuchung eines grossen Parameterbereichs verschiedene dynamische Zustände, welche sowohl synchronisierte Oszillationen innerhalb als auch ausserhalb der Scherebene beeinhalten. Bemerkenswert ist insbesondere die Beobachtung eines symmetriebrechenden Verhaltens für bestimmte Parameterwerte. Hierbei weisen die beiden Mischungskomponenten verschiedene, aber phasengleiche oszillatorische Zustände auf.

Contents

Chapter 1

Introduction

This work contains many things which are new and interesting. Unfortunately, everything that is new is not interesting, and everything which is interesting, is not new.
– Lev Davidovich Landau

Fluids composed of orientable particles form the basis for a range of high–end technologies such as drug delivery, immunodetection and the design of new functional materials. In general, these devices are composed of colloidal suspensions, where anisotropic particles (in the micrometer range) are suspended in liquids. Typically, applications require stable suspensions which are often obtained at very high solute concentrations. However, in practice, these systems are highly polydisperse (*i.e.*, composed of various shapes and sizes) and this may have strong effects in the stability of the system. Thus, in order to tune key properties of such systems, external fields, like shear and electro–magnetic fields, are usually applied.

The goal of this chapter is to introduce the reader to the study of mixtures of rigid anisotropic particles in and out of equilibrium. To this end, we address some recent experimental and theoretical developments of the behavior of such systems. In particular, we discuss the underlying equilibrium phenomenology and the effect of shear on the structure and rheological signature of these fluids. Finally, at the end of the chapter, we list the motivation, goals and an outline of this thesis.

1.1 Colloidal systems of rigid rod–like particles

A colloidal suspension is a system where microscopic particles, ranging from nano– to micrometer dimensions, are dispersed in a solvent composed of atomic–sized molecules. In this thesis, we focus on the study of mixtures of rigid anisotropic particles embedded in aqueous solutions.

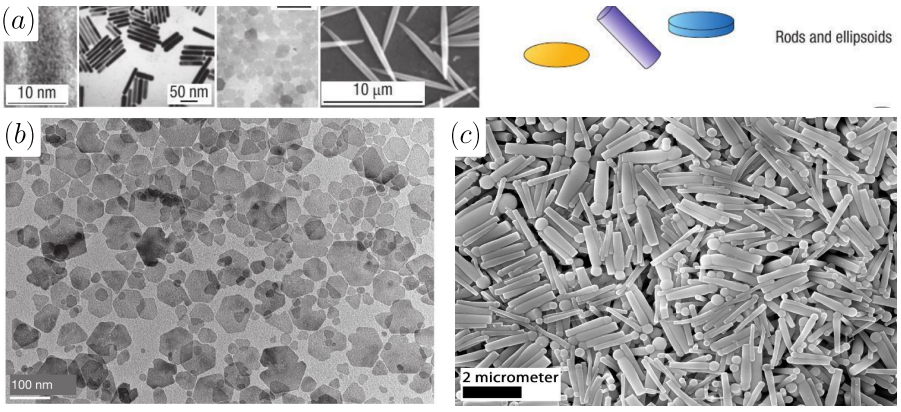

Figure 1.1: (a) Example of single component dispersions of rod–like, disk–like and ellipsoidal particles in aqueous solutions (see Ref. [8]). (b) Transmission electron microscopy image of a mixture of magnetic platelets embedded in a nematic host (see Ref. [1]). (c) Scanning electron microscopy image of a polydisperse solution of "matchstick" rod–like particles (see Ref. [2]).

To be more specific, we deal with particles having *simple* morphologies characterized by their aspect ratio, *i.e.*, the ratio between their length and diameter. Examples include magnetic platelets embedded in nematic hosts [1] and polydisperse "matchstick" rod–like particles [2] (see Fig. 1.1). The versatility of these systems has allowed their successful application in *high–end* technologies, e.g., panels and photographic devices [3, 4], *smart* windows [5] and even in drug delivery and immunodetection [6, 7].

To ensure an effective performance, almost all devices depend on the optimization of key material properties, e.g., rotational viscosity and dielectric anisotropy. Consequently mixtures of colloidal rod–like particles are designed to be thermodynamically stable at very high concentrations [9]. However, because of the complex orientational behavior and high sensitivity to external perturbations, this is often a difficult task. Thus, it is often necessary to apply external fields such as shear (see e.g. [10]) and electro–magnetic fields (see e.g. [11]) to tune the performance of the fluid.

1.2 Equilibrium behavior of mixtures

Already in thermodynamic equilibrium, mixtures of rigid anisotropic particles display a very rich phase behavior typically dominated by repulsive interactions arising from the particle's shape. In general, these fluids exhibit two kinds of long range ordering: ordering of the centers of mass and ordering of the orientations of the particles. In the absence of translational ordering, as the density increases, systems with little long–range orientational order undergo a phase transition from the isotropic (orientationally disordered) to the nematic (orientationally ordered) phase.

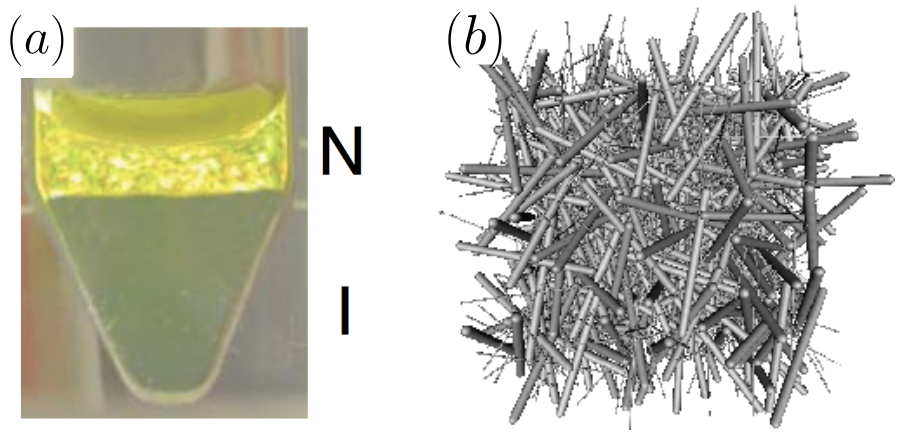

Figure 1.2: Phase separation of binary mixtures of thin and thick rod–like particles. (a) Highly fractionated isotropic–nematic coexistence of thin and thick *fd*–viruses [16]. Here N denotes the location of the nematic fluid (rich in thick particles) whereas I denotes the isotropic fluid (rich in thin particles) (b) Snapshot of computer simulations of binary mixtures of thick and thin hard spherocylinders [17]. Here the domain is splitted into isotropic rich long–spherocylinders in the front and isotropic rich short–spherocylinders in the back.

A prominent example of the complicated equilibrium behavior of true polydisperse fluids is the experimental study of clay rods in Ref. [12]. Here they measure the collective reorientation of the particles by looking at changes of the optical properties of the sample, e.g. birefringence and light transmittance. However, recent studies focus on binary mixtures as the first step towards understanding polydisperse fluids.

In fact, recent investigations of binary mixtures of rod–like particles show that these systems display a very rich, entropy–driven phase behavior, including phase separation, demixing and order–disorder phase transitions [13, 14, 15, 16, 17, 18] (see Fig. 1.2). Noteworthy are the phase diagrams of short and long molecules obtained by Monte Carlo simulations [14], and the experimental phase diagrams of binary mixtures of thin and thick *fd*–viruses [16].

From a theoretical standpoint, such phase behavior may be studied using two different levels of description: a phenomenological (mesoscopic) description and a particle–based (microscopic) description.

The phenomenological approach is based on a very simple idea: In orientationally ordered phases the particles are, on average, aligned along a common direction; in this case the system is said to be in a nematic state, and the local direction of alignment is given in terms of the nematic director $\hat{\boldsymbol{n}} = \hat{\boldsymbol{n}}(\mathbf{r}, t)$ [19]. In the same way, it is possible to describe the *spatial distortions* of the nematic director using a more general theory which includes spatial derivatives of $\hat{\boldsymbol{n}}$ [20, 21]. Further, the degree of orientational

order is then measured by defining a suitable set of order parameters. In the scope of the $\mathbf{Q}$–tensor theory, one can define a *mesoscopic* order parameter in terms of the one–body orientational distribution function $f(\hat{\boldsymbol{u}})$ (where $\hat{\boldsymbol{u}}$ contains the set of Euler angles describing the particle's orientation [19, 22]). The resulting order parameter, $\mathbf{Q}$, is a second–rank tensor which corresponds to the lowest non–vanishing moment of $f(\hat{\boldsymbol{u}})$ and it can be measured in experiments looking at the birefringence and fluorescence of the sample [19, 23]. In terms of $\mathbf{Q}$ and its spatial derivatives, the phase behavior of the system is described using the phenomenological Landau–de Gennes (LdG) theory [19]. However, this description lacks quantitative measurement of the microscopic characteristics of the system.

The microscopical description studies the equilibrium behavior of the system in terms of all degrees of freedom of each particle. In certain approximations, this has been achieved successfully, e.g., for needle–like particles in the low density limit [24]. More generally, one can employ the framework of classical density functional theory (DFT) [25, 26], whose main idea is to minimize a (free energy) functional of the singlet density $\rho(\mathbf{r}, \hat{\boldsymbol{u}})$ where $\mathbf{r}$ and $\hat{\boldsymbol{u}}$ account for translational and rotational degrees of freedom, respectively [27, 28].

For one component systems several studies have been devoted to construct free energy functionals for homogeneous states of anisotropic fluids. Their common goal is to describe the isotropic–nematic phase transition [27, 29] or the distortions of the nematic phase [30, 31, 32]. Considering binary mixtures, the effects of shape (and in some cases flexibility) have been accounted for in various theoretical studies (see e.g. [33, 34] and references therein). Of special importance for the present study are the DFT description of spatial homogeneous phases of mixtures of Malijevsky *et al.* [35] and the Phase–Field–Crystal Model for liquid crystals of Wittkowski *et al.* [36]. These theoretical descriptions are derived, respectively, as a generalization of the ideas of Parsons [37] and Lee [38] for pure component systems, and an extension of a second–order perturbation theory in the Ramakrishnan-Youssuf approximation [39, 40, 41].

1.3 Non–equilibrium behavior under shear

While the equilibrium behavior of mixtures is already challenging by itself, a further level of complexity is reached when these systems are considered under shear [42, 43, 44].

Shear flow is a fundamental example of driving a soft–matter system out of equilibrium [45]. From a fundamental perspective, the combination of shear and the complex morphologies of the particles can generate a variety of instabilities in the system. Prominent examples are the shear induced shift of the isotropic–nematic transition and the stabilization of the nematic phase [46, 47], the appearance of orientational oscillatory states [48, 49, 50], rheochaos [51, 52] and the occurrence of spatially inhomogeneous instabilities like shear banding [53, 54]. Thus, investigating the impact of shear is crucial for understanding the system's rheological behavior.

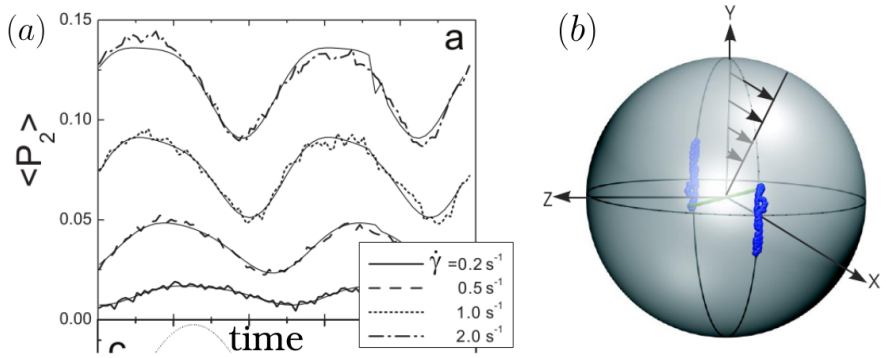

Figure 1.3: (a) Order parameter P_2 as a function of time showing the dynamics of the system in an orientational oscillatory states (adapted form Ref. [60]). (b) The path of the nematic director in the unit sphere in the wagging oscillatory state [55].

Here, we are interested in the study of two different types of shear induced phenomena occurring in fluids of rigid anisotropic particles: shear induced oscillatory states and shear banding instabilities. In general, these non–equilibrium phenomena are characterized by a time–dependent collective behavior of the orientable particles. However, modeling these collective shear induced phenomena on a microscopic level is still a challenge. Thus, one typically employs particle based computer simulations [55, 56] or non–linear mesoscopic theories for the dynamics of the orientational order parameter $\mathbf{Q}$ [57, 23, 58, 59]. The later assumes that the nematic director $\hat{\boldsymbol{n}}(\mathbf{r},t)$ is effectively coupled with the hydrodynamic flow field $\mathbf{v}(\mathbf{r},t)$.

Shear induced oscillatory states: Already for homogeneous systems, particles in a shear flow can display spontaneous time–dependent oscillations. A prime example is the wagging motion (characterized by the alternation of the nematic director around zero along the shear direction) which has been observed in experiments [60] as well as in particle–resolved computer simulations [55] (see Fig. 1.3).

A well–established path to explore the orientational dynamics under shear are the mesoscopic equations describing the evolution of $\mathbf{Q}$ in time. Within the Doi–Hess approach [57, 23], the time dependence of $\mathbf{Q}$ hinges on a competition between flow–induced perturbations, and a contribution accounting for the relaxation of the system towards equilibrium (stemming from the functional derivative of the phenomenological LdG free energy [19]). Depending on the initial equilibrium (un–sheared) state of the system, these nonlinear equations uncover a huge variety of complex dynamical behavior characterized by different (regular) oscillatory states [48, 49, 50], chaotic behavior [51] and complex spatiotemporal patterns [61, 62, 63].

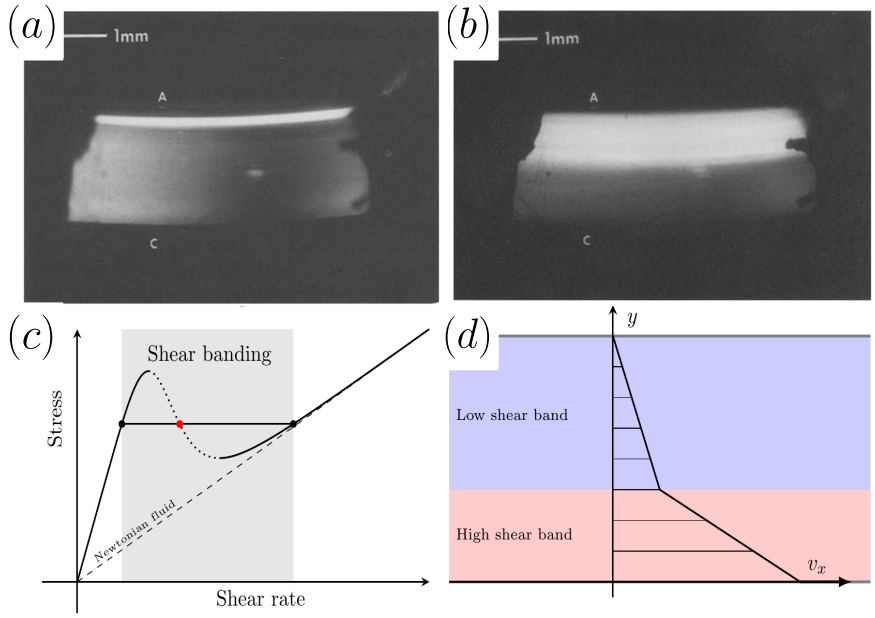

Figure 1.4: (First row) Flow birefringence experiments showing shear banding structures on a CTAB (cetyltrimethyammoniumbromide) solution in a Couette cell upon increasing shear rate from (a) $\dot{\gamma} \simeq 3s^{-1}$ to (b) $\dot{\gamma} \simeq 16s^{-1}$ (taken from Ref. [70]). (Second row) (c) Flow curve of a shear banding fluid. (d) Velocity profile in a shear banded flow (taken from Ref. [71]).

Shear banding instabilities: The manifestation of shear induced orientational dynamics must have a direct impact on the rheological properties of the system. Thus, the emerging oscillatory states may be associated with a non–Newtonian behavior of the viscosity. In fact, when the applied shear rate goes beyond a critical value, the homogeneous system becomes unstable and separates into macroscopic bands with different *local* shear rates (or stresses) (see Fig. 1.4(d)). This phenomenon is often referred to as *shear banding* and was observed (for the first time) in worm–like micellar solutions by Rehage and Hoffmann [64, 65] (see e.g. Refs. [66, 67, 68] for recent reviews). More recently, Chen *et al* and Decruppe *et al* have shown that this phenomenon can be observed in rod–like colloidal dispersions [69] and liquid–crystalline polymers [70] (see Figs. 1.4(a) and 1.4(b)). In all mentioned cases, the flow induced reorganization of the fluid's microstructure leads to a non–monotonic relation between shear stress and shear rate, the so–called flow curve of the fluid (see Fig. 1.4(c)).

Theoretically, shear banding (and the related vorticity banding [72]) has been studied mainly via continuum models. A standard theory is the diffusive Johnson-Segelman (DJS) model [73, 74] in which the viscosity decreases with the stress (shear thinning) and the shear bands are formed along the gradient direction. In contrast, recent theoretical

studies [52, 75] have used the Doi–Hess model, by choosing a suitable parameter range, to study the emergence irregular dynamical shear banding corresponding to rheochaos. The choice of the Doi–Hess model over the DJS model is because the first one depends on $\mathbf{Q}$. Thus, the study of spatiotemporal complex dynamics and spatial inhomogeneities, at the same time, is accessible.

1.4 Motivation, goals and scope of the thesis

The purpose of this thesis is to investigate the collective behavior of binary mixtures of rod–like colloids under shear. The focus of our investigations is to study the nature of the shear induced oscillatory states arising in such systems with respect to the mixture's components, as well as the possible occurrence of shear banding instabilities and the related rheological behavior.

Specifically, we aim to develop novel techniques based on quantities that are directly accessible to experiments, e.g., the orientational order parameter tensor $\mathbf{Q}$. The starting point of our investigations is related to the complex equilibrium phase behavior of binary mixtures. In fact, as shown for one–component fluids, a deep understanding of the underlying equilibrium behavior of the system leads to straightforward investigations of the non–equilibrium setup. Thus, the first goal of our approach, is to construct an expression for the equilibrium free energy functional capable of describing the thermodynamic phase behavior of the mixture. To this end we use techniques from classical DFT to develop a mesoscopic functional given in terms of the orientational order parameter tensors, $\mathbf{Q}^\alpha$ where $\alpha = A, B$ (one for each component of the mixture).

Second, we couple the $\mathbf{Q}$–tensors to the hydrodynamic flow field $\mathbf{v}(\mathbf{r}, t)$. For this purpose, the free energy functional resulting from the equilibrium study is used as an input to extend the well–known Doi–Hess theory to the study of binary mixtures. Finally, by expanding the tensorial system of equations in terms of an appropriate tensor basis, we analyze the resulting equations, exploring a vast range of range of parameters.

1.4.1 Outline

In order to cover the content listed above, this work is organized as follows: First, in Chapters 2 and 3 we introduce the theoretical background necessary to understand the phenomenological and microscopic descriptions of rod–like systems in equilibrium.

We start our own investigations in Chapter 4. There we use the multicomponent Parsons–Lee theory [35] and a second–order perturbation theory for mixtures as a starting point to construct an approximate free energy functional given in terms of the tensorial order parameters, $\mathbf{Q}^\alpha$, and its gradients, $\nabla\mathbf{Q}^\alpha$, where $\alpha = 1, \cdots, n$ labels the n components of the mixture.

Further, in Chapter 5 we concentrate on the study of binary mixtures in equilibrium. Special attention is given to the semi–dilute regime in Section 5.2, where we investigate

the stability of isotropic and nematic states (for fixed densities). In Section 5.3 we briefly discuss the mesoscopic free energy density of distortion for binary mixtures.

In Chapter 6, we combine our equilibrium theory with the theory of irreversible processes in order to extend the Doi-Hess theory to binary mixtures of rigid anisotropic particles. In Section 6.5, upon expanding the alignment tensors and the stress in terms of an appropriate tensor basis, we obtain a set of coupled differential equations for the independent components of $\mathbf{Q}^{\alpha}$ and $\mathbf{T}$.

In Chapter 7, we present numerical results of the shear banding in one component systems and shear induced orientational dynamics of binary mixtures. This work then finishes in Chapter 8 with concluding remarks and an outlook. Some technical details are given in the Appendices A and B.

Chapter 2

Phenomenological description

Fluids consisting of anisotropic particles exhibit two kinds of long range ordering: ordering of the centers of mass and ordering of the orientations of the particles. In a system characterized by little to no long–range orientational order, as the density is gradually increased, the ordering of the molecules becomes larger. This behavior constitutes the general picture of the isotropic–nematic phase transition.

In classic liquid crystal theories, the phenomenology of this transition is described in terms of a set of appropriate order parameters. The aim of this chapter is to introduce the tensor order parameter $\mathbf{Q}$ and the ideas behind the well established phenomenological Landau–de Gennes theory. This theory is a standard premise used in the study of suspensions of rod–like (disc–like) particles and liquid crystals. [1]

2.1 Measure of orientational order

In the absence of long range positional ordering the particles are, on average, aligned along a common direction. In this case the system is in a nematic state, where the local direction of alignment is defined by the nematic director. In different regions of the fluid, this director changes from point to point and may also depend on time, thus, $\hat{\boldsymbol{n}} = \hat{\boldsymbol{n}}(\mathbf{r}, t)$. When both, positional and orientational order vanish, the system is in an isotropic fluid phase. A sketch of this behavior is shown in Fig. (2.1). The director $\hat{\boldsymbol{n}}$ is a local measure of the average molecular orientation of the particles in the fluid.

A single particle has its own orientation which is specified by the unit vector $\hat{\boldsymbol{u}}$. In general, depending on the complexity of the particles $\hat{\boldsymbol{u}}$ is a complicated vector dependent

[1] This chapter is based on four publications: *Landau theory of nematic–isotropic phase transition* by E. F. Gramsbergen *et al* [76], *The physics of liquid crystals* by P. G. de–Gennes [19], *Introduction to Q–tensor theory* by N. J. Mottram *et al* [77] and *Tensors for physics* by S. Hess [22].

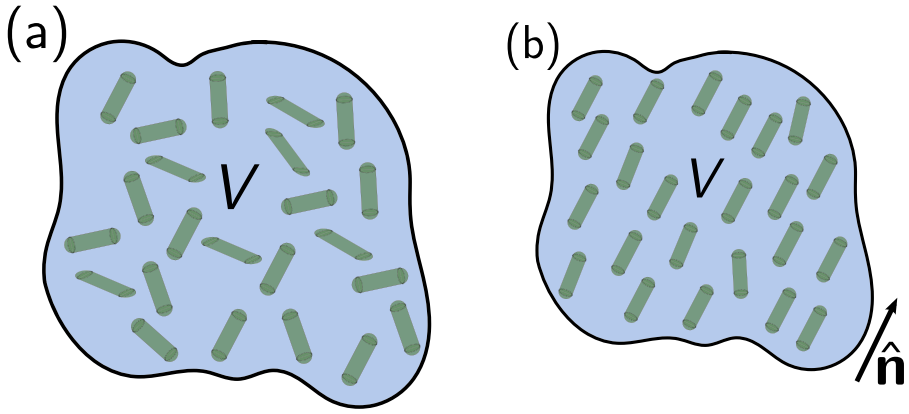

Figure 2.1: Rod–like particles in the (a) isotropic fluid phase and (b) nematic phase. In the isotropic phase there is not an average orientation of the particles, whereas, in the nematic phase the average orientation is given by the nematic director $\hat{\boldsymbol{n}}$.

on Euler angles and presents no symmetries. However, for uniaxial particles the head–to–tail symmetry is conserved and $\hat{\boldsymbol{u}} = -\hat{\boldsymbol{u}}$. For these systems, a measure of how spread out is the particle's orientation with respect to the nematic director is given by the angle θ_p, defined by the relation

$$\cos\theta_p = \hat{\boldsymbol{u}} \cdot \hat{\boldsymbol{n}}\,. \tag{2.1}$$

In real systems it is impossible to track the amount of orientational order of each particle with respect to the director. Hence the statistical state of the fluid is characterized by a probability distribution function in terms of the molecular orientations, $f = f(\hat{\boldsymbol{u}}, \mathbf{r}, t)$. In terms of f, the probability to find a molecule in $[\mathbf{r}, \mathbf{r} + d\mathbf{r}]$ with an orientation $[\hat{\boldsymbol{u}}, \hat{\boldsymbol{u}} + d\hat{\boldsymbol{u}}]$ at a given time t is $f(\hat{\boldsymbol{u}}, \mathbf{r}, t) d\mathbf{r} d\hat{\boldsymbol{u}}$. The orientational distribution function satisfies the normalization condition

$$\int_{\mathbb{S}^2} f(\hat{\boldsymbol{u}}, \mathbf{r}, t) d\hat{\boldsymbol{u}} = 1\,, \tag{2.2}$$

where $f(\hat{\boldsymbol{u}}, \mathbf{r}, t)$ is integrated over the an arbitrary surface $\mathbb{S}^2$, corresponding to the solid angle integral. As a last remark, one should note that considering all the molecules in a volume V, the mean value of $f(\hat{\boldsymbol{u}}, \mathbf{r}, t)$ defines the direction of the nematic director $\hat{\boldsymbol{n}}$.

2.1.1 Scalar order parameter

The usual measure of the amount of order in fluids of anisotropic particles is the scalar order parameter S introduced by A. Saupe and W. Maier in 1959 [78]. Like in any order parameter theory, a common requirement is that it satisfies the following: it should vanish in the more symmetric (less ordered) phase and it must be different from zero in the less symmetric (more ordered) phase [76].

According to this principle, Saupe and Meier defined a scalar order parameter S as a weighted average in terms of the second order Legendre polynomial. This order parameter is given by

$$S = \int_{\mathbb{S}^2} P_2(\hat{\boldsymbol{u}} \cdot \hat{\boldsymbol{n}}) f(\hat{\boldsymbol{u}}) d\hat{\boldsymbol{u}} \,. \tag{2.3}$$

When the material has all its molecules exactly aligned with the director, $\langle \cos^2 \theta_p \rangle = 1$ and therefore $S = 1$. In contrast, when all molecules are randomly oriented in a plane perpendicular to the director $\langle \cos^2 \theta_p \rangle = 0$ and thus $S = -1/2$. In the isotropic liquid phase the molecules are randomly oriented, $f(\hat{\boldsymbol{u}}) = 1/4\pi$ and as a result $S = 0$. When greater accuracy is required it is usual to define an order parameter in terms of higher order polynomials of the Legendre expansion [77].

In general the nematic state is not only defined by a single nematic director. In fact, in some materials there are two or three axis of complete rotational symmetry. For such materials a set of perpendicular axes $\{\hat{\boldsymbol{l}}, \hat{\boldsymbol{m}}, \hat{\boldsymbol{n}}\}$ may be defined. The uniaxial or biaxial macroscopic nature of the system should not be confused with the geometry of the particles. In principle uniaxial particles (e.g. rods or discs) may be arranged into biaxial phases [19, 77].

There are some theories able to describe biaxial nematic phases using scalar order parameters. These theories generalize the ideas of Maier and Saupe and often involve a representation of rotational invariants in terms of Euler angles. The disadvantage of such theories is that in some specific cases they may present some multi–valuedness problems [77]. Therefore there is a need of a further generalization of the scalar order parameter S in Eq. (2.3).

2.1.2 Tensor order parameter

A natural extension from a scalar order parameter is a tensor one. This arbitrary function should be a non–zero rank Cartesian tensor [2] containing all the information of the rotational and reflective symmetries of the nematic phase. In contrast to the scalar order parameter, the tensor order parameter is not defined in terms of a set of perpendicular axes, but instead it is a quantity defined in terms of the moments of the orientational distribution function.

A proper construction of the tensor order parameter involves the evaluation of the average of a hierarchy of dyadic products $\hat{\boldsymbol{u}}^{(k)}$[3] over $f_{iso} = 1/4\pi$ and $f(\hat{\boldsymbol{u}})$. In general,

[2] For background information about this topic please refer to the Appendix A.

[3] Here we consider the k–order dyadic product of $\hat{\boldsymbol{u}}$ with itself given by the relation

$$\hat{\boldsymbol{u}}^{(k)} = \underbrace{\hat{\boldsymbol{u}} \otimes \hat{\boldsymbol{u}} \otimes \cdots \otimes \hat{\boldsymbol{u}}}_{k-times} \quad \text{and} \quad \hat{\boldsymbol{u}}^{(k)} \in \underbrace{\mathbb{R}^3 \otimes \mathbb{R}^3 \otimes \cdots \otimes \mathbb{R}^3}_{k-times} .$$

these moments are defined by the relation

$$\langle \hat{\boldsymbol{u}}^{(k)} \rangle = \int_{\mathbb{S}^2} \hat{\boldsymbol{u}}^{(k)} f(\hat{\boldsymbol{u}}) d\hat{\boldsymbol{u}} \,. \tag{2.4}$$

With respect to the isotropic orientational distribution function f_{iso} the first two moments are

$$\langle \hat{\boldsymbol{u}} \rangle_{iso} = 0 \quad \text{and} \quad \langle \hat{\boldsymbol{u}}\hat{\boldsymbol{u}} \rangle_{iso} = \frac{1}{3}\delta \,. \tag{2.5}$$

Note that the first moment, and in fact all odd moments of the distribution vanish since $f(\hat{\boldsymbol{u}}) = f(-\hat{\boldsymbol{u}})$. Therefore the hierarchy of dyadic products $\hat{\boldsymbol{u}}^{(k)}$ is restricted for values of $k = 2n$ where n is an integer.

In analogy to S, the new tensor order parameter $\mathbf{Q}_{(k)}$ should be a function of a deviation of the full tensor $\hat{\boldsymbol{u}}^{(k)}$ with respect to the isotropic phase, *i.e.*

$$\hat{\boldsymbol{u}}^{(k)} - \langle \hat{\boldsymbol{u}}^{(k)} \rangle_{iso} \,. \tag{2.6}$$

In terms of $\hat{\boldsymbol{u}}\hat{\boldsymbol{u}}$ using Eq. (2.5) it follows

$$\hat{\boldsymbol{u}}\hat{\boldsymbol{u}} - \langle \hat{\boldsymbol{u}}\hat{\boldsymbol{u}} \rangle_{iso} = \hat{\boldsymbol{u}}\hat{\boldsymbol{u}} - \frac{1}{3}\delta = \overline{\hat{\boldsymbol{u}}\hat{\boldsymbol{u}}} \,, \tag{2.7}$$

where $\overline{\mathbf{x}}$ stands for the symmetric traceless part of the tensor $\mathbf{x}$. The first non–vanishing moment which distinguishes the anisotropic distribution from the isotropic one is the second rank tensor order parameter $\mathbf{Q}_{(2)} = \mathbf{Q}$ [22]. This quantity is defined as an ensemble average of the deviation $\overline{\hat{\boldsymbol{u}}\hat{\boldsymbol{u}}}$ over the orientational distribution function $f(\hat{\boldsymbol{u}})$, *i.e.*

$$\mathbf{Q}(\mathbf{r}, t) = \sqrt{\frac{15}{2}} \left\langle \overline{\hat{\boldsymbol{u}}\hat{\boldsymbol{u}}} \right\rangle . \tag{2.8}$$

The translational dependency of the second rank order parameter $\mathbf{Q}_{(2)} = \mathbf{Q}_{(2)}(\mathbf{r}, t)$ is implicit since $\hat{\boldsymbol{u}} = \hat{\boldsymbol{u}}(\mathbf{r})$ [19, 22]. In most phenomenological theories, all physical quantities depending on the orientation $\hat{\boldsymbol{u}}$ of the particles can be described in terms of the order parameter $\mathbf{Q}$ also known as the *alignment tensor* [63]. In Eq. (2.8) the factor $\sqrt{15/2}$ is a convention [23].

The construction of the second rank alignment tensor can be generalized in a very direct manner in terms of $\hat{\boldsymbol{u}}^{(k)}$ so that

$$\mathbf{Q}_{(k)}(\mathbf{r}, t) = \sqrt{\frac{(2k+1)!!}{k!}} \left\langle \overline{\hat{\boldsymbol{u}}^{(k)}} \right\rangle , \tag{2.9}$$

is the k–th order alignment tensor [22]. As mentioned before, for systems involving particles presenting head–to–tail symmetry it is sufficient to consider tensors with even values of k. In the following we will focus only on the second rank alignment tensor $\mathbf{Q}$ in Eq. (2.8) since it is in terms of this quantity that the phenomenological Landau–de Gennes theory is given.

2.1.3 Some properties of the second rank alignment tensor

By definition $\mathbf{Q}$ is a 3×3 symmetric traceless matrix. It has five independent components where three of them may be fixed to the molecular reference frame and the other two can be used to describe the average orientational order. In the molecular reference frame, $\mathbf{Q}$ is written as a linear combination of the principal eigenvectors (parallel to the molecule's principal axes) $\boldsymbol{l}, \boldsymbol{m}$ and $\boldsymbol{n}$, *i.e.*

$$\mathbf{Q}(\mathbf{r},t) = \mu_1 \boldsymbol{ll} + \mu_2 \boldsymbol{mm} + \mu_3 \boldsymbol{nn}\,. \tag{2.10}$$

Here μ_1, μ_2 and μ_3 are the eigenvalues of the matrix satisfying $\mu_1+\mu_2+\mu_3 = 0$. In terms of these eigenvalues it is possible to characterize different states of order. The following distinction should be made: if all eigenvalues are zero the system presents an isotropic state; if two of these eigenvalues are equal then the system is in a uniaxial nematic state; finally, if all eigenvalues are different the system presents a biaxial nematic state.

For the special case of uniaxial phases, the order parameter can be found contracting $\mathbf{Q}$ and the principal direction $\boldsymbol{n}$, *i.e.*, $\boldsymbol{nn} : \mathbf{Q}$. Hence

$$\mathbf{Q}(\mathbf{r},t) = \frac{3}{2}\mu_3 \overline{\mathbf{nn}} \tag{2.11}$$

where μ_3 is the largest eigenvalue in Eq. (2.10). The equilibrium value μ_3 is proportional to the Maier–Saupe order parameter via $\mu_3 = \sqrt{10/3}\,S$ [22]. Using the definition of the Maier–Saupe scalar order parameter we find that the bounds of μ_3 are

$$-\sqrt{\frac{5}{6}} \leq \mu_3 \leq \sqrt{\frac{10}{3}}\,. \tag{2.12}$$

For biaxial nematic states the description is more complicated. In this case the full tensor $\mathbf{Q}$ should be contracted as well with the tensors $\boldsymbol{ll}$ and $\boldsymbol{mm}$. However, due to the symmetries of the tensor, the three principal values are not independent. A proper description of the biaxial states of the system can be done in terms of the rotational invariants of $\mathbf{Q}$. By definition, a second rank symmetric traceless tensor has three rotational invariants: the trace, the norm and the determinant. Using the Einstein convention these are:

$$\begin{aligned} I_1 &= Q_{\mu\mu}\,, \\ I_2 &= Q_{\mu\nu}Q_{\mu\nu}\,, \\ I_3 &= Q_{\mu\nu}Q_{\nu\lambda}Q_{\lambda\mu}\,. \end{aligned} \tag{2.13}$$

Since $\mathbf{Q}$ is traceless $I_1 = 0$. In terms of I_2 and I_3 a suitable measure of the biaxiality is b, the biaxiality parameter, given by [79]

$$b^2 = 1 - \frac{I_3^2}{I_2^3}\,. \tag{2.14}$$

With this parameter one realizes that in the case of uniaxial alignment $b = 0$ and in the case of biaxial alignment $b = 1$.

2.2 The isotropic–nematic phase transition

Normally depending on the temperature, concentration or the applied electric or magnetic field these systems show a variety of phases. Therefore the total free energy $\mathcal{F}$ of the material may include terms such as: elastic energy due to any distortion of the structure of the material; lyotropic energy which dictates the preferred phase of the material; and, surface energy terms representing the interaction between the boundaries of the system and the particles at the surface [77]. Therefore, the total energy of the system is:

$$\mathcal{F} = \mathcal{F}_{elastic} + \mathcal{F}_{lyotropic} + \mathcal{F}_{surface}\,. \tag{2.15}$$

In terms of the energy densities F_e, F_l and F_s, Eq. (2.15) may be written as

$$\mathcal{F} = \int_V (F_e + F_l) d\mathbf{r} + \int_{\mathbb{S}^2} F_s ds\,, \tag{2.16}$$

where the energy densities depend on the tensor order parameter $\mathbf{Q}$.

2.2.1 Lyotropic energy

The lyotropic energy density F_l is the function which dictates the state the fluid would be, *e.g.* uniaxial order, biaxial nematic or isotropic fluid phase [77]. At low concentration this free energy density should have a minimum energy in the isotropic state $\mathbf{Q} = 0$ whereas at high concentration there should be minima at three uniaxial states, *i.e.* the states where any two of the eigenvalues of $\mathbf{Q}$ are equal. The simplest form of such function is a truncated Taylor expansion about $\mathbf{Q} = 0$ which up to 4–th order reads [19, 77],

$$F_l = \frac{1}{2} A\, Q_{\mu\nu} Q_{\mu\nu} - \frac{1}{3} B\, Q_{\mu\nu} Q_{\nu\lambda} Q_{\lambda\mu} + \frac{1}{4} C\, (Q_{\mu\nu} Q_{\mu\nu})^2\,. \tag{2.17}$$

It is immediate to recognize that this expansion is given in terms of the scalar rotational invariants I_n [see Eqs. (2.13)] of the tensor order parameter $\mathbf{Q}$. In fact, a more general expression of F_l is constructed in terms of a multiplication of the scalar rotational invariants as shown in Ref. [76]. However, for this study we will focus in the classical Landau–de Gennes expression in (2.17).

The numerical coefficients in Eq. (2.17) are introduced for future convenience, however, the most important information is given by the coefficients A, B and C. These coefficients may or may not depend on the concentration of the system. For simplicity here we assume that

$$A(c) = A_0 \left(1 - \frac{c}{c^*}\right)\,, \tag{2.18}$$

and A_0, B and C are positive dimensionless coefficients that may be related to molecular properties of the system [19, 57, 23, 80]. In Eq. (2.18) the characteristic concentration

c^* is a model parameter known as the pseudo–critical concentration [22]. Before going any further, it is important that to take into account the following remarks [76]:

1. There is no linear term in $\mathbf{Q}$. This allows the possibility of an isotropic phase.
2. Odd terms of order three are allowed. This causes the isotropic–nematic phase transition to be of first order.
3. The isotropic–nematic phase transition takes place in the neighborhood of $A = 0$. Therefore the density dependence of the free energy density of the system is contained in A alone.

The minimum of the Landau–de Gennes free energy density

Considering only uniaxial nematic phases inserting the uniaxial nematic order parameter given by Eq. (2.11) in Eq. (2.17) the lyotropic energy becomes

$$F_l^{uni} = \frac{9}{8}A(c)\mu_3^2 - \frac{9}{8}B\mu_3^3 + \frac{81}{64}C\mu_3^4 \,. \tag{2.19}$$

Equation (2.19) has stationary points when the second derivative vanishes, *i.e.* $dF_l^{uni}/d\mu_3 = 0$, thus

$$\mu_3^0 = 0 \,, \tag{2.20}$$

$$\mu_3^{\pm} = \frac{1}{3C}\left(B \pm \sqrt{B^2 - 4AC}\right) \,. \tag{2.21}$$

For the system it would be energetically favorable to lie in one of the minima of F_l^{uni}. By calculating the second derivative $(d^2F_l^{uni}/d\mu_3^2)$ and comparing the energies of each solution one finds that:

- At μ_3^0 the isotropic state is globally stable for $A > \frac{2B^2}{9C}$, metastable for $0 < A < \frac{2B^2}{9C}$ and unstable for $A < 0$.
- At μ_3^+ the nematic state is globally stable for $A < \frac{2B^2}{9C}$, metastable for $\frac{2B^2}{9C} < A < \frac{B^2}{4C}$ and not defined for $A > \frac{B^2}{4C}$.
- At μ_3^- the nematic state has negative (non–physical) values and is usually discarded.

There are three important values of A: $\frac{B^2}{4C}$ the low concentration $c^\dagger$ where the nematic state disappears; $\frac{2B^2}{9C}$ the concentration c^{IN} at which the energy of the isotropic and nematic are exactly equal; $A = 0$ the high concentration c^* where the isotropic state loses stability. Using the ansatz in Eq. (2.19) these critical concentrations are:

$$c^\dagger = \left(1 - \frac{B^2}{4C}\right)c^* \quad \text{and} \quad c^{IN} = \left(1 - \frac{2B^2}{9C}\right)c^* \,. \tag{2.22}$$

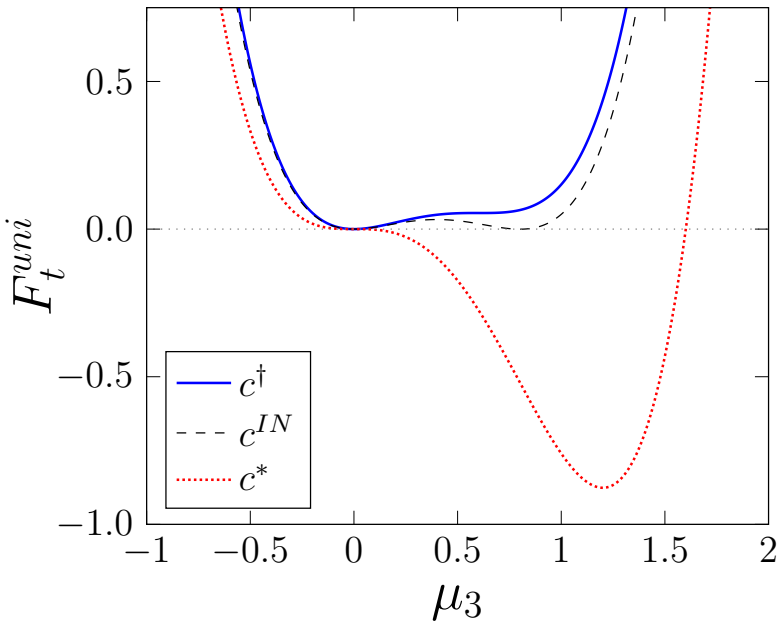

Figure 2.2: Free energy density F_t^{uni} as a function of the scalar order parameter μ_3 for the concentrations $c^\dagger, c^{IN}$ and c^*, for $\mu_3^{IN} = 0.4$.

In Fig. (2.2) the Landau–de Gennes free energy density in Eq. (2.19) is shown as a function of the scalar order parameter μ_3 for the special concentrations $c^\dagger, c^{IN}$ and c^* with $\mu_3^{IN} = 0.4$.

It is important to say that by construction the Landau–de Gennes free energy density does not restrict the order parameter to be within its bounds [see Eq. (2.12)]. Thus it is common to introduce an ansatz such that the magnitude of the alignment tensor is bounded. In Ref. [63] an amended free energy density is given in terms of a *maximum value* for the magnitude of $\mathbf{Q}$. However, the differences between these ansatz and the Landau–de Gennes free energy are small and it is convenient to maintain the original one [63].

2.2.2 Elastic energy

The most general theory of curvature-elasticity of uniaxial fluids is due to F. C. Frank extending the seminal work of C. W. Oseen from 1933 [20]. In his work of 1958 *On the theory of liquid crystals* Frank derives a phenomenological elastic energy density in terms of the nematic director $\hat{\boldsymbol{n}}$ [21] . For non–chiral particles the Frank–Oseen elastic free energy density is:

$$F_e = \frac{K_{11}}{2}(\nabla \cdot \hat{\boldsymbol{n}})^2 + \frac{K_{22}}{2}(\hat{\boldsymbol{n}} \cdot \nabla \times \hat{\boldsymbol{n}})^2 + \frac{K_{33}}{2}(\hat{\boldsymbol{n}} \times \nabla \times \hat{\boldsymbol{n}})\,. \tag{2.23}$$

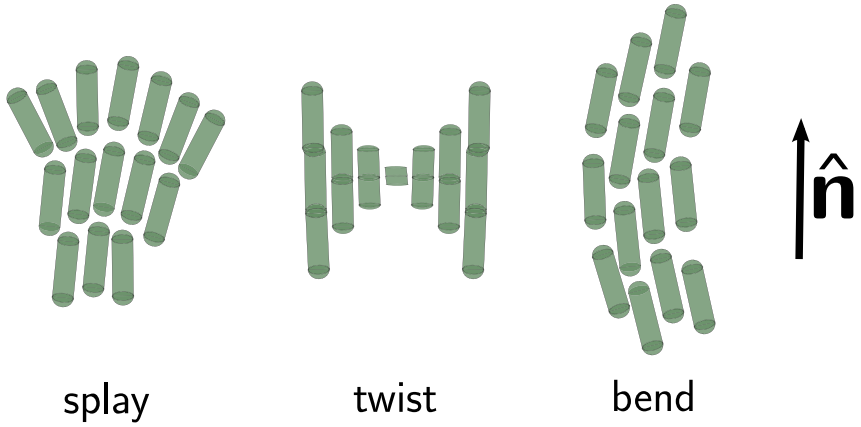

Figure 2.3: Splay, twist and bend deformations of the nematic director $\hat{\boldsymbol{n}}$.

This elastic energy takes into account 3 different types of distortion that can occur in the system: splay, twist and bend [see Fig. (2.3)]. The Frank constants are dependent on the particular fluid being described and can be determined by experimental measurements of the structure factor of the material [19].

The Landau–de Gennes free energy density can also be extended to a description of spatially inhomogeneous alignment only by including combinations of gradients, divergence and curl of the order parameter $\mathbf{Q}$ [19]. The contribution due to distortion in space of the alignment tensor is such that any gradients in $\mathbf{Q}$ would lead to an increase of the elastic energy density F_e [77].

However, in order to write a phenomenological description of these phenomena in terms of $\mathbf{Q}$ we have to take into account that given a fixed distortion in space of Q the elastic energy must remain unchanged under translations and rotations of the material. Such restrictions imply that not all combinations of derivatives of $\mathbf{Q}$ in space are allowed [77]. A common expression of the phenomenological elastic energy density is:

$$F_e = \frac{L_1}{2}(\nabla_\lambda Q_{\mu\nu})^2 + \frac{L_2}{2}(\nabla_\lambda Q_{\mu\lambda})(\nabla_\gamma Q_{\mu\gamma})\,, \tag{2.24}$$

where the elastic coefficient L_1 and L_2 are phenomenologic elastic constants. A more general elastic free energy density contains terms proportional to $\nabla_\lambda Q_{\mu\gamma}\nabla_\gamma Q_{\mu\lambda}$ and cubic in the alignment tensor [19], but in the following they will not be considered.

The elastic parameters L_1 and L_2 are related to the Frank elastic constants K_{ij}

in (2.23) by [81]

$$L_1 = \frac{1}{6S_{eq}^2}(K_{33} - K_{11} + 3K_{22})\,, \tag{2.25}$$

$$L_2 = \frac{1}{S_{eq}^2}(K_{11} - K_{22})\,, \tag{2.26}$$

where S_{eq} is the equilibrium uniaxial order parameter of the fluid [81]. In terms of elastic constant L_1 order parameter fluctuations are correlated over a distance of order

$$\xi = \sqrt{\frac{L_1}{A(c)}}\,, \tag{2.27}$$

where $A(c)$ is given in Eq. (2.19). In normal lyotropic fluids this correlation length is at most a few tens of nanometers even close the isotropic–nematic transition [82].

2.2.3 Surface energy

In experiments surfaces can be treated in different ways. Usually the surface undergoes a special type of chemical or physical modification such that there is a preferred direction of alignment near the boundaries [83, 84, 85, 86]. Associated with this preferred direction of alignment directly at the border is the amount of order in a vicinity close to it. These restrictions imply that the surface energy density F_s has minimum at the preferred state. If $\mathcal{S}$ is the surface in contact with the fluid

$$F_s = F_s(\mathbf{Q}|_{\mathcal{S}})\,. \tag{2.28}$$

Sometimes the variables near the boundaries are forced to move out of the minima of F_s because the bulk of the fluid is in some alternate state. Finally the competition between the surface energy and the bulk energy reaches a balance such that the total energy of the system in Eq. (2.15) is minimized.

The most commonly obtained types of anchoring are characterized by a particular anchoring direction. One these is the so called weak anchoring condition. In this type of anchoring F_s has a single minimum at the point where the magnitude of $\mathbf{Q}|_{\mathcal{S}}$ is reached. Another common type of anchoring is the strong (infinite) anchoring, which corresponds to the usual Dirichlet boundary condition at the surface. Finally, another common anchoring condition is the planar anchoring condition. In this situation the physical boundaries are prepared such that the directors of the fluid lie parallel to the substrate [84].

Chapter 3

Microscopical description

In this chapter we revisit the basic concepts of standard statistical physics starting with the Hamiltonian of a one component system and the pair interaction potential between uniaxial rigid molecules. We continue introducing the main ideas behind the variational principle known as classical density functional theory (DFT) and familiarize with the theories developed (within this formalism) for systems of one–component non–spherical bodies. Further, we briefly introduce the density functional theories for mixtures of non–spherical particles. We focus mainly on two theories: the Many–fluid Parsons–Lee theory [35] which is focused on spatially homogeneous one–body densities; and an extension of the Ramakrishnan–Youssuf approximation [39] (Second–order perturbation theory) for mixtures which focus on spatially inhomogeneous one–body densities.

3.1 Systems of rigid anisotropic particles

Consider a system of N identical uniaxial anisotropic rigid particles filling a simply connected volume $V \subset \mathbb{R}^3$. Due to their anisotropy the complete set of variables necessary to describe the k–th particle in V is: $\{\mathbf{r}_k, \hat{\boldsymbol{u}}_k\}$. This set accounts for translational and rotational degrees of freedom. Here $\mathbf{r}_k$ denotes the center of mass position and $\hat{\boldsymbol{u}}_k = \hat{\boldsymbol{u}}_k(\{\phi_k, \theta_k\})$ is a unit vector dependent on the set of Euler angles that fix the particle's orientation.

In absence of external fields, the Hamiltonian of the system, $\mathcal{H}(\{\mathbf{r}_k, \hat{\boldsymbol{u}}_k\})$, is a sum of kinetic energy K and interaction energy H given by

$$K = \sum_{i=1}^{N} \frac{\mathbf{p}_i^2}{2m} + \frac{1}{2} I \boldsymbol{\omega}_i^2 \quad \text{and} \quad H = \mathcal{U}(\{\mathbf{r}_k, \hat{\boldsymbol{u}}_k\}) \,, \tag{3.1}$$

where $\mathbf{p}_i$ is the linear momenta of particles of mass m, I the moment of inertia, $\boldsymbol{\omega}_i$ the angular velocity of rotation and $\mathcal{U}(\{\mathbf{r}_k, \hat{\boldsymbol{u}}_k\})$ is the total inter molecular potential energy [87]. Assuming that the interactions occur solely by pairs $\mathcal{U}(\{\mathbf{r}_k, \hat{\boldsymbol{u}}_k\})$ is given by

$$\mathcal{U}(\{\mathbf{r}_k, \hat{\boldsymbol{u}}_k\}) = \frac{1}{2}\sum_{i=1}^{N}\sum_{j=1}^{N}\mathcal{U}(\mathbf{r}_i - \mathbf{r}_j, \hat{\boldsymbol{u}}_i, \hat{\boldsymbol{u}}_j) \tag{3.2}$$

where $\mathcal{U}(\mathbf{r}_{ij}, \hat{\boldsymbol{u}}_i, \hat{\boldsymbol{u}}_j)$ is the pair interaction potential between the particle i and the particle j at positions $\mathbf{r}_i$ and $\mathbf{r}_j$ having orientations $\hat{\boldsymbol{u}}_i$ and $\hat{\boldsymbol{u}}_j$, respectively.

In accordance with classical statistical mechanics in the canonical ensemble, the configurational partition function is

$$\mathcal{Q} = \frac{1}{N!}\prod_{k=1}^{N}\int_V d\mathbf{r}_k \int_{\mathbb{S}^2} d\hat{\boldsymbol{u}}_k \exp\left(-\frac{1}{2}\sum_{i=1}^{N}\sum_{j=1}^{N}\frac{\mathcal{U}(\mathbf{r}_{ij}, \hat{\boldsymbol{u}}_i, \hat{\boldsymbol{u}}_j)}{k_B T}\right), \tag{3.3}$$

where $\mathbb{S}^2$ is the unit sphere and k_B is Boltzmann's constant. Given the configurational partition function, Eq. (3.3), the conformational ensemble average of an observable $\mathcal{A}$ is given by

$$\langle \mathcal{A} \rangle = \frac{1}{\mathcal{Q}}\prod_{k=1}^{N}\int_V d\mathbf{r}_k \int_{\mathbb{S}^2} d\hat{\boldsymbol{u}}_k \mathcal{A} \exp\left(-\frac{1}{2}\sum_{i=1}^{N}\sum_{j=1}^{N}\frac{\mathcal{U}(\mathbf{r}_{ij}, \hat{\boldsymbol{u}}_i, \hat{\boldsymbol{u}}_j)}{k_B T}\right). \tag{3.4}$$

In statistical mechanics, the properties of a system are obtained after the partition function (3.4). However, in most cases, the configurational integral, $\mathcal{Q}$, and the conformational ensemble average of an observable, $\langle \mathcal{A} \rangle$, cannot be calculated analytically for a given pair potential $\mathcal{U}(\mathbf{r}_{ij}, \hat{\boldsymbol{u}}_i, \hat{\boldsymbol{u}}_j)$. Nevertheless, it is possible to write these functions in the form of series expansions. In fact, there are several ways to do this and the simplest is one is the Mayer cluster expansion [87, 88, 89]. This expansion [90] consists of a power series of the configurational partition function (3.3) around a system of non-interacting particles. Here, the two particle function

$$f_{ij}(\mathbf{r}_{ij}, \hat{\boldsymbol{u}}_i, \hat{\boldsymbol{u}}_j) = \exp\left(-\frac{\mathcal{U}(\mathbf{r}_{ij}, \hat{\boldsymbol{u}}_i, \hat{\boldsymbol{u}}_j)}{k_B T}\right) - 1, \tag{3.5}$$

is introduced, and in terms of this function the cluster expansion is performed. For homogeneous rigid anisotropic fluids the Mayer function plays a key role in the context of Onsager's theory [24] and Density Functional Theory [29].

3.1.1 Pair interaction potential

The structure and thermodynamic properties of a system in equilibrium are determined by inter molecular forces. These forces, or rather their related interaction potentials, can

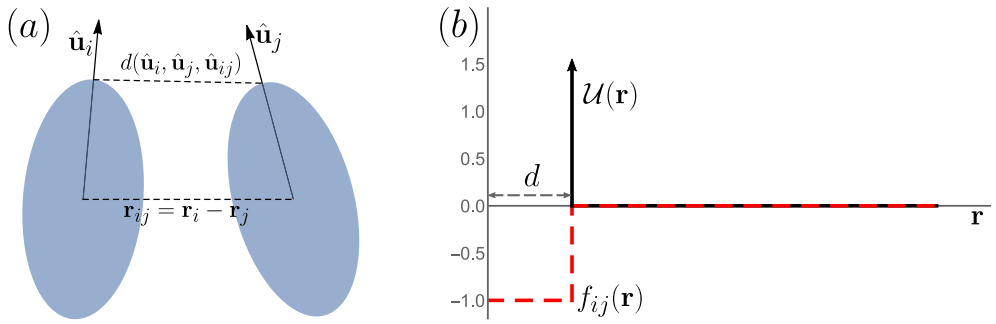

Figure 3.1: (a) Interaction between two anisotropic particles. Here $\mathbf{r}_{ij}$ denotes the center of mass distance between the particles and $d(\hat{\boldsymbol{u}}_i, \hat{\boldsymbol{u}}_j, \hat{\boldsymbol{u}}_{ij})$ is the orientational dependent distance of closest approach. (b) Schematic representation of the inter particle potential energy $\mathcal{U}(\mathbf{r}_{ij})$ and Mayer function $f_{ij}(\mathbf{r}_{ij})$ of a couple of hard anisotropic particles with fixed orientation. Since the orientation of the molecules is fixed the distance of closest approach between the particles is d.

be obtained, e.g., from *ab initio* calculations based on quantum mechanics [91]. However even for simple fluids these calculations are complex and computationally demanding. For this reason theorists resort to model these interactions using suitable analytic functions determined by a number of parameters.

Restricting ourselves to apolar and uniaxial rigid molecules, the pair interaction potential must have the following regularities [87]

$$\mathcal{U}(\mathbf{r}_{ij}, \hat{\boldsymbol{u}}_i, \hat{\boldsymbol{u}}_j) = \mathcal{U}(-\mathbf{r}_{ij}, \hat{\boldsymbol{u}}_i, \hat{\boldsymbol{u}}_j) = \mathcal{U}(\mathbf{r}_{ij}, -\hat{\boldsymbol{u}}_i, \hat{\boldsymbol{u}}_j) = \mathcal{U}(\mathbf{r}_{ij}, \hat{\boldsymbol{u}}_i, -\hat{\boldsymbol{u}}_j)\,, \tag{3.6}$$

where $\mathbf{r}_{ij} = \mathbf{r}_i - \mathbf{r}_j$. For this reason, the average orientation of the particles present the so called *head–tail* symmetry. Some examples of pair interaction potentials suitable to describe such anisotropic fluids are generalizations of the Gay-Berne potential [92] and excluded volume interactions [24].

The simplest model is one of hard core interactions. Hard particle systems combine conceptual simplicity and computational tractability, qualities that make them accessible to theoretical studies. For these systems the pair potential is given by

$$\mathcal{U}(\mathbf{r}_{ij}, \hat{\boldsymbol{u}}_i, \hat{\boldsymbol{u}}_j) = \begin{cases} \infty & r < d(\hat{\boldsymbol{u}}_i, \hat{\boldsymbol{u}}_j, \hat{\boldsymbol{u}}_{ij}) \\ 0 & \text{otherwise} \end{cases}\,, \tag{3.7}$$

where $d(\hat{\boldsymbol{u}}_i, \hat{\boldsymbol{u}}_j, \hat{\boldsymbol{u}}_{ij})$ is the orientational dependent distance of closest approach between the particles, and $\mathbf{r}_{ij} = r_{ij}\hat{\boldsymbol{u}}_{ij}$ [see Fig. 3.1(a)][1]. For a system of rigid anisotropic

[1]The simplest hard core pair potential model is the one of a hard–sphere liquid where the particles have isotropic shape and d represents the effective diameter of the particle.

particles the Mayer function (3.5) is given by

$$f_{ij}(\mathbf{r}_{ij},\hat{\boldsymbol{u}}_i,\hat{\boldsymbol{u}}_j)=\begin{cases}-1 & r<d(\hat{\boldsymbol{u}}_i,\hat{\boldsymbol{u}}_j,\hat{\boldsymbol{u}}_{ij})\\ 0 & \text{otherwise}\end{cases}. \tag{3.8}$$

In Fig. 3.1(b) we show schematically the inter particle potential energy $\mathcal{U}(\mathbf{r}_{ij})$ and Mayer function $f_{ij}(\mathbf{r}_{ij})$ for a couple of hard anisometric particles with fixed orientation.

Due to the singular nature of the hard particle potential $\mathcal{U}(\mathbf{r}_{ij},\hat{\boldsymbol{u}}_i,\hat{\boldsymbol{u}}_j)$ the temperature T does not appear on the right hand side of Eq. (3.8), consequently, hard particle fluids are often called *athermal*. In turn, the configurational energy depends only on the density and is determined by the non–overlapping configurations in space.

3.1.2 Onsager's second virial theory

Historically the first attempt to describe the structural and thermodynamical properties of anisotropic fluids from a microscopic point of view was made by Lars Onsager in 1949. In his seminal work *The effects of shape on the interaction of colloidal particles* he considered a low density gas of needle–like particles and wrote down the orientational free energy introducing a much more efficient way of using the virial expansion [24]. To this end, he did a cluster expansion of the free energy following the work of Mayer [90]. This expansion reads

$$\frac{\mathcal{F}}{Nk_BT}=c(T)+\ln\rho-1-\frac{\beta_1}{2}\rho-\frac{\beta_2}{3}\rho^2+\cdots, \tag{3.9}$$

where $c(T)$ is a constant that depends only on the temperature and β_n are the irreducible cluster integrals [2], given in terms of Mayer functions as

$$\beta_1=\frac{1}{V}\int_{\mathbb{S}^2} f_{12}\,d\hat{\boldsymbol{u}}_1 d\hat{\boldsymbol{u}}_2 \quad\text{and}\quad \beta_2=\frac{1}{2V}\int_{\mathbb{S}^2} f_{12}f_{23}f_{31}\,d\hat{\boldsymbol{u}}_1 d\hat{\boldsymbol{u}}_2 d\hat{\boldsymbol{u}}_2\,. \tag{3.10}$$

For hard–core potentials $-\beta_1$ determines the excluded volume between particles. Indeed, excluded volume effects can account for most ordering transitions in simple liquids and liquid crystals [93].

For a pair of hard–spheres of radius r the excluded volume is obviously a sphere of radius $2r$. However, the determination of an exact expression of the excluded volume between non–spherical particles is not an easy task. In fact, this assignment normally includes concepts from analytic geometry and integral geometry[3]. Onsager himself determined the pair–excluded volume of hard–spherocylinders (see Ref. [24]). Hard spherocylinders are cylinders of length l caped at both ends with hemispheres whose diameters

[2] For a modern and didactic introduction to the Mayer cluster integrals and its formalism we refer the reader to Chapter 3 in the book of Hansen and McDonald *Theory of simple liquids*, Ref. [88].

[3] A very nice introduction to the topic is given in the book: *Theory of anisotropic colloidal solutions* by A. Isihara, Ref. [94].

are the same as the diameter of the cylinder d. They are characterized by their aspect ratio $\kappa = l/d$ and possess a particle volume of $v = (\pi/12)(3\kappa + 2)d^3$. The excluded volume between a pair of spherocylinders (i, j) is

$$V_{exc}(\gamma) = \frac{\pi}{4}(\kappa_i d_i^3 + \kappa_j d_j^3) + \frac{\pi}{4} d_i d_j (d_i + d_j) \sin\gamma + \frac{\pi}{4}(\kappa_i d_i d_j^2 + \kappa_j d_j d_i^2)|\cos\gamma| + \kappa_i \kappa_j d_i d_j (d_i + d_j) \sin\gamma + (\kappa_i d_i + \kappa_j d_j) d_i d_j E(\sin\gamma)\,, \quad (3.11)$$

where $E(\sin\gamma)$ denotes the complete elliptic integral of the second kind and $\gamma = \arccos(\hat{\boldsymbol{u}}_i \cdot \hat{\boldsymbol{u}}_j)$. A modern derivation in the framework of general expressions for generalized hard sphero–zonotopes can be found in Ref. [93].

The irreducible cluster integrals (3.10) are related to the well known virial coefficients B_n by $B_{n+1} = -n/(n+1)\beta_n$ [82]. Omitting all constants that are independent of density Eq. (3.10) can be rewritten as

$$\frac{\mathcal{F}}{N k_B T} = \ln\rho + \rho B_2 + \frac{1}{2}\rho^2 B^3 + \cdots . \quad (3.12)$$

For highly elongated spherocylinders ($\kappa \to \infty$) Onsager showed that the contribution to Eq. (3.12) of all virial coefficients beyond the second goes to zero. As it is confirmed by numerous simulations, in this limit all higher order terms vanish and may be neglected for all finite densities $\rho B_2 \ll \kappa$ [82].

Up to this point we have assumed that the density of the system is constant. However, we should allow the possibility of an orientational ordered phase with a lower free energy. To this end the density of the system should be a one–particle density distribution of the form $\rho = \rho(\mathbf{r}, \hat{\boldsymbol{u}})$. Although this approach is made in a very clear fashion by Onsager in Ref. [24] we will turn to a much more modern description. For this purpose we use the density functional description for fluids which is described in the following sections.

3.2 Density functional theory

In its original form, the density functional formalism was developed in 1964 to deal with a gas of interacting electrons in an external potential. Hohenberg and Kohn [95] derived a variational principle to determine the ground state of this quantum mechanical system. One year later this theoretical approach was generalized to non-zero temperatures by Mermin [96].

In Soft Matter theory this formalism was introduced by R. Evans in *The nature of the liquid-vapor interface and other topics in the statistical mechanics of nonuniform, classical fluids* in 1979 [25, 26]. The following summary of the theory is based on the above mentioned publications as well as in the review articles *Density Functional Theories of Hard Particle Systems* by P. Tarazona et al [28] and *Density functional theory of inhomogeneous classical fluids: recent developments and new perspectives* by H. Löwen [97].

In short, density functional theory (DFT) consists on a variational principle of the grand canonical free energy functional $\Omega(T, \mu, [\rho(\mathbf{r}, \hat{\boldsymbol{u}})])$. Here T is the temperature of the system and μ is its chemical potential [96, 25]. Within this formalism, the basic variables describing the microscopic degrees of freedom of a many–body fluid are the one–particle densities $\rho(\mathbf{r}, \hat{\boldsymbol{u}})$. Here $\rho(\mathbf{r}, \hat{\boldsymbol{u}})\, dV$ is the average number of particles in an infinitesimal volume dV located at position $\mathbf{r}$ with orientation $\hat{\boldsymbol{u}}$. In terms of $\{\mathbf{r}_k, \hat{\boldsymbol{u}}_k\}$ the one–particle density is defined as

$$\rho(\mathbf{r}, \hat{\boldsymbol{u}}) \equiv \left\langle \sum_{k=1}^{N} \delta(\mathbf{r} - \mathbf{r}_k)\delta(\hat{\boldsymbol{u}} - \hat{\boldsymbol{u}}_k) \right\rangle , \tag{3.13}$$

where $\langle \cdots \rangle$ denotes the conformational average in Eq. (3.4). In the DFT the structural an thermodynamic properties of the system will be described in terms of $\rho(\mathbf{r}, \hat{\boldsymbol{u}})$. The one–particle density distribution $\rho(\mathbf{r}, \hat{\boldsymbol{u}})$ gives the probability of finding a particle at position $\mathbf{r}$ with orientation $\hat{\boldsymbol{u}}$.

At fixed T and μ, $\Omega(T, \mu, [\rho(\mathbf{r}, \hat{\boldsymbol{u}})])$, the functional $\Omega([\rho(\mathbf{r}, \hat{\boldsymbol{u}})])$ becomes minimal for the equilibrium one–particle density $\rho_0(\mathbf{r}, \hat{\boldsymbol{u}})$, i.e.,

$$\left.\frac{\delta\Omega[\rho]}{\delta\rho}\right|_{\rho=\rho_0} = 0\,, \quad \Omega[\rho_0(\mathbf{r}, \hat{\boldsymbol{u}})] = \Omega\,. \tag{3.14}$$

Here, the value of the functional at the equilibrium density Ω_0 is the real equilibrium grand canonical free energy. Moreover, the functional $\Omega(T, \mu, [\rho(\mathbf{r}, \hat{\boldsymbol{u}})])$ can be decomposed as

$$\Omega[\rho] = \mathcal{F}[\rho] + \int_V d\mathbf{r} \int_{\mathbb{S}^2} d\hat{\boldsymbol{u}}\, \rho(\mathbf{r}, \hat{\boldsymbol{u}}))(V_{\text{ext}}(\mathbf{r}, \hat{\boldsymbol{u}})) - \mu)\,, \tag{3.15}$$

where $V_{\text{ext}}(\mathbf{r}, \hat{\boldsymbol{u}}))$ is the external potential acting on the particles. Normally, this external potential is in charge of describing the system boundaries and external fields (gravitational, electro–magnetic, etc.).

The free energy functional $\mathcal{F}[\rho]$ appearing in Eq. (3.15) may be splitted in an ideal contribution, $\mathcal{F}_{\text{id}}[\rho]$, plus an excess free energy, $\mathcal{F}_{\text{exc}}[\rho]$, that accounts for the particles interaction. In k_BT units $\mathcal{F}[\rho]$ is written as

$$\beta\mathcal{F}[\rho] = \beta\mathcal{F}_{\text{id}}[\rho] + \beta\mathcal{F}_{\text{exc}}[\rho]\,, \tag{3.16}$$

where $\beta = 1/k_BT$. The ideal free energy functional is known exactly [29] and reads

$$\beta\mathcal{F}_{\text{id}}[\rho] = \int_V \int_{\mathbb{S}^2} \rho(\mathbf{r}, \hat{\boldsymbol{u}})\{\ln\left(\Lambda^3\rho(\mathbf{r}, \hat{\boldsymbol{u}})\right) - 1\}\, d\hat{\boldsymbol{u}}\, d\mathbf{r}\,, \tag{3.17}$$

where $\Lambda^2 = h^2/2\pi m k_BT$ is the thermal de Broglie wavelength with m the particle's mass and includes the translational and rotational contributions of the kinetic energy. If the system is an ideal gas, $\mathcal{F}_{\text{exc}}[\rho]$ vanishes. For a system of non-vanishing pair interaction the excess part is not known in general and one has to rely on approximations.

3.2.1 Excess free energy

The effects of particle interactions are introduced through the excess free energy functional $\mathcal{F}_{\text{exc}}[\rho]$. For its construction it is useful to introduce an effective one–body potential known as the direct correlation function. The direct correlation function $c^{(1)}$ is related to the excess free energy functional via

$$c^{(1)}[\rho(\mathbf{r},\hat{\boldsymbol{u}})] \equiv -\beta \frac{\delta \mathcal{F}_{\text{exc}}[\rho]}{\delta \rho} \,. \tag{3.18}$$

In fact, $c^{(1)}[\rho(\mathbf{r},\hat{\boldsymbol{u}})]$ is only the first member of a hierarchy of correlation functions generated by $\mathcal{F}_{\text{exc}}[\rho]$. Higher order functions are obtained by differentiation

$$c^{(n)}[\rho] = -\beta \frac{\delta^n \mathcal{F}_{\text{exc}}[\rho]}{\delta\rho_1 \cdots \delta\rho_n} = -\beta \frac{\delta^n \mathcal{F}_{\text{exc}}[\rho]}{\delta\rho_n \cdots \delta\rho_1} \,, \tag{3.19}$$

where $\rho_i = \rho(\mathbf{r}_i, \hat{\boldsymbol{u}}_i)$. Of particular interest is the second derivative of this hierarchy, the so–called direct correlation function

$$c^{(2)}(\mathbf{r}_{12}, \hat{\boldsymbol{u}}_1, \hat{\boldsymbol{u}}_2) = -\beta \frac{\delta^2 \mathcal{F}_{\text{exc}}[\rho(\mathbf{r},\hat{\boldsymbol{u}})]}{\delta\rho(\mathbf{r}_1,\hat{\boldsymbol{u}}_1)\delta\rho_(\mathbf{r}_2,\hat{\boldsymbol{u}}_2)} \,. \tag{3.20}$$

The direct correlation function serves as a measure of the structure and the properties of the fluid [98] and is related to the total pair correlation function which can be measured using diffraction experiments and computer simulations.

In terms of the direct correlation function the total pair correlation function $h(\mathbf{r}_{12}, \hat{\boldsymbol{u}}_1, \hat{\boldsymbol{u}}_2)$ is given by[4]:

$$h(\mathbf{r}_{12}, \hat{\boldsymbol{u}}_1, \hat{\boldsymbol{u}}_2) = c^{(2)}(\mathbf{r}_{12}, \hat{\boldsymbol{u}}_1, \hat{\boldsymbol{u}}_2) + \rho_0 \int_V d\mathbf{r}_3 \langle c^{(2)}(\mathbf{r}_{13}, \hat{\boldsymbol{u}}_1, \hat{\boldsymbol{u}}_2) h(\mathbf{r}_{32}, \hat{\boldsymbol{u}}_3, \hat{\boldsymbol{u}}_2) \rangle_{\hat{\boldsymbol{u}}_3} \,, \tag{3.21}$$

and it measures the total effect of a molecule 1 on a molecule 2 at a separation $\mathbf{r}_{12}$ and with orientations $\hat{\boldsymbol{u}}_1$ and $\hat{\boldsymbol{u}}_2$. Equation (3.21) is a generalization of the *Ornstein–Zernike* equation to non–spherical molecules for a homogeneous fluid [99]. This expression indicates that the total pair correlation between two particles consists of two contributions: the direct correlation function between them and an indirect correlation arising because of their interactions with the remaining particles in the system[91]. In general, the knowledge of the direct correlation function allows us to calculate many fluid properties, for example, the isothermal compressibility.

Approximations work on different levels. The usual virial expansion of Onsager can be obtained directly from Eqs. (3.20) and (3.21) doing a cluster expansion of the pair correlation function in a system with uniform density ρ_0, i.e.,

$$-c^{(2)}(\mathbf{r}_{12}, \hat{\boldsymbol{u}}_1, \hat{\boldsymbol{u}}_2; \rho_0) = f_{12} + \rho_0 f_{12} \int_V \int_{\mathbb{S}^2} f_{23} f_{31} \, d\hat{\mathbf{u}}' \, d\hat{\mathbf{u}} \, d\mathbf{r}' \, d\mathbf{r} + \cdots \,, \tag{3.22}$$

[4] For an inhomogeneous fluid ρ_0 will depend on $\mathbf{r}_3$ and $\hat{\boldsymbol{u}}_3$ and cannot be taken outside the integral.

where $f_{ij} = f_{ij}(\mathbf{r}_{ij}, \hat{\boldsymbol{u}}_i, \hat{\boldsymbol{u}}_j)$ is the corresponding Mayer function. This choice is asymptotically exact in the dilute limit [24, 82]. Another choice is a the mean field approximation which is asymptotically exact at very high densities for bounded potentials [100]. A perturbative treatment out of the homogeneous liquid which needs the direct correlation function as an input is the Ramakrishnan–Youssuf (RY) approximation [39]. It is a functional Taylor expansion of $\mathcal{F}_{\text{exc}}[\rho]$ in terms of the density difference $\Delta\rho = \rho(\mathbf{r}, \hat{\boldsymbol{u}}) - \rho_0$ where ρ_0 is the homogeneous density in the isotropic phase. It follows from Eqs. (3.20) and (3.21) that

$$-c^{(2)}(\mathbf{r}_{12}, \hat{\boldsymbol{u}}_1, \hat{\boldsymbol{u}}_2; \rho_0) = \beta \frac{\delta^2 \mathcal{F}_{\text{exc}}[\rho(\mathbf{r}, \hat{\boldsymbol{u}})]}{\delta\rho(\mathbf{r}_1, \hat{\boldsymbol{u}}_1)\delta\rho_(\mathbf{r}_2, \hat{\boldsymbol{u}}_2)}\bigg|_{\rho_0}, \tag{3.23}$$

with the second functional derivative of $\mathcal{F}_{\text{exc}}[\rho]$ evaluated at $\rho(\mathbf{r}, \hat{\boldsymbol{u}}) = \rho_0$. Therefore,

$$\beta\mathcal{F}_{\text{exc}}[\{\rho\}] \simeq -\frac{1}{2} \iint_V \iint_{\mathbb{S}^2} c^{(2)}(\mathbf{r} - \mathbf{r}'; \hat{\boldsymbol{u}}, \hat{\boldsymbol{u}}')\Delta\rho(\mathbf{r}, \hat{\boldsymbol{u}})\Delta\rho(\mathbf{r}', \hat{\boldsymbol{u}}')\, d\hat{\boldsymbol{u}}'\, d\hat{\boldsymbol{u}}\, d\mathbf{r}'\, d\mathbf{r}\,. \tag{3.24}$$

For hard spheres, the RY approximation leads to freezing and was the first demonstration that freezing can be described within DFT. There are a couple of non–perturbative functionals based on Rosenfeld's fundamental measure theory [101]. These are more accurate approximations of the excluded energy of hard convex bodies and can be found in Refs. [102, 103].

3.2.2 Density functional theories for systems of hard rods

In this section we summarize the most important results regarding isotropic and nematic phases in the DFT formalism. We discuss different theories for systems of hard rods using the smoothed density approximation of Poniewierski and Holyst [29] as a starting point.

The smoothed density approximation in its original form is a DFT of a homogeneous hard–sphere system (see for example Refs. [27, 104]). For systems of hard rods, it relies on the definition of a weight function which is related to the direct correlation function. The ideal gas contribution to the free energy is given as usual [see Eq. (3.17)] by

$$\beta\mathcal{F}_{\text{id}}[\rho] = \int_V \int_{\mathbb{S}^2} \rho(\mathbf{r}, \hat{\boldsymbol{u}})\{\ln\left(\Lambda^3\rho(\mathbf{r}, \hat{\boldsymbol{u}})\right) - 1\}\, d\hat{\boldsymbol{u}}\, d\mathbf{r}\,, \tag{3.25}$$

where $\rho(\mathbf{r}, \hat{\boldsymbol{u}})$ is the one–particle density function. On the other hand, within this approximation the excess free energy of the system is

$$\mathcal{F}_{exc}[\rho] = \int_V \rho(\mathbf{r})\Delta\psi(\bar{\rho}(\mathbf{r})\, d\mathbf{r} \tag{3.26}$$

where $\rho(\mathbf{r})$ and $\bar{\rho}(\mathbf{r})$ are the physical and smoothed densities and $\Delta\psi$ is the excess free energy per particle of the reference fluid, which, in this case, is a homogeneous and isotropic fluid of hard rods. The first nontrivial step beyond the SDA corresponds to a relation between ρ and $\bar{\rho}$. To this end Poniewierski *et al* used the following expression

$$\bar{\rho}(\mathbf{r},\hat{\boldsymbol{u}}) = \int_V \iint_{\mathcal{S}^2} w(\mathbf{r}-\mathbf{r}',\hat{\boldsymbol{u}},\hat{\boldsymbol{u}}')f(\mathbf{r},\hat{\boldsymbol{u}})f(\mathbf{r}',\hat{\boldsymbol{u}}')d\mathbf{r}'d\hat{\boldsymbol{u}}d\hat{\boldsymbol{u}}' \,. \tag{3.27}$$

Here $f(\mathbf{r},\hat{\boldsymbol{u}}) = \rho(\mathbf{r},\hat{\boldsymbol{u}})/\rho(\mathbf{r})$ is the angular distribution function also known as *orientational distribution function* and $w(\mathbf{r}-\mathbf{r}',\hat{\boldsymbol{u}},\hat{\boldsymbol{u}}')$ is a weight function satisfying the normalization condition

$$\int_V \iint_{\mathcal{S}^2} w(\mathbf{r}-\mathbf{r}',\hat{\boldsymbol{u}},\hat{\boldsymbol{u}}')d\mathbf{r}'d\hat{\boldsymbol{u}}d\hat{\boldsymbol{u}}' = (4\pi)^2 \,. \tag{3.28}$$

For the isotropic fluid the orientational distribution function is given by $f = 1/\int d\hat{\boldsymbol{u}} = 1/4\pi$. In general, the weight function w should be calculated via the direct correlation function of a homogeneous and isotropic fluids of hard rods. However any analytic form of $c^{(2)}$ is in general unknown. Instead of making approximations on the level of $c^{(2)}$ Poniewierski and Holyst did some approximations on the weight function itself.

Onsager's approximation

Onsager's second virial theory can be obtained directly from the SDA assuming that

$$w(\mathbf{r}-\mathbf{r}',\hat{\boldsymbol{u}},\hat{\boldsymbol{u}}') = -\frac{f_{12}(\mathbf{r}-\mathbf{r}',\hat{\boldsymbol{u}},\hat{\boldsymbol{u}}')}{2B_2} \,, \tag{3.29}$$

together with

$$\beta\Delta\psi(\rho) = \rho B_2 + \mathcal{O}(3) \,. \tag{3.30}$$

Here f_{12} is the Mayer function for hard rods and B_2 is the second virial coefficient given by

$$B_2 = \frac{1}{2}\int_V \iint_{\mathcal{S}^2} f_{12}(\mathbf{r}-\mathbf{r}',\hat{\boldsymbol{u}},\hat{\boldsymbol{u}}')d\hat{\boldsymbol{u}}d\hat{\boldsymbol{u}}' \,. \tag{3.31}$$

For uniform fluids ($\rho \neq \rho(\mathbf{r})$) the Mayer function only depends on the orientational degrees of freedom and determines the volume of exclusion between the particles. In this limit the second virial coefficient is

$$B_2 = \frac{1}{2}\rho V \iint_{\mathcal{S}^2} V^{exc}(\hat{\boldsymbol{u}},\hat{\boldsymbol{u}}')f(\hat{\boldsymbol{u}})f(\hat{\boldsymbol{u}}')d\hat{\boldsymbol{u}}d\hat{\boldsymbol{u}}' \,, \tag{3.32}$$

where V is the volume of the system[5]. As we can see, introducing the simple ansatz (3.28) in the DFT formalism develops into the well known Onsager approximation [see Eq. (3.12)]. Finally the excess contribution to the free energy is

$$\frac{\beta\mathcal{F}_{exc}}{V} = \frac{1}{2}\rho^2 \iint_{\mathcal{S}^2} V^{exc}(\hat{\boldsymbol{u}}, \hat{\boldsymbol{u}}') f(\hat{\boldsymbol{u}}) f(\hat{\boldsymbol{u}}') d\hat{\boldsymbol{u}} d\hat{\boldsymbol{u}}' \,. \tag{3.33}$$

One can obtain the isotropic and nematic coexistence densities directly from the total free energy Eqs. (3.25) and (3.32). To this end one needs to do functional minimization of the total free energy with respect to $f(\hat{\boldsymbol{u}})$. After this procedure one gets the integral equation

$$f(\theta) = \frac{\exp\left[-\frac{8\rho^*}{\pi}\int_{-1}^{1} d(\cos\theta') K(\theta,\theta') f(\theta')\right]}{\int_{-1}^{1} d(\cos\theta) \exp\left[-\frac{8\rho^*}{\pi}\int_{-1}^{1} d(\cos\theta') K(\theta,\theta') f(\theta')\right]} \,, \tag{3.34}$$

where $\rho^* = \rho^* B_2^I$ is a dimensionless density scaled with respect to the value of B_2 for the isotropic fluid and the kernel function $K(\theta,\theta')$ is

$$K(\theta,\theta') = \int_0^{2\pi} d\phi \sqrt{1 - (\cos\theta\cos\theta'\cos\phi + \sin\theta\sin\theta')^2} \,, \tag{3.35}$$

Equation (3.32) can be solved for $f(\theta)$ using an iterative procedure at a fixed ρ^*. The resulting function should be inserted back into the total free energy and after using the Maxwell construction (see Ref. [105]) obtain the coexistence densities [28, 106]. The main drawback of this theory is that it is limited to very long aspect ratios and it is only valid in the dilute regime (very low densities).

Parsons–Lee Approximation

For finite values of κ further virial coefficients should be included in order to obtain with increased accuracy the $I - N$ coexistence densities. In the original treatment in Ref. [29] the ansatz for $\Delta\psi$ [see Eq. (3.30)] has an additional contribution which takes into account the packing between the particles. This inclusion corresponds to the virial expansion of Parsons and Lee [37, 38, 107]. Parsons and Lee proposed an excess free energy density given by

$$\frac{\beta\mathcal{F}_{exc}[f(\hat{\boldsymbol{u}})]}{V} = \rho G_{HS}(\eta) \frac{B_2[f(\hat{\boldsymbol{u}})]}{B_2^{HS}} \,. \tag{3.36}$$

[5] The excluded volume between the particles 1 and 2 is related to the contact distance (see Eq. (3.7)) via

$$V^{exc}(\hat{\boldsymbol{u}}_1, \hat{\boldsymbol{u}}_2) = \frac{1}{3}\int_{\mathcal{S}^2} d(\hat{\boldsymbol{u}}_1, \hat{\boldsymbol{u}}_2, \hat{\boldsymbol{u}}_{12}) d\hat{\boldsymbol{u}}_{12} \,.$$

where $B_2^{HS} = 4v$ is the second virial coefficient of the hard sphere model with a molecular volume v equal to the volume of the hard rod. The prefactor $G_{HS}(\eta)$ is the *compressibility factor* of the system and corresponds to the usual Carnahan–Sterling free energy per particle of the hard sphere fluid. The compressibility factor $G_{HS}(\eta)$ is given by

$$G_{HS}(\eta) = \frac{\eta(4-3\eta)}{(1-\eta)^2}\,, \tag{3.37}$$

with $\eta = \rho v$ the packing fraction. From construction, this approximation recovers the second virial low–density limit when $\rho \to 0$. For a system of spherocylinders with aspect ratios $\kappa \simeq 5-8$, this simple approach is very accurate. As it is proven by Bolhuis *et al* in Ref. [108] using Gibbs-ensemble simulations.

Density-functional theory of distortion

The distortions of the nematic director can be formulated within the DFT formalism. A first approximation was done by A. Poniewierski and J. Stecki in 1979–1982 [40, 41]. Later, in a series of studies between 1985 and 1987, Y. Singh and K. Singh derived an excess free energy of the aligned nematic liquids in terms of the direct correlation functions of the isotropic fluids [30, 31, 32].

In both approximations the Frank elastic constants [see Eq. (2.23)] are expressed in terms of the direct correlation function $c^{(2)}(\mathbf{r}_{12}, \hat{\boldsymbol{u}}_1, \hat{\boldsymbol{u}}_2)$ and the one–particle density distribution function. These studies are based on the assumption that the one–particle density is such that

$$\rho(\mathbf{r}, \hat{\boldsymbol{u}}) = \rho_0(\hat{\boldsymbol{n}}(\mathbf{r}) \cdot \hat{\boldsymbol{u}})\,, \tag{3.38}$$

where $\hat{\boldsymbol{n}}$ is the nematic director specifying the axis of symmetry of the uniaxial homogeneous sample. In terms of the director field and the one–particle density the free energy of deformation is [40]:

$$\begin{aligned}\beta\mathcal{F}_{\mathsf{def}}[\rho] = \int_V A_{\alpha\mu}(\mathbf{r})\nabla_\alpha n_\mu \, d\mathbf{r} + \frac{1}{2}\int_V [M_{\alpha\beta\mu\nu}(\mathbf{r}) + H_{\alpha\beta\mu\nu}(\mathbf{r})] \times \nabla_\alpha n_\mu \nabla_\beta n_\nu \, d\mathbf{r} \\ + \frac{1}{2}\int_{\mathbb{S}^2} B_{\alpha\beta\mu}(\mathbf{r})\nabla_\alpha n_\mu \, d\sigma_\beta\,.\end{aligned} \tag{3.39}$$

where the coefficients $A_{\alpha\mu}$, $B_{\alpha\beta\mu}$, $M_{\alpha\beta\mu\nu}$, and $H_{\alpha\beta\mu\nu}$ are functions of $\mathbf{r}$ defined as integrals of a hierarchy of direct correlation functions integrated over $\rho_0(\hat{\boldsymbol{n}}(\mathbf{r}) \cdot \hat{\boldsymbol{u}})$, (see Ref. [40]).

Finally, in terms of the direct correlation function of the undistorted nematic state

$c^{(2)}(\mathbf{r}_{12}, \hat{\boldsymbol{u}}_1, \hat{\boldsymbol{u}}_2; \rho_0)$ in Eq. (3.24) the Frank elastic coefficients are

$$K_1 = \frac{1}{2} \int_V \iint_{\mathbb{S}^2} (r_{12})_x^2 \, c^{(2)}(\mathbf{r}_{12}; \hat{\boldsymbol{u}}, \hat{\boldsymbol{u}}'; \rho_0) \rho_0(\hat{\boldsymbol{n}} \cdot \hat{\boldsymbol{u}}) \rho_0(\hat{\boldsymbol{n}} \cdot \hat{\boldsymbol{u}}') \, \hat{u}_x \hat{u}'_x d\hat{\mathbf{u}} d\hat{\mathbf{u}}' d\mathbf{r} \ , \tag{3.40}$$

$$K_2 = \frac{1}{2} \int_V \iint_{\mathbb{S}^2} (r_{12})_x^2 \, c^{(2)}(\mathbf{r}_{12}; \hat{\boldsymbol{u}}, \hat{\boldsymbol{u}}'; \rho_0) \rho_0(\hat{\boldsymbol{n}} \cdot \hat{\boldsymbol{u}}) \rho_0(\hat{\boldsymbol{n}} \cdot \hat{\boldsymbol{u}}') \, \hat{u}_y \hat{u}'_y d\hat{\mathbf{u}} d\hat{\mathbf{u}}' d\mathbf{r} \ , \tag{3.41}$$

$$K_3 = \frac{1}{2} \int_V \iint_{\mathbb{S}^2} (r_{12})_z^2 \, c^{(2)}(\mathbf{r}_{12}; \hat{\boldsymbol{u}}, \hat{\boldsymbol{u}}'; \rho_0) \rho_0(\hat{\boldsymbol{n}} \cdot \hat{\boldsymbol{u}}) \rho_0(\hat{\boldsymbol{n}} \cdot \hat{\boldsymbol{u}}') \, \hat{u}_y \hat{u}'_y d\hat{\mathbf{u}} d\hat{\mathbf{u}}' d\mathbf{r} \ , \tag{3.42}$$

where $(r_{12})_i$ denotes the magnitude of the i–th component of the vector $\mathbf{r}_{12} = \mathbf{r} - \mathbf{r}'$. To calculate these constants for a model nematic fluid we must know the direct correlation function and the orientational distribution function calculated in the undistorted homogeneous nematic [40, 41].

3.3 Density functional theories for mixtures

For an n–component mixture of non spherical hard–body particles, the total number of molecules of all species is

$$\mathcal{N} = \sum_{\alpha=1}^{n} N^{\alpha} \, .$$

where α labels the components of the mixture. In the scope of DFT, there is a one–body density ρ_α for each component of the fluid and it is such that $\rho_\alpha(\mathbf{r}, \hat{\boldsymbol{u}}) \, dV$ is the average number of α–molecules in an infinitesimal volume dV located at position $\mathbf{r}$ with orientation $\hat{\boldsymbol{u}}$. In terms of $\{\mathbf{r}_k^\alpha, \hat{\boldsymbol{u}}_k^\alpha\}$ the one–body density is

$$\rho_\alpha(\mathbf{r}, \hat{u}) \equiv \left\langle \sum_{k=1}^{N^\alpha} \delta(\mathbf{r} - \mathbf{r}_k^\alpha) \delta(\hat{\boldsymbol{u}} - \hat{\boldsymbol{u}}_k^\alpha) \right\rangle , \tag{3.43}$$

where $\langle \cdots \rangle$ denotes the conformational average. Since, the density functional approach focuses on the Helmholtz free energy $\mathcal{F}$ as a unique functional of these one–body densities ρ_α then $\mathcal{F}[\rho_\alpha]$. The free energy functional, $\mathcal{F}[\rho_\alpha]$, is splitted in an ideal contribution, $\mathcal{F}_{\mathsf{id}}[\rho_\alpha]$, plus an excess free energy, $\mathcal{F}_{\mathsf{ex}}[\rho_\alpha]$, that accounts for the particles' interaction. In $\beta = 1/k_B T$ units $\mathcal{F}[\rho_\alpha]$ is written as

$$\beta\mathcal{F}[\rho_\alpha] = \beta\mathcal{F}_{\mathsf{id}}[\rho_\alpha] + \beta\mathcal{F}_{\mathsf{ex}}[\rho_\alpha] \, . \tag{3.44}$$

Ideal contribution

A straightforward generalization of the single component system (see Ref. [29]) of the ideal free energy for the n–component mixture reads

$$\beta\mathcal{F}_{\mathsf{id}}[\rho_\alpha] = \sum_{\alpha=1}^{n} \int_V \int_{\mathbb{S}^2} \rho_\alpha(\mathbf{r},\hat{\boldsymbol{u}})\{\ln\left(\Lambda_\alpha^3\rho_\alpha(\mathbf{r},\hat{\boldsymbol{u}})\right) - 1\}\, d\hat{\boldsymbol{u}}\, d\mathbf{r}\,, \tag{3.45}$$

where Λ_α is the thermal de Broglie wavelength of component α of mass m_α and is given by

$$\Lambda_\alpha = \left(\frac{h^2}{2\pi m_\alpha k_B T}\right)^{1/2}.$$

Excess contribution

As stated previously, the excess free energy functional $\mathcal{F}_{\mathsf{ex}}[\rho_\alpha]$ is unknown and therefore one has to rely on several approximations. In the following we present two approximations of the one–body density of each component α which lead to two very distinct density functionals. First we consider spatially homogeneous densities where the dependency of ρ_α on the translational degrees of freedom is disregarded. Later we assume that the dependence of the one–body densities on the translational degrees of freedom is inherited through $\hat{\boldsymbol{u}}$ with the ansatz $\hat{\boldsymbol{u}} = \hat{\boldsymbol{u}}(\mathbf{r})$.

3.3.1 Many–fluid Parsons–Lee theory

Here we focus on spatially homogeneous densities such that

$$\rho_\alpha(\mathbf{r},\hat{\boldsymbol{u}}) = \rho_\alpha\, f_\alpha(\hat{\boldsymbol{u}})\,, \tag{3.46}$$

where $\rho_\alpha = N_\alpha/V$ is the number density of species α (with V being the volume) and $f_\alpha(\hat{\boldsymbol{u}})$ is the orientational distribution function (ODF), which is normalized such that $\int d\hat{\boldsymbol{u}} f_\alpha(\hat{\boldsymbol{u}}) = 1$. This ansatz allows us to describe isotropic and nematic phases of the system.

With this specification, the ideal part of the free energy functional [see Eq. (3.45)] can be written as

$$\frac{\beta\mathcal{F}_{id}^H}{V}[\rho_\alpha] = \sum_{\alpha=1}^{n} \rho_\alpha \left(\ln(\rho_\alpha\Lambda_\alpha^3) - 1 + \sigma[f_\alpha]\right)\,, \tag{3.47}$$

where $\sigma[f_\alpha]$ is the orientational entropy given by

$$\sigma[f_\alpha] = \int_{\mathbb{S}^2} d\hat{\boldsymbol{u}} f_\alpha(\hat{\boldsymbol{u}}) \ln(4\pi f_\alpha(\hat{\boldsymbol{u}})), \tag{3.48}$$

The quantity σ is zero in the isotropic state, where $f_\alpha(\boldsymbol{u}) = f_0 = (4\pi)^{-1}$ and becomes positive in the nematic state. It thus reflects the loss of orientational entropy due to ordering.

Regarding the excess part of the free energy, we here employ a generalization of the so–called Parsons–Lee theory [37, 38] to mixtures, as suggested by Malijevsky *et al.* [35]. This approach is derived by starting from the virial expression for the pressure, which involves (apart from the singlet densities) the spatial derivative of the pair potential, $\mathcal{U}_{\alpha\beta}$ and the pair correlation function $g_{\alpha\beta}$. Noting that $\mathcal{U}_{\alpha\beta}$ can be re–expressed in terms of a hard–sphere (HS) potential with scaled distance $r_{ij}/d_{\alpha\beta}(\hat{\boldsymbol{u}}_i, \hat{\boldsymbol{u}}_j, \boldsymbol{u}_{ij})$, the same assumption is made for the correlation function, i.e., $g_{\alpha\beta} = g^{HS}_{\alpha\beta}(r_{ij}/d_{\alpha\beta})$ (note that this is an approximation). By integrating over the total density $\rho = \sum_\alpha \rho_\alpha$ (and noting that $\partial \mathcal{U}^{HS}_{\alpha\beta}(y)/\partial y$ is proportional to a delta function in space), one obtains the excess free energy

$$\frac{\beta \mathcal{F}^H_{ex}}{V}[\rho_\alpha] = \frac{1}{2}\sum_{\alpha=1}^{n}\sum_{\beta=1}^{n}\rho_\alpha\rho_\beta G_{\alpha\beta}\int_{\mathbb{S}^2} d\hat{\boldsymbol{u}}_i \int_{\mathbb{S}^2} d\hat{\boldsymbol{u}}_j V^{exc}_{\alpha\beta}(\hat{\boldsymbol{u}}_i, \hat{\boldsymbol{u}}_j) f_\alpha(\hat{\boldsymbol{u}}_i) f_\beta(\hat{\boldsymbol{u}}_j)\,. \tag{3.49}$$

In (3.49), $V^{exc}_{\alpha\beta}$ is the excluded volume between particles i and j, which is related to the contact distance via

$$V^{exc}_{\alpha\beta}(\hat{\boldsymbol{u}}_i, \hat{\boldsymbol{u}}_j) = \frac{1}{3}\int_{\mathbb{S}^2} d\hat{\boldsymbol{u}}_{ij}\; d^3_{\alpha\beta}(\hat{\boldsymbol{u}}_i, \hat{\boldsymbol{u}}_j, \hat{\boldsymbol{u}}_{ij})\,. \tag{3.50}$$

The quantities $G_{\alpha\beta}$ are averages (in terms of the total density) of the contact values of the HS pair correlation functions, $g^{HS}_{\alpha\beta}(1_+)$, in the considered density range [35].

As discussed extensively in Ref. [35], the free energy given in (3.49) reduces to the familiar second–virial theory of Onsager [24] in the limit of low densities. Then, one has $g^{HS}_{\alpha\beta}(1_+) \to 1$, and therefore $G_{\alpha\beta} = 1$ for all combinations α, β. Although the Onsager theory provides an intuitive approach regarding the effects related to the geometry of the particles, it is known to become inaccurate for particles of finite length at the densities close to orientational phase transitions [108, 109]. In this respect the generalized Parsons–Lee approach provides a significant improvement, as demonstrated by comparison with Monte Carlo simulations of hard Gaussian molecules with different elongations and concentrations [14].

3.3.2 Second–order perturbation theory for mixtures

To our account the excess free energy functional of a mixture of hard–body particles in terms of spatially inhomogeneous one–body densities has not been addressed in literature. To this end we assume that the one–body density of the α component of the mixture can be written as:

$$\rho_\alpha(\mathbf{r}, \hat{\boldsymbol{u}}) = \rho_\alpha\, f_\alpha(\hat{\boldsymbol{u}}(\mathbf{r}))\,. \tag{3.51}$$

This ansatz of the one–body densities is similar to the one in Ref. [40, 41], however, the spatial dependence of the orientational degrees of freedom is not given in terms of the nematic director but in terms of full vector $\hat{\boldsymbol{u}}$. This allows a description of the fluid in terms of the space–fixed frame of reference instead of the usual director dependent frame of reference. With this assumption the ideal contribution of the free energy [see Eq. (3.45)] is simply given by:

$$\beta\mathcal{F}^{I}_{\mathsf{id}}[\rho_\alpha] = \sum_{\alpha=1}^{n} \int_V \int_{\mathbb{S}^2} \rho_\alpha(\hat{\boldsymbol{u}}(\mathbf{r}))\{\ln\left(\Lambda_\alpha^3 \rho_\alpha(\hat{\boldsymbol{u}}(\mathbf{r})) - 1\right\} d\hat{\boldsymbol{u}}\, d\mathbf{r}\,, \tag{3.52}$$

where Λ_α is the thermal de Broglie wavelength of component α.

Since our interest is to study spatially homogeneous nematic phases a first choice of the excess free energy functional may be an extension of Onsager's second virial theory for mixtures or a mean field approximation. However, inspired on previous results for the one component system [39, 40, 41, 30, 31, 32] we use a second order perturbation theory of the full excess free energy functional, $F_{\mathsf{ex}}[\rho_\alpha]$. This perturbation resolves on an extension of the well known Ramakrishnan–Youssuf [39] to a mixture of n–components which is:

$$\beta\mathcal{F}^{I}_{\mathsf{ex}} = -\frac{1}{2}\sum_{\alpha=1}^{n}\sum_{\beta=1}^{n} \iint_V \iint_{\mathbb{S}^2} c^{(2)}_{\alpha\beta}(\mathbf{r}-\mathbf{r}';\hat{\boldsymbol{u}},\hat{\boldsymbol{u}}')\Delta\rho_\alpha(\mathbf{r},\hat{\boldsymbol{u}})\Delta\rho_\beta(\mathbf{r}',\hat{\boldsymbol{u}}')\, d\hat{\boldsymbol{u}}'\, d\hat{\boldsymbol{u}}\, d\mathbf{r}'\, d\mathbf{r}\,. \tag{3.53}$$

Here $\Delta\rho_\alpha(\mathbf{r},\hat{\boldsymbol{u}}) = \rho_\alpha(\mathbf{r},\hat{\boldsymbol{u}}) - \bar{\rho}_\alpha$ with the mean number density $\bar{\rho}_\alpha = \rho_\alpha f_0$ and the direct correlation function $c^{(2)}_{\alpha\beta}(\mathbf{r}-\mathbf{r}';\hat{\boldsymbol{u}},\hat{\boldsymbol{u}}')$ calculated in the isotropic phase. As it is discussed previously, with this assumption $\mathcal{U}_{\alpha\beta}(\mathbf{r}_{ij},\hat{\boldsymbol{u}}_i,\hat{\boldsymbol{u}}_j)$ is a smoothly varying long range function of the distance and orientation [110, 36, 39].

Chapter 4

Bridging microscopic and mesoscopic theories

The first goal of our investigations is to construct an expression of the equilibrium free energy functional capable of describing the thermodynamic phase behavior of a mixture. In addition, this functional should contain microscopic features of the system such as, number density, length and diameter of the particles, etc. In this chapter we take on the task of *bridging* the microscopic and phenomenological descriptions introduced in the preceding chapters. We address this issue for both, spatially homogeneous and inhomogeneous systems, starting from the previously discussed density functional theories for mixtures (Many–fluid Parsons–Lee theory and the Ramakrishnan-Youssuf approximation for mixtures).

4.1 DFT based Q–tensor theory for mixtures

The aim of this chapter is to rewrite the free energy functionals consisting of ideal and excess contributions [see Eqs. (3.47)–(3.53)] in terms of the k–th order alignment tensors $\mathbf{Q}^{\alpha}_{(k)}$ (one for each component of the mixture) where $\alpha = 1, \cdots, n$ [see Chapter 2]. These tensors are defined in terms of the k–fold product $\hat{\boldsymbol{u}}^{(k)}$ as [22]

$$\mathbf{Q}^{\alpha}_{(k)} = \sqrt{\frac{(2k+1)!!}{k!}} \left\langle \overline{\hat{\boldsymbol{u}}^{(k)}} \right\rangle_{\alpha} . \tag{4.1}$$

where $\langle \cdots \rangle_{\alpha}$ denotes the configurational ensemble average of $\hat{\boldsymbol{u}}^{(k)}$ with respect to the orientational distribution function $f_{\alpha}(\hat{\boldsymbol{u}})$. For most systems of rigid particles, it is sufficient to consider tensors with even k due to the head–to–tail symmetry. Within this subset, the tensors of rank $k = 2$ and $k = 4$ are of particular importance since they may be related to the birefringence and fluorescence of the sample [19, 23].

4.2 Homogeneous systems

First we will discuss the construction of the Q-tensor functional for homogeneous systems based on the publication *Binary mixtures of rod–like colloids under shear: microscopically–based equilibrium theory and order–parameter dynamics* which was written in collaboration with S. H. L. Klapp [111].

4.2.1 Ideal contribution

The first task is to rewrite the orientational entropy, given in (3.48). Here we follow earlier approaches [23, 112], where the one–particle ODF was expressed as $f_\alpha(\hat{\boldsymbol{u}}) = f_0\,(1+\psi_\alpha(\hat{\boldsymbol{u}}))$, with $\psi(\hat{\boldsymbol{u}})$ being a small deviation from the isotropic state, $f_0 = 1/4\pi$. Inserting this ansatz into (3.48) and performing a Taylor expansion of the logarithm yields [23, 113]

$$\sigma[f_\alpha] = \sum_{n=2}^{\infty} \frac{(-1)^n}{n(n-1)} \langle \psi_\alpha^n(\hat{\boldsymbol{u}})\rangle_0\,, \tag{4.2}$$

where $\langle\cdots\rangle_0$ denotes the orientational average evaluated with f_0. Due to normalization of the ODF the term $n=1$ is zero and thus it is disregarded. Next, one assumes that the function $\psi(\hat{\boldsymbol{u}})$ may be expanded in terms of the tensor quantities $((2k+1)!!/k!)\;\overline{\hat{\boldsymbol{u}}^{(k)}}$ [see (4.1)], where the prefactors are determined by their orientational averages, $\mathbf{Q}^\alpha_{(k)}$. Following [23, 113], we restrict this expansion to terms involving $k=2$ and $k=4$. Inserting the resulting *ansatz* for ψ_α into (4.2) and retaining terms up to fourth power in $\mathbf{Q}^\alpha_{(2)}$ and up to second power in $\mathbf{Q}^\alpha_{(4)}$, one obtains

$$\begin{aligned}\sigma[\mathbf{Q}^\alpha_{(2)},\mathbf{Q}^\alpha_{(4)}] = \frac{1}{2}\mathbf{Q}^\alpha_{(2)}\odot\mathbf{Q}^\alpha_{(2)} - \frac{\sqrt{30}}{21}\mathbf{Q}^\alpha_{(2)}\cdot\mathbf{Q}^\alpha_{(2)}\odot\mathbf{Q}^\alpha_{(2)} + \frac{5}{28}\left[\mathbf{Q}^\alpha_{(2)}\odot\mathbf{Q}^\alpha_{(2)}\right]^2 \\ + \frac{1}{2}\mathbf{Q}^\alpha_{(4)}\odot\mathbf{Q}^\alpha_{(4)} + \mathcal{O}(\mathbf{Q}^\alpha_{(4)})^2\,.\end{aligned} \tag{4.3}$$

In (4.3), the product $\mathbf{A}_{(k)}\cdot\mathbf{B}_{(k)}$ yields a tensor of rank k [see Appendix A].

4.2.2 Excess contribution

We now turn to the reformulation of the excess free energy as functions of the $\mathbf{Q}^\alpha_{(k)}$. To our knowledge, before our publication [111], this problem has not been addressed in the literature so far.

As a starting point we expand the excluded volume of the hard–core particles appearing in Eq. (3.49) in terms of the Legendre polynomials (following Refs. [35, 114] and references therein),

$$V^{exc}_{\alpha\beta}(\hat{\boldsymbol{u}}_i,\hat{\boldsymbol{u}}_j) = \sum_{k=0}^{\infty} V_k^{\alpha\beta} P_k(\cos\gamma), \tag{4.4}$$

where γ is the angle between $\hat{\boldsymbol{u}}_i$ and $\hat{\boldsymbol{u}}_j$ (see Appendix B) and the coefficients $V_k^{\alpha\beta}$ are calculated using the relation

$$V_k^{\alpha\beta} = \frac{2k+1}{2}\int_{-1}^{1} d\cos\gamma P_k(\cos\gamma) V_{\alpha\beta}^{exc}(\gamma). \tag{4.5}$$

Next, we replace P_k in (4.4) by using the addition theorem for spherical harmonics [99] (see Appendix B), yielding

$$V_{\alpha\beta}^{exc}(\hat{\boldsymbol{u}}_i, \hat{\boldsymbol{u}}_j) = \sum_{k=0}^{\infty} \frac{4\pi V_k^{\alpha\beta}}{2k+1} \sum_{m=-k}^{k} \mathsf{Y}_{km}^*(\hat{\boldsymbol{u}}_i)\mathsf{Y}_{km}(\hat{\boldsymbol{u}}_j)\,. \tag{4.6}$$

The sum on the right side of Eq. (4.6) can be rewritten as a full scalar product of the two tensors $\overline{\hat{\boldsymbol{u}}^{(k)}}$ [99]. One obtains

$$V_{\alpha\beta}^{exc}(\hat{\boldsymbol{u}}_i, \hat{\boldsymbol{u}}_j) = \sum_{k=0}^{\infty} V_k^{\alpha\beta} \frac{(2k+1)!!}{(2k+1)k!} \overline{\hat{\boldsymbol{u}}_i^{(k)}} \odot \overline{\hat{\boldsymbol{u}}_j^{(k)}}\,. \tag{4.7}$$

Inserting (4.7) into (3.49), noting that the angular integrals (weighted by the ODFs) in (3.49) lead to orientational averages, and using the definition of the tensor order parameter [see (4.1)] one finds

$$\frac{\beta\mathcal{F}_{exc}^H}{V} = \frac{1}{2}\sum_{\alpha=1}^{n}\sum_{\beta=1}^{n}\rho_\alpha\rho_\beta G_{\alpha\beta}\sum_{k=0}^{\infty}\frac{V_k^{\alpha\beta}}{2k+1}\mathbf{Q}_{(k)}^{\alpha}\odot\mathbf{Q}_{(k)}^{\beta}\,. \tag{4.8}$$

Equation (4.8) provides the excess free energy as a function of order parameter tensors. It still depends on the microscopic parameters of the mixture, that is, the geometry of the particles (defining the excluded volume) and the densities.

4.2.3 Full free energy

We now turn to the full free energy containing ideal and excess parts, $\mathcal{F}^H = \mathcal{F}_{id}^H + \mathcal{F}_{ex}^H$. Restricting to terms involving $2nd$– and $4th$– rank tensors we have

$$\frac{\beta\mathcal{F}_{id}^H[\mathbf{Q}]}{V} = \sum_{\alpha=1}^{n}\left[\mathcal{F}_{00}^{\alpha} + \rho_\alpha\sigma\left(\mathbf{Q}_{(2)}^{\alpha}, \mathbf{Q}_{(4)}^{\alpha}\right)\right]\,, \tag{4.9}$$

where $\mathcal{F}_{00}^{\alpha} = \rho_\alpha(\ln(\rho_\alpha\Lambda_\alpha^3) - 1)$, σ is given in (4.3), and the notation $[\mathbf{Q}]$ on the left side indicates the dependence of the (ideal) free energy on all four order parameter tensors ($k = 2, 4$, $\alpha = 1, \cdots, n$). Further, we obtain from Eq. (4.8)

$$\frac{\beta\mathcal{F}_{ex}^H[\mathbf{Q}]}{V} = \frac{1}{2}\sum_{\alpha=1}^{n}\sum_{\beta=1}^{n}\rho_\alpha\rho_\beta G_{\alpha\beta}\left[V_0^{\alpha\beta} + \frac{V_2^{\alpha\beta}}{5}(\mathbf{Q}_{(2)}^{\alpha}\odot\mathbf{Q}_{(2)}^{\beta}) + \frac{V_4^{\alpha\beta}}{9}(\mathbf{Q}_{(4)}^{\alpha}\odot\mathbf{Q}_{(4)}^{\beta})\right]\,. \tag{4.10}$$

These expressions can be further simplified by using a "closure" relation expressing the $4th$–rank tensor with the one of second rank. For uniaxial systems characterized by a (nematic) director $\mathbf{n}$ [115, 116], there exists the *exact* relation $S_2^2\mathbf{Q}_{(4)} = S_4\,\overline{\mathbf{Q}_{(2)}\mathbf{Q}_{(2)}}$, where $S_2 = \langle P_2(\hat{\boldsymbol{u}}\cdot\hat{\mathbf{n}})\rangle$ and $S_4 = \langle P_4(\hat{\boldsymbol{u}}\cdot\hat{\mathbf{n}})\rangle$. In strongly aligned systems one has $S_4 \approx S_2^2 \approx 1$. In that limit, the closure thus takes the form $\mathbf{Q}_{(4)} \equiv \overline{\mathbf{Q}_{(2)}\mathbf{Q}_{(2)}}$. This choice is the simplest and most widely used approximation without requiring further assumptions in the ODF. In this direction, one could have used the Bingham closure which is suitable for rotational flows but loses precision for simple shear flow [117].

Since we can now express all quantities in terms of the second–rank tensor, we ease notation and set $\mathbf{Q}^\alpha = \mathbf{Q}^\alpha_{(2)}$ $(\alpha = 1, \cdots, n)$. Further, we rewrite the notation for the tensor products appearing in Eq. (4.10) into the form commonly used for second–rank tensors, that is $\mathbf{Q}^\alpha \odot \mathbf{Q}^\alpha = \mathbf{Q}^\alpha : \mathbf{Q}^\alpha = \mathsf{Tr}(\mathbf{Q}\cdot\mathbf{Q}) = Q_{\mu\nu}Q_{\mu\nu}$. Adding ideal and excess contributions of the free energy, we obtain

$$\begin{aligned}\Phi^H[\mathbf{Q}] =& \frac{\beta\mathcal{F}^H[\mathbf{Q}]}{V}\\ \Phi^H[\mathbf{Q}] =& \sum_{\alpha=1}^{n}\left(\mathcal{F}_0^\alpha + A_\alpha(\mathbf{Q}^\alpha:\mathbf{Q}^\alpha) - B_\alpha\mathsf{Tr}(\mathbf{Q}^\alpha\cdot\mathbf{Q}^\alpha\cdot\mathbf{Q}^\alpha) + C_\alpha(\mathbf{Q}^\alpha:\mathbf{Q}^\alpha)^2\right)\\ &+\frac{1}{2}\sum_{\alpha=1}^{n}\sum_{\beta=1}^{n}\left(\mathcal{F}_0^{\alpha\beta} + A_{\alpha\beta}(\mathbf{Q}^\alpha:\mathbf{Q}^\beta) + C_{\alpha\beta}(\mathbf{Q}^\alpha:\mathbf{Q}^\beta)^2\right), \qquad (4.11)\end{aligned}$$

where the coefficients are functions of the number densities, the factors $G_{\alpha\beta}$ and the coefficients of the excluded volume. Explicitly, they are given by

$$\mathcal{F}_0^\alpha = \rho_\alpha\left(\ln(\rho_\alpha\Lambda_\alpha^3) - 1\right) + \frac{1}{2}\rho_\alpha^2 G_{\alpha\alpha}V_0^{\alpha\alpha}\,, \qquad (4.12)$$

$$A_\alpha = \frac{1}{2}\rho_\alpha + \frac{1}{10}\rho_\alpha^2 G_{\alpha\alpha}V_2^{\alpha\alpha}\,, \qquad (4.13)$$

$$B_\alpha = \frac{\sqrt{30}}{21}\rho_\alpha\,, \qquad (4.14)$$

$$C_\alpha = \frac{19}{28}\rho_\alpha + \frac{1}{18}\rho_\alpha^2 G_{\alpha\alpha}V_4^{\alpha\alpha}\,, \qquad (4.15)$$

$$\mathcal{F}_0^{\alpha\beta} = \rho_\alpha\rho_\beta G_{\alpha\beta}V_0^{\alpha\beta}\,, \qquad (4.16)$$

$$A_{\alpha\beta} = \frac{1}{5}\rho_\alpha\rho_\beta G_{\alpha\beta}V_2^{\alpha\beta}\,, \qquad (4.17)$$

$$C_{\alpha\beta} = \frac{1}{9}\rho_\alpha\rho_\beta G_{\alpha\beta}V_4^{\alpha\beta}\,. \qquad (4.18)$$

As seen from Eq. (4.11), the mesoscopic free energy derived here has the standard Landau–de Gennes (LdG) form [19] in the sense that it involves an expansion into order parameters. Contrary to standard LdG theory, however, the coefficients are related to microscopic properties of the system. We also note that the free energy does not depend

explicitly on the temperature, which reflects the hard–core character of the interactions. Consequently, the ordering behavior of the resulting "lyotropic" system is essentially controlled by the concentration of the system.

4.3 Inhomogeneous systems

In the previous Subsection (4.2) we took on the task of writing the mesoscopic free energy functional of the mixture in terms of tensor order parameters of second and fourth rank. This was done using an expansion of the excluded volume between anisotropic particles in terms of the spherical harmonic functions. Here we propose a different but at the same time complementary approach based on a particular ansatz for the one–particle density $\rho_\alpha(\mathbf{r}, \hat{\boldsymbol{u}})$.

As in Eq. (3.51) in the following we assume that the one–particle density is of the form

$$\rho_\alpha(\mathbf{r}, \hat{\boldsymbol{u}}) = \rho_\alpha f_\alpha(\hat{\boldsymbol{u}}(\mathbf{r}))\,, \tag{4.19}$$

where $\rho = N/V$ is the number density and $f(\hat{\boldsymbol{u}})$ is the normalized orientational distribution function with $\hat{\boldsymbol{u}} = \hat{\boldsymbol{u}}(\mathbf{r})$) [see Chapter 3]. Following Ref. [112] assuming simple angle dependence of the ODF viz $f(\hat{\boldsymbol{u}}) = f_0(1 + \varphi(\hat{\boldsymbol{u}}))$ we employ the ansatz

$$\rho_\alpha(\mathbf{r}, \hat{\boldsymbol{u}}) = \rho_\alpha f_0(1 + \varphi_\alpha(\hat{\boldsymbol{u}})) \tag{4.20}$$

$$= \rho_\alpha f_0 \left(1 + \sqrt{\frac{15}{2}}\, \overbrace{\hat{\mathbf{u}}\hat{\mathbf{u}}} : \mathbf{Q}^\alpha\right)\,, \tag{4.21}$$

where $\varphi(\hat{\boldsymbol{u}})$ describes a small deviation from f_0 corresponding to anisotropic states. In expressions (4.20–4.21) the explicit dependence of $\hat{\boldsymbol{u}}$ and $Q_{\mu\nu}$ with the space dependent vector $\mathbf{r}$ is not written to avoid any confusion.

Equation (4.20) implies that the one–particle density is comparable with the mean number density of the fluid in the isotropic phase given by $\bar{\rho} = \rho f_0$. Inserting Eq. (4.21) in the density difference $\Delta\rho_\alpha(\mathbf{r}, \hat{\boldsymbol{u}}) = \rho_\alpha(\mathbf{r}, \hat{\boldsymbol{u}}) - \bar{\rho}_\alpha$ given by the RY approximation [see Eq. (3.53)] results in

$$\begin{aligned}\Delta\rho_\alpha(\mathbf{r}, \hat{\boldsymbol{u}}) &= \rho_\alpha f_0\, \varphi_\alpha(\hat{\boldsymbol{u}})\,, \\ &= \rho_\alpha f_0 \sqrt{\frac{15}{2}}\, \overbrace{\hat{\mathbf{u}}\hat{\mathbf{u}}} : \mathbf{Q}^\alpha\,.\end{aligned} \tag{4.22}$$

With the above expressions of the one–particle density and the difference $\Delta\rho_\alpha(\mathbf{r}, \hat{\boldsymbol{u}})$, Eqs. (4.21–4.22), we will proceed writing the ideal (3.52) and excess (3.53) contributions of the free energy functional in terms of the spatially inhomogeneous second rank tensor order parameters $\mathbf{Q}^\alpha(\mathbf{r})$.

4.3.1 Ideal contribution

The first assignment is to write the ideal contribution of the free energy (3.52) in terms of $\mathbf{Q}^{\alpha}(\mathbf{r})$. Using the initial assumption for inhomogeneous systems Eq. (4.19), the ideal free energy functional in Eq. (3.52) is given by [1]

$$\beta\mathcal{F}_{id}^{I}[\rho_{\alpha}] = \sum_{\alpha=1}^{n}\int_{V}\left\{\rho_{\alpha}\left(\ln(\rho_{\alpha}\Lambda_{\alpha}^{3}) - 1 + \sigma[f_{\alpha}]\right)\right\}d\boldsymbol{r}\,, \tag{4.23}$$

where $\sigma[f_{\alpha}]$ is the inhomogeneous orientational entropy given by

$$\sigma[f_{\alpha}] = \int_{\mathbb{S}^2} d\hat{\boldsymbol{u}} f_{\alpha}(\hat{\boldsymbol{u}})\ln(4\pi f_{\alpha}(\hat{\boldsymbol{u}}))\,. \tag{4.24}$$

Inserting the ansatz (4.20) in Eq. (4.24) results in

$$\sigma[f_{\alpha}] = f_0\int_{\mathbb{S}^2}(1+\varphi_{\alpha}(\hat{\boldsymbol{u}}))\ln((1+\varphi_{\alpha}(\hat{\boldsymbol{u}})))d\hat{\boldsymbol{u}}\,. \tag{4.25}$$

For small non–zero deviations we expand the integrand in (4.25) up to fourth order, thus

$$(1+\varphi_{\alpha}(\hat{\boldsymbol{u}}))\ln((1+\varphi_{\alpha}(\hat{\boldsymbol{u}}))) \approx \varphi_{\alpha}(\hat{\boldsymbol{u}}) + \frac{1}{2}\varphi_{\alpha}(\hat{\boldsymbol{u}})^2 - \frac{1}{6}\varphi_{\alpha}(\hat{\boldsymbol{u}})^3 + \frac{1}{12}\varphi_{\alpha}(\hat{\boldsymbol{u}})^4 + \mathcal{O}(\varphi_{\alpha}^5)\,, \tag{4.26}$$

yielding to the inhomogeneous orientational entropy

$$\sigma[f_{\alpha}] = f_0\int_{\mathbb{S}^2}\left(\varphi_{\alpha}(\hat{\boldsymbol{u}}) + \frac{1}{2}\varphi_{\alpha}(\hat{\boldsymbol{u}})^2 - \frac{1}{6}\varphi_{\alpha}(\hat{\boldsymbol{u}})^3 + \frac{1}{12}\varphi_{\alpha}(\hat{\boldsymbol{u}})^4\right)d\hat{\boldsymbol{u}}\,. \tag{4.27}$$

Due to normalization of the ODFs the first integral in (4.27) must vanish. Further, inserting the explicit ansatz (4.21) in each term of the right side of (4.27) results in

$$\sigma[\mathbf{Q}(\mathbf{r})] = \frac{1}{2}\left(\mathbf{Q}^{\alpha}:\mathbf{Q}^{\alpha}\right) - \frac{\sqrt{30}}{21}\mathrm{Tr}\left(\mathbf{Q}^{\alpha}\cdot\mathbf{Q}^{\alpha}\cdot\mathbf{Q}^{\alpha}\right) + \frac{5}{28}\left(\mathbf{Q}^{\alpha}:\mathbf{Q}^{\alpha}\right)^2\,, \tag{4.28}$$

Evidently the above derivation is consistent with the one for homogeneous systems [see Eq. (4.3)]. Finally, inserting Eq. (4.28) in Eq. (4.23) results in

$$\beta\mathcal{F}_{\mathsf{id}}^{I}[\mathbf{Q}(\mathbf{r})] = \int_{V}\left\{\Phi_0^{\alpha} + \Phi_{\mathsf{id}}[\mathbf{Q}(\mathbf{r})]\right\}d\mathbf{r}\,. \tag{4.29}$$

[1] Note that the form of the ideal contribution to the free energy is similar to the one for spatially homogeneous phases [see Eq. (3.47)] with the difference that here the integration over the volume V is in general more complicated because of the implicit dependence $\hat{\boldsymbol{u}}(\mathbf{r})$.

where $\Phi_0^\alpha = \sum_\alpha \rho_\alpha \left(\ln(\rho_\alpha \Lambda_\alpha^3) - 1\right)$ and $\Phi_{\mathsf{id}}[\mathbf{Q}(\mathbf{r})]$ is the ideal contribution of the mesoscopic free energy density (per unit volume)

$$\Phi_{\mathsf{id}}[\mathbf{Q}(\mathbf{r})] = \sum_{\alpha=1}^{n} \left\{ \frac{1}{2}\rho_\alpha \left(\mathbf{Q}^\alpha : \mathbf{Q}^\alpha\right) - \frac{1}{7}\sqrt{\frac{10}{3}}\rho_\alpha \,\mathsf{Tr}\left(\mathbf{Q}^\alpha \cdot \mathbf{Q}^\alpha \cdot \mathbf{Q}^\alpha\right) + \frac{5}{28}\rho_\alpha \left(\mathbf{Q}^\alpha : \mathbf{Q}^\alpha\right)^2 \right\}. \tag{4.30}$$

4.3.2 Excess contribution

Now we turn to the reformulation of the excess free energy as function of $\mathbf{Q}(\mathbf{r})$. To our knowledge this has not been done systematically from a DFT basis, however, some attempts have been reported following Taylor expansions of the one–particle densities and moments of the Mayer function [118] similar to the generalized DFT for weakly twisted director fields [119].

Here we use the extension to mixtures of the RY approximation [see Eq. (3.53)]. Inserting the ansatz given for the density difference in (4.22) into Eq. (3.53) and after some rearrangement yields[2]

$$\begin{aligned}\beta\mathcal{F}_{\mathsf{ex}}^I[\mathbf{Q}(\mathbf{r})] = -\frac{1}{2}\sum_{\alpha=1}^{n}\sum_{\beta=1}^{n}\int_V d\mathbf{r}\int_V d\mathbf{r}'\left(\frac{\rho_\alpha}{4\pi}\right)\left(\frac{\rho_\beta}{4\pi}\right)\left(\frac{15}{2}\right) Q_{\mu\nu}^\alpha(\mathbf{r}) Q_{\mu\nu}^\beta(\mathbf{r}') \\ \times \int_{\mathbb{S}^2} d\hat{\boldsymbol{u}}\int_{\mathbb{S}^2} d\hat{\boldsymbol{u}}'\, c_{\alpha\beta}^{(2)}(\mathbf{r}-\mathbf{r}';\hat{\boldsymbol{u}},\hat{\boldsymbol{u}}')\left(\overline{\hat{u}_\mu \hat{u}_\nu}\right)\left(\overline{\hat{u}'_\mu \hat{u}'_\nu}\right).\end{aligned} \tag{4.31}$$

Now, the task is to rewrite the integrals over the unit sphere, i.e.,

$$\mathsf{Int}_{\hat{\boldsymbol{u}}\hat{\boldsymbol{u}}'} = \int_{\mathbb{S}^2} d\hat{\boldsymbol{u}}\int_{\mathbb{S}^2} d\hat{\boldsymbol{u}}'\, c_{\alpha\beta}^{(2)}(\mathbf{r}-\mathbf{r}';\hat{\boldsymbol{u}},\hat{\boldsymbol{u}}')\left(\overline{\hat{u}_\mu \hat{u}_\nu}\right)\left(\overline{\hat{u}'_\mu \hat{u}'_\nu}\right), \tag{4.32}$$

in terms of the tensor quantities $\mathbf{Q}^\alpha$. Here it is important to mention, once again, that according to the RY approximation [39] the direct correlation function is calculated in the isotropic phase.

Referred to an arbitrary space–fixed reference frame the direct correlation function $c_{\alpha\beta}^{(2)}(\mathbf{r}-\mathbf{r}';\hat{\boldsymbol{u}},\hat{\boldsymbol{u}}')$ can be expanded in terms of the spherical invariants as (see e.g. Refs. [88, 99])

$$c_{\alpha\beta}^{(2)}(\mathbf{r}-\mathbf{r}';\hat{\boldsymbol{u}},\hat{\boldsymbol{u}}') = \sum_{l_1 l_2 l} c_{\alpha\beta}^{(2)}(l_1 l_2 l;\mathbf{r}-\mathbf{r}')\Phi(l_1 l_2 l;\hat{\boldsymbol{u}},\hat{\boldsymbol{u}}',\hat{\boldsymbol{u}}_x), \tag{4.33}$$

[2] For simplicity in the following expressions Einstein's index convention will be used.

where $\hat{\boldsymbol{u}}_x$ is the unit vector pointing in the direction of the vector difference $\mathbf{x} = \mathbf{r} - \mathbf{r}'$ and $c^{(2)}_{\alpha\beta}(l_i l_2 l; \mathbf{r} - \mathbf{r}')$ are the harmonic expansion coefficients of the direct correlation function

$$c^{(2)}_{\alpha\beta}(l_1 l_2 l; \mathbf{x}) = \frac{(2l_1+1)(2l_2+1)}{4\pi(2l+1)} \int\limits_{\mathbb{S}^2} d\hat{\boldsymbol{u}} \int\limits_{\mathbb{S}^2} d\hat{\boldsymbol{u}}' c^{(2)}_{\alpha\beta}(\mathbf{r}-\mathbf{r}'; \hat{\boldsymbol{u}}, \hat{\boldsymbol{u}}') \Phi(l_1 l_2 l; \hat{\boldsymbol{u}}, \hat{\boldsymbol{u}}', \hat{\boldsymbol{u}}_x)\,. \tag{4.34}$$

Here, the rotational invariants $\Phi(l_1 l_2 l; \hat{\boldsymbol{u}}, \hat{\boldsymbol{u}}', \hat{\boldsymbol{u}}_x)$ are given by

$$\Phi(l_1 l_2 l; \hat{\boldsymbol{u}}, \hat{\boldsymbol{u}}', \hat{\boldsymbol{u}}_x) = \sum_{m_1 m_2 m} C(l_1 l_2 l; m_1 m_2 m) \mathsf{Y}_{l_1 m_1}(\hat{\boldsymbol{u}}) \mathsf{Y}_{l_2 m_2}(\hat{\boldsymbol{u}}') \mathsf{Y}^*_{lm}(\hat{\boldsymbol{u}}_x)\,, \tag{4.35}$$

where Y_{lm} are the spherical harmonics and $C(l_1 l_2 l; m_1 m_2 m)$ are the Clebsch–Gordan coefficients [see Appendix B] [3]. Inserting the series expansion (4.33) in Eq. (4.32) yields

$$\mathsf{Int}_{\hat{\boldsymbol{u}}\hat{\boldsymbol{u}}'} = \int\limits_{\mathbb{S}^2} d\hat{\boldsymbol{u}} \int\limits_{\mathbb{S}^2} d\hat{\boldsymbol{u}}' \sum_{l_1 l_2 l} c^{(2)}_{\alpha\beta}(l_1 l_2 l; \mathbf{x}) \Phi(l_1 l_2 l; \hat{\boldsymbol{u}}, \hat{\boldsymbol{u}}', \hat{\boldsymbol{u}}_x) \left(\overbrace{\hat{u}_\mu \hat{u}_\nu} \right) \left(\overbrace{\hat{u}'_\mu \hat{u}'_\nu} \right)\,. \tag{4.36}$$

Since the Cartesian product $\overbrace{\hat{u}_\mu \hat{u}_\nu}$ is isomorphic to the $l = 2$ spherical harmonics [see Appendix B], i.e.,

$$\left(\overbrace{\hat{\mathbf{u}}\hat{\mathbf{u}}} \right)_m = \sqrt{\frac{8\pi}{15}}\, \mathsf{Y}_{2m}(\hat{\mathbf{u}})\,, \tag{4.37}$$

then we find after substitution of the isomorphism (4.37) in Eq. (4.36)

$$\mathsf{Int}_{\hat{\boldsymbol{u}}\hat{\boldsymbol{u}}'} = \frac{8\pi}{15} \int\limits_{\mathbb{S}^2} d\hat{\boldsymbol{u}} \int\limits_{\mathbb{S}^2} d\hat{\boldsymbol{u}}' \sum_{l_1 l_2 l} c^{(2)}_{\alpha\beta}(l_1 l_2 l; \mathbf{x}) \Phi(l_1 l_2 l; \hat{\boldsymbol{u}}, \hat{\boldsymbol{u}}', \hat{\boldsymbol{u}}_x) \mathsf{Y}_{2m_1}(\hat{\boldsymbol{u}}) \mathsf{Y}_{2m_2}(\hat{\boldsymbol{u}}')\,. \tag{4.38}$$

Considering that the rotational invariants $\Phi(l_1 l_2 l; \hat{\boldsymbol{u}}, \hat{\boldsymbol{u}}', \hat{\boldsymbol{u}}_x)$ are given in terms of spherical harmonics [see Eq. (4.35)] and since [see Appendix B]

$$\int\limits_{\mathbb{S}^2} \mathsf{Y}^*_{l_1 m_1}(\hat{\boldsymbol{u}}) \mathsf{Y}_{l_2 m_2}(\hat{\boldsymbol{u}}) d\hat{\boldsymbol{u}} = \delta_{l_1 l_2} \delta_{m_1 m_2}\,, \quad \text{and} \quad \mathsf{Y}^*_{l_1 m_1}(\hat{\boldsymbol{u}}) = (-1)^{-m_1} \mathsf{Y}_{l_1 -m_1}(\hat{\boldsymbol{u}})\,,$$

[3] The notation in Eqs. (4.33) and (4.35) represents explicitly the following [see Appendix B]:

$$\sum_{l_1 l_2 l} \to \sum_{l_1=0}^{\infty} \sum_{l_2=0}^{\infty} \sum_{l=|l_1-l_2|}^{|l_1+l_2|} \quad \text{and} \quad \sum_{m_1 m_2 m} \to \sum_{m_1=-l_1}^{l_1} \sum_{m_2=-l_2}^{l_2} \sum_{m=-l}^{l} \delta_{m,m_1+m_2}.$$

the integral over $\hat{\boldsymbol{u}}$ and $\hat{\boldsymbol{u}}'$ in Eq. (4.38) reduces to

$$\mathrm{Int}_{\hat{\boldsymbol{u}}\hat{\boldsymbol{u}}'} = \frac{8\pi}{15}\sum_{l=0}^{4}\sum_{m=-l}^{l} c^{(2)}(22l;\mathbf{x})C(22l;00m)\mathsf{Y}^{*}_{lm}(\hat{\boldsymbol{u}}_x)\,. \tag{4.39}$$

Equation (4.39) defines the *reduced* direct correlation function (independent of $\hat{\boldsymbol{u}}$ and $\hat{\boldsymbol{u}}'$) as

$$\bar{c}^{(2)}_{\alpha\beta}(\mathbf{r}-\mathbf{r}') = \sum_{l=0}^{4}\sum_{m=-l}^{l} c^{(2)}_{\alpha\beta}(22l;\mathbf{x})C(22l;00m)\mathsf{Y}^{*}_{lm}(\hat{\boldsymbol{u}}_x)\,. \tag{4.40}$$

Finally, writing Eq. (4.31) in terms of the reduced direct correlation function (4.39) yields

$$\beta\mathcal{F}^{I}_{\mathsf{ex}}[\mathbf{Q}(\mathbf{r})] = -\frac{1}{2}\sum_{\alpha=1}^{n}\sum_{\beta=1}^{n}\int_V d\mathbf{r}\int_V d\mathbf{r}'\,\frac{\rho_\alpha\,\rho_\beta}{4\pi}\,\bar{c}^{(2)}(\mathbf{r}-\mathbf{r}')Q^{\alpha}_{\mu\nu}(\mathbf{r})Q^{\beta}_{\mu\nu}(\mathbf{r}')\,. \tag{4.41}$$

4.3.3 Gradient expansion of the direct correlation function

As mentioned in Chapter 3, $c^{(2)}_{\alpha\beta}(\mathbf{r}-\mathbf{r}')$ is related to the pair interaction between particles. To gain an insight of the properties of the system and compare them with experimental results (often obtained by small–angle X–ray or neutron scattering see e.g. Ref. [120]) it is useful to write the direct correlation function in the Fourier space (see e.g. Ref. [88, 89]).

Here, we follow Ref. [121], to write a gradient expansion of the pair correlation function. First we focus on the integral over $\mathbf{r}'$ appearing on the right hand side of Eq. (4.41),

$$J(\mathbf{r}) = \int_V d\mathbf{r}'\,\bar{c}^{(2)}_{\alpha\beta}(\mathbf{r}-\mathbf{r}')Q^{\beta}_{\mu\nu}(\mathbf{r}')\,. \tag{4.42}$$

Taking the Fourier transform of Eq. (4.42),

$$\mathfrak{F}\Big\{J(\mathbf{r})\Big\} = \mathfrak{F}\Big\{\int_V d\mathbf{r}'\,\bar{c}^{(2)}_{\alpha\beta}(\mathbf{r}-\mathbf{r}')Q^{\beta}_{\mu\nu}(\mathbf{r}')\Big\}\,, \tag{4.43}$$

and after using the convolution theorem (see e.g. Ref. [122]) from Eq. (4.43) it follows

$$\widehat{J}(\mathbf{k}) = \frac{1}{(2\pi)^{3/2}}\,\widehat{\bar{c}^{(2)}_{\alpha\beta}}(\mathbf{k})\widehat{Q^{\beta}_{\mu\nu}}(\mathbf{k})\,. \tag{4.44}$$

where $\mathbf{k}$ is the wave number and the notation $\widehat{f}(\mathbf{k})$ represents the Fourier transform of the real valued function $f(\mathbf{r})$. Second, in the small wave number approximation ($\mathbf{k}\approx 0$)

we expand $\widehat{\bar{c}^{(2)}_{\alpha\beta}}(\mathbf{k})$ in the series

$$\widehat{\bar{c}^{(2)}_{\alpha\beta}}(\mathbf{k}) = M_0^{\alpha\beta} + M_2^{\alpha\beta}|\mathbf{k}|^2 + M_4^{\alpha\beta}|\mathbf{k}|^4 + \mathcal{O}(|\mathbf{k}|^6)\,, \tag{4.45}$$

where $M_n^{\alpha\beta}$ are expansion coefficients related to the moments of the direct correlation function in the Fourier space [89]. Inserting (4.45) back into Eq. (4.44) we obtain

$$\widehat{J}(\mathbf{k}) = \frac{1}{(2\pi)^{3/2}}\left(M_0^{\alpha\beta} + M_2^{\alpha\beta}|\mathbf{k}|^2 + M_4^{\alpha\beta}|\mathbf{k}|^4\right)\widehat{Q^{\beta}_{\mu\nu}}(\mathbf{k})\,. \tag{4.46}$$

Back in real space the Fourier transform (4.46) corresponds to the product between the gradient expansion of the direct correlation function and the tensor $Q^{\beta}_{\mu\nu}$, *i.e.*

$$J(\mathbf{r}) = \int_V d\mathbf{r}'\left(\mathcal{M}_0^{\alpha\beta} - \mathcal{M}_2^{\alpha\beta}\nabla^2 + \mathcal{M}_4^{\alpha\beta}\nabla^4\right)\delta(\mathbf{r}-\mathbf{r}')\,Q^{\beta}_{\mu\nu}(\mathbf{r}')\,, \tag{4.47}$$

where the operator ∇ is taken with respect to the $\mathbf{r}'$ coordinates. Finally, upon integration of (4.47) with respect to $\mathbf{r}'$ one obtains

$$J(\mathbf{r}) = \left(\mathcal{M}_0^{\alpha\beta} - \mathcal{M}_2^{\alpha\beta}\nabla^2 + \mathcal{M}_4^{\alpha\beta}\nabla^4\right)Q^{\beta}_{\mu\nu}(\mathbf{r})\,, \tag{4.48}$$

where the coefficients $\mathcal{M}_n^{\alpha\beta}$ are the moments of the expansion coefficients of the direct correlation function given by

$$\mathcal{M}_n^{\alpha\beta} = \frac{1}{(2\pi)^{3/2}}\int_V d\mathbf{x}\;\bar{c}^{(2)}_{\alpha\beta}(\mathbf{x})\,|\mathbf{x}|^n\,. \tag{4.49}$$

In this analysis the properties of the mixture are parametrized only by the moments $\mathcal{M}_0^{\alpha\beta}$, $\mathcal{M}_2^{\alpha\beta}$ and $\mathcal{M}_4^{\alpha\beta}$. In general, these moments depend on the thermodynamic properties of the mixture expressed in terms of the mean number densities ρ_α. For example, the $k=0$ term is related to the liquid phase isothermal compressibility whereas the $k=2$ and $k=4$ terms are usually related with the bulk modulus of the isotropic system and the Frank elastic constants [121].

Inserting Eq. (4.48) into the excess free energy contribution Eq. (4.41) yields:

$$\beta\mathcal{F}^{I}_{\text{ex}}[\mathbf{Q}(\mathbf{r})] = -\frac{1}{2}\sum_{\alpha=1}^{n}\sum_{\beta=1}^{n}\frac{\rho_\alpha\,\rho_\beta}{4\pi}\int_V d\mathbf{r}\;Q^{\alpha}_{\mu\nu}(\mathbf{r})\left(\mathcal{M}_0^{\alpha\beta} - \mathcal{M}_2^{\alpha\beta}\nabla^2 + \mathcal{M}_4^{\alpha\beta}\nabla^4\right)Q^{\beta}_{\mu\nu}(\mathbf{r})\,. \tag{4.50}$$

Equation (4.50) may be interpreted as the excess free energy cost due to the spatial inhomogeneities of the mixture. However, as it is written it does not measure properly

how the inhomogeneities of the tensor quantities $\mathbf{Q}^\alpha$ and $\mathbf{Q}^\beta$ are correlated. To this end it is useful to re–write Eq. (4.50) in terms of gradients of the alignment tensors $\mathbf{Q}^\alpha$ and $\mathbf{Q}^\beta$.

Focusing on the integral

$$-\int_V d\mathbf{r}\; Q^\alpha_{\mu\nu}(\mathbf{r})\left(\mathcal{M}_2^{\alpha\beta}\nabla^2 - \mathcal{M}_4^{\alpha\beta}\nabla^4\right) Q^\beta_{\mu\nu}(\mathbf{r})\,, \tag{4.51}$$

we note that the ∇^2 and ∇^4 operators are acting (only) on $\mathbf{Q}^\beta$. However, both may be rewritten in terms of the derivatives of the product $\mathbf{Q}^\alpha : \mathbf{Q}^\beta$.

Focusing on second order derivatives and using Green's tensor identity [see Appendix A]

$$\begin{aligned}\nabla^2(Q^\alpha_{\mu\nu}Q^\beta_{\mu\nu}) = Q^\alpha_{\mu\nu}(\nabla^2 Q^\beta_{\mu\nu}) + 2(\nabla_\lambda Q^\alpha_{\mu\nu})(\nabla_\lambda Q^\beta_{\mu\nu}) \\ + (\nabla_\lambda Q^\alpha_{\lambda\nu})(\nabla_\mu Q^\beta_{\mu\nu}) + Q^\alpha_{\mu\nu}(\epsilon_{\mu\gamma\delta}\nabla_\gamma(\epsilon_{\delta\kappa\lambda}\nabla_\kappa Q^\beta_{\lambda\nu}))\,,\end{aligned} \tag{4.52}$$

equation (4.51) after integration by parts yields (where we used the property of the Levi–Civita symbol $\epsilon_{\mu\gamma\delta}\epsilon_{\delta\kappa\lambda} = \delta_{\mu\kappa}\delta_{\gamma\lambda} - \delta_{\mu\lambda}\delta_{\kappa\gamma}$)

$$\begin{aligned}-\int_V d\mathbf{r} Q^\alpha_{\mu\nu}(\mathbf{r})\left(\mathcal{M}_2^{\alpha\beta}\nabla^2\right) Q^\beta_{\mu\nu}(\mathbf{r}) = \\ = \int_V d\mathbf{r}\mathcal{M}_2^{\alpha\beta}\left\{\left(\nabla_\lambda Q^\alpha_{\mu\nu}\nabla_\lambda Q^\beta_{\mu\nu}\right) + \left(\nabla_\nu Q^\alpha_{\mu\nu}\nabla_\lambda Q^\beta_{\mu\lambda}\right) + \left(\nabla_\nu Q^\alpha_{\mu\lambda}\nabla_\lambda Q^\beta_{\mu\nu}\right)\right\}.\end{aligned} \tag{4.53}$$

Finally, the excess free energy contribution Eq. (4.41) in terms of gradients of $\mathbf{Q}^\alpha$ and $\mathbf{Q}^\beta$ is

$$\beta\mathcal{F}^I_{\text{ex}}[\mathbf{Q}(\mathbf{r})] = -\int_V \Phi_{\text{ex}}[\mathbf{Q}(\mathbf{r})]\, d\mathbf{r}\,, \tag{4.54}$$

where $\Phi_{\text{ex}}[\mathbf{Q}(\mathbf{r})]$ is the excess contribution of the mesoscopic free energy density (per unit volume) which in the tensor notation is

$$\begin{aligned}\Phi_{\text{ex}} = \frac{1}{2}\sum_{\alpha=1}^{n}\sum_{\beta=1}^{n}\frac{\rho_\alpha\rho_\beta}{4\pi}\Big\{\mathcal{M}_0^{\alpha\beta}\big(\boldsymbol{Q}^\alpha : \boldsymbol{Q}^\beta\big) + \mathcal{M}_2^{\alpha\beta}\big(\nabla\boldsymbol{Q}^\alpha \odot \nabla\boldsymbol{Q}^\beta\big) \\ + \mathcal{M}_2^{\alpha\beta}\big(\nabla\cdot\boldsymbol{Q}^\alpha\big)\cdot\big(\nabla\cdot\boldsymbol{Q}^\beta\big) + \mathcal{M}_2^{\alpha\beta}\big(\nabla\times\boldsymbol{Q}^\alpha\big) : \big(\nabla\times\boldsymbol{Q}^\beta\big)\Big\}.\end{aligned} \tag{4.55}$$

In general each gradient term on the right hand side of Eq. (4.55) contributes differently to the excess free energy. However, this expression indicates that in our approximation, all distortions of the fluid (splay, twist, bend and saddle–splay) contribute equally to the energy cost of deformation. Taking this into account Eq. (4.55) may be rewritten as

$$\Phi_{\text{ex}} = \frac{1}{2}\sum_{\alpha=1}^{n}\sum_{\beta=1}^{n}\frac{\rho_\alpha\rho_\beta}{4\pi}\Big\{\mathcal{M}_0^{\alpha\beta}\big(\boldsymbol{Q}^\alpha : \boldsymbol{Q}^\beta\big) + \mathcal{M}_2^{\alpha\beta}\big(\nabla\boldsymbol{Q}^\alpha \odot \nabla\boldsymbol{Q}^\beta\big)\Big\}. \tag{4.56}$$

4.3.4 Full free energy

As in Subsection (4.2), in the following we write the full free energy given by the sum of ideal and excess parts $\mathcal{F}^I = \mathcal{F}^I_{\text{id}} + \mathcal{F}^I_{\text{ex}}$. Adding ideal (4.29) and excess (4.54) contributions we get

$$\beta\mathcal{F}^I[\mathbf{Q}(\mathbf{r})] = \int_V \left\{ \Phi_0^\alpha + \Phi_{\text{id}}[\mathbf{Q}(\mathbf{r})] - \Phi_{\text{ex}}[\mathbf{Q}(\mathbf{r})] \right\} d\mathbf{r}\,,$$

where Φ_0^α, $\Phi_{\text{id}}[\mathbf{Q}(\mathbf{r})]$ and $\Phi_{\text{ex}}[\mathbf{Q}(\mathbf{r})]$ are the ideal (4.30) and excess (4.56) contributions of the mesoscopic free energy density (per unit volume), respectively.

In terms of the alignment tensors the mesoscopic free energy density of the system:

$$\begin{aligned}\Phi[\mathbf{Q}(\mathbf{r})] = \sum_{\alpha=1}^{n} \left(\Phi_0^\alpha + \mathcal{A}_\alpha \left(\mathbf{Q}^\alpha : \mathbf{Q}^\alpha\right) - \mathcal{B}_\alpha \,\text{Tr}\left(\mathbf{Q}^\alpha \cdot \mathbf{Q}^\alpha \cdot \mathbf{Q}^\alpha\right) + \mathcal{C}_\alpha \,\left(\mathbf{Q}^\alpha : \mathbf{Q}^\alpha\right)^2 \right) \\ + \frac{1}{2}\sum_{\alpha=1}^{n}\sum_{\beta=1}^{n} \left(\mathcal{A}_{\alpha\beta}\big(\boldsymbol{Q}^\alpha : \boldsymbol{Q}^\beta\big) + \mathcal{C}_{\alpha\beta}\big(\nabla\boldsymbol{Q}^\alpha \odot \nabla\boldsymbol{Q}^\beta\big) \right). \end{aligned} \tag{4.57}$$

where the coefficients Φ_0^α, $\mathcal{A}_\alpha$, $\mathcal{B}_\alpha$, $\mathcal{C}_\alpha$, $\mathcal{A}_{\alpha\beta}$ and $\mathcal{C}_{\alpha\beta}$ are given by

$$\Phi_0^\alpha = \rho_\alpha \left(\ln(\rho_\alpha \Lambda_\alpha^3) - 1 \right) , \tag{4.58}$$

$$\mathcal{A}_\alpha = \frac{1}{2}\rho_\alpha \,, \tag{4.59}$$

$$\mathcal{B}_\alpha = \frac{\sqrt{30}}{21}\rho_\alpha \,, \tag{4.60}$$

$$\mathcal{C}_\alpha = \frac{5}{28}\rho_\alpha \,, \tag{4.61}$$

$$\mathcal{A}_{\alpha\beta} = \frac{\rho_\alpha\rho_\beta}{4\pi}\mathcal{M}_0^{\alpha\beta} \,, \tag{4.62}$$

$$\mathcal{C}_{\alpha\beta} = \frac{\rho_\alpha\rho_\beta}{4\pi}\mathcal{M}_2^{\alpha\beta} \,. \tag{4.63}$$

and the moments of the direct correlation function $\bar{c}^{(2)}_{\alpha\beta}(\mathbf{r}-\mathbf{r}')$ in Eq. (4.49) are given by

$$\mathcal{M}_n^{\alpha\beta} = \frac{1}{(2\pi)^{3/2}} \int_V d\mathbf{x}\; \bar{c}^{(2)}_{\alpha\beta}(\mathbf{x})\, |\mathbf{x}|^n \,.$$

As in the case of homogeneous systems, the mesoscopic free energy density derived for inhomogeneous systems (4.57) has the standard de Gennes form of the elastic energy [19] in terms of an expansion in terms of the order parameters and its gradients [see Chapter 2]. The main difference with the de Gennes's approximation and our approach is that terms with third order derivatives vanish. It is important to note that the microscopical

information entering in Eq. (4.57) through the expansion coefficients is closely related to the intrinsic properties of the fluid namely the number density and the moments of the direct correlation function [see Eq. (4.49)]. We have to remark that similar expressions of these moments are given in various previous studies in Refs. [110, 36, 123, 124] based on a particle–fixed frame description (parallel to $\hat{e}_z$). Both descriptions are equivalent, however, with our approach the connection with simulation analysis and experiments may be simpler.

4.4 Comparison between mesoscopic free energies

To conclude this chapter it is necessary to discuss and establish the connection between the full mesoscopic free energy density for homogeneous systems, Eq. (4.11)], and the one corresponding to inhomogeneous systems, Eq. (4.57). This can be done in straightforwardly focusing only on the part of the free energy which depends on the orientational order parameters $\mathbf{Q}^\alpha$. With this specialization the mesoscopic free energy densities (per unit volume), $\Phi[\mathbf{Q}]$ are:

Homogeneous systems:

$$\Phi^H[\mathbf{Q}] = \sum_{\alpha=1}^{n}\left(A_\alpha(\mathbf{Q}^\alpha:\mathbf{Q}^\alpha) - B_\alpha \mathsf{Tr}(\mathbf{Q}^\alpha\cdot\mathbf{Q}^\alpha\cdot\mathbf{Q}^\alpha) + C_\alpha(\mathbf{Q}^\alpha:\mathbf{Q}^\alpha)^2\right) + \frac{1}{2}\sum_{\alpha=1}^{n}\sum_{\beta=1}^{n}\left(A_{\alpha\beta}(\mathbf{Q}^\alpha:\mathbf{Q}^\beta) + C_{\alpha\beta}(\mathbf{Q}^\alpha:\mathbf{Q}^\beta)^2\right), \tag{4.64}$$

Inhomogeneous systems:

$$\Phi^I[\mathbf{Q}] = \sum_{\alpha=1}^{n}\left(\mathcal{A}_\alpha\left(\mathbf{Q}^\alpha:\mathbf{Q}^\alpha\right) - \mathcal{B}_\alpha\,\mathsf{Tr}\left(\mathbf{Q}^\alpha\cdot\mathbf{Q}^\alpha\cdot\mathbf{Q}^\alpha\right) + \mathcal{C}_\alpha\,\left(\mathbf{Q}^\alpha:\mathbf{Q}^\alpha\right)^2\right) + \frac{1}{2}\sum_{\alpha=1}^{n}\sum_{\beta=1}^{n}\left(\mathcal{A}_{\alpha\beta}\big(\boldsymbol{Q}^\alpha{:}\boldsymbol{Q}^\beta\big) + \mathcal{C}_{\alpha\beta}\big(\nabla\boldsymbol{Q}^\alpha\odot\nabla\boldsymbol{Q}^\beta\big)\right), \tag{4.65}$$

where the coefficients appearing in Eqs. (4.64) and (4.65) are listed (for convenience) on Table 4.1. Clearly, the first point of convergence between both expressions is that for each independent component α terms of second, third and fourth terms of $\mathbf{Q}^\alpha$ appear. This confirms that both derivations result in a Landau–like expression of the single component system.

The coefficients appearing in Eqs. (4.64) and (4.65) depend on the number densities of each components of the mixture and on different microscopic details. On the one hand, for homogeneous systems the dependency of the excluded volume coefficients implies short–range structural properties of the fluid. On the other hand, for inhomogeneous systems the microscopic dependence on the direct correlation function of the isotropic

	Homogeneous systems Eq. (4.64)	**Inhomogeneous systems** Eq. (4.65)
$\mathbf{Q}^\alpha : \mathbf{Q}^\alpha$	$\frac{1}{2}\rho_\alpha + \frac{1}{10}\rho_\alpha^2 G_{\alpha\alpha} V_2^{\alpha\alpha}$	$\frac{1}{2}\rho_\alpha$
$\mathrm{Tr}\,(\mathbf{Q}^\alpha \cdot \mathbf{Q}^\alpha \cdot \mathbf{Q}^\alpha)$	$\frac{\sqrt{30}}{21}\rho_\alpha$	$\frac{\sqrt{30}}{21}\rho_\alpha$
$(\mathbf{Q}^\alpha : \mathbf{Q}^\alpha)^2$	$\frac{19}{28}\rho_\alpha + \frac{1}{18}\rho_\alpha^2 G_{\alpha\alpha} V_4^{\alpha\alpha}$	$\frac{5}{28}\rho_\alpha$
$\mathbf{Q}^\alpha : \mathbf{Q}^\beta$	$\frac{1}{5}\rho_\alpha\rho_\beta G_{\alpha\beta} V_2^{\alpha\beta}$	$\frac{\rho_\alpha\rho_\beta}{4\pi}\mathcal{M}_0^{\alpha\beta}$
$\left(\mathbf{Q}^\alpha : \mathbf{Q}^\beta\right)^2$	$\frac{1}{9}\rho_\alpha\rho_\beta G_{\alpha\beta} V_4^{\alpha\beta}$	—
$\nabla\boldsymbol{Q}^\alpha \odot \nabla\boldsymbol{Q}^\beta$	—	$\frac{\rho_\alpha\rho_\beta}{4\pi}\mathcal{M}_2^{\alpha\beta}$

Table 4.1: Comparison of the coefficients appearing on the final forms of the mesoscopic free energy densities for homogeneous (4.11) and inhomogeneous systems (4.57).

system implies an measure of the mean interaction of the particles. This feature is what makes both descriptions, albeit independent, complementary.

Regarding the coupling terms between component α and component β we see that the derivation of the mesoscopic free energy for homogeneous systems includes and extra term of the type $\left(\mathbf{Q}^\alpha : \mathbf{Q}^\beta\right)^2$ which is evidently due to the detailed expansion of the excluded volume interaction up 4–th rank tensors (see Section 3.3.1). On the other hand, this term is not present on the derivation for inhomogeneous systems due to the simple angle dependence assumption introduced in Eq. (4.20). However, what is recovered by this assumption are terms of gradients of the alignment tensors $\mathbf{Q}^\alpha$. Therefore we conclude that both derivations do not exclude each other but are indeed complementary and, to certain extent, reciprocal.

4.5 Summary

In this chapter we established a *bridge* between density functional theory and mesoscopic $\mathbf{Q}$–tensor theory. To create this link we proposed two different, but at the same time complementary strategies. First, based on the many fluid Parson-Lee theory, we performed an expansion of the free energy functional in powers of the $\mathbf{Q}$–tensors of each species. This procedure yields a spatially homogeneous Landau–like expression for

the orientational part of the free energy. On the other hand, starting with an ansatz of the one–particle densities (which assumes small deviations from the isotropic state), we expressed the second order perturbation theory (Ramakrishnan–Youssuf approximation) in terms of powers of $\mathbf{Q}$ and its gradients. The resulting expressions for the free energy density are:

Homogeneous systems:

$$\begin{aligned}\Phi^H[\mathbf{Q}] =& \sum_{\alpha=1}^{n}\left(A_\alpha(\mathbf{Q}^\alpha:\mathbf{Q}^\alpha) - B_\alpha \mathsf{Tr}(\mathbf{Q}^\alpha\cdot\mathbf{Q}^\alpha\cdot\mathbf{Q}^\alpha) + C_\alpha(\mathbf{Q}^\alpha:\mathbf{Q}^\alpha)^2\right)\\ &+\frac{1}{2}\sum_{\alpha=1}^{n}\sum_{\beta=1}^{n}\left(A_{\alpha\beta}(\mathbf{Q}^\alpha:\mathbf{Q}^\beta) + C_{\alpha\beta}(\mathbf{Q}^\alpha:\mathbf{Q}^\beta)^2\right),\end{aligned}$$

Inhomogeneous systems:

$$\begin{aligned}\Phi^I[\mathbf{Q}] =& \sum_{\alpha=1}^{n}\left(\mathcal{A}_\alpha\left(\mathbf{Q}^\alpha:\mathbf{Q}^\alpha\right) - \mathcal{B}_\alpha\,\mathsf{Tr}\left(\mathbf{Q}^\alpha\cdot\mathbf{Q}^\alpha\cdot\mathbf{Q}^\alpha\right) + \mathcal{C}_\alpha\,\left(\mathbf{Q}^\alpha:\mathbf{Q}^\alpha\right)^2\right)\\ &+\frac{1}{2}\sum_{\alpha=1}^{n}\sum_{\beta=1}^{n}\left(\mathcal{A}_{\alpha\beta}\big(\boldsymbol{Q}^\alpha:\boldsymbol{Q}^\beta\big) + \mathcal{C}_{\alpha\beta}\big(\nabla\boldsymbol{Q}^\alpha\odot\nabla\boldsymbol{Q}^\beta\big)\right),\end{aligned}$$

where the coefficients appearing in these expressions are functions of the microscopic properties of the system, namely, the number density, aspect ratio and, in the case of spatially inhomogeneous systems, moments of the inter–component direct correlation function.

The combination of microscopic (DFT) and mesoscopic descriptions makes our approach a part of the theories aiming to contribute to a scale–bridging characterization of complex colloidal mixtures. However, the biggest restriction of our approach is that we focused on the orientational distribution function alone. This enhances a clear qualitative difference with classical density functional theories for fluids which describe a variety of density driven transitions (such as demixing). In the future, it would be interesting to understand to what extent the above–mentioned expressions are preempted (or modified) by coupling to density fluctuations.

Chapter 5

Application to binary mixtures

Athermal mixtures of non spherical particles are widely used in functional materials. These include liquid crystal displays, adaptive optic devices and switchable windows. Typically these mixtures are characterized by their polydispersity, *i.e.*, non uniform range of lengths and diameters. The lowest form of polydispersity is constituted by binary mixtures. In this chapter we aim to connect our theoretical approach with real systems.

There are a number of studies focusing on the equilibrium behavior of binary mixtures [13, 14, 15, 16, 17, 18]. However, for our theoretical investigations we focused on two of them: particle based simulations [14] and experimental measurements [16]. First, based on a standard Monte Carlo simulations in Ref. [14] the behavior of a binary mixture of Hard Gaussian particles is studied. In this study, they observed the spontaneous formation of orientationally ordered phases in systems of short and long molecules. On the other hand, the first experimental observation of such phenomena is due to Purdy *et al* [16]. Here, for a system composed of thin semi flexible *fd*–viruses and thick PEG coated *fd*–viruses, they observed that as the concentration of the system is higher, a vast variety of coexisting phases (isotropic–nematic, isotropic–nematic–nematic and nematic–nematic) appear. Interestingly, for sufficiently low concentrations there is a clear separation of an isotropic (thin–rich) and nematic (thick–rich) phases. As we can see both studies describe systems of rigid rod–like particles with very different geometry which develops in different quantitative results. However, the overall qualitative behavior of both, simulations and experiments, is very similar.

5.1 Binary mixtures of hard spherocylinders

Since the derivation presented in Chapter 4 can be applied to binary mixtures of any type of rigid anisotropic particles (as long as they are uniaxial and have head–tail symmetry),

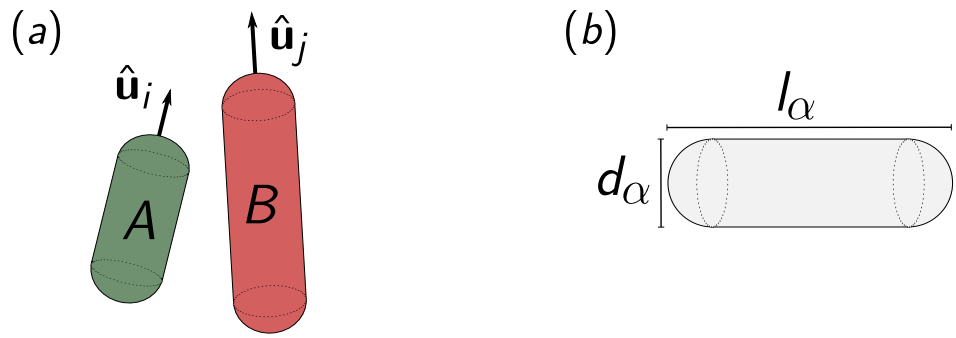

Figure 5.1: (a) Binary mixture of A (short) and B (long) molecules (in this case hard spherocylinders) having the molecular orientations $\hat{\boldsymbol{u}}_i$ and $\hat{\boldsymbol{u}}_j$. (b) Hard spherocylinders are cylinder cape at both sides with hemispheres characterized by two geometrical parameters: their length l_α and their diameter d_α which defines their aspect ratio, *i.e.*, $\kappa_\alpha = l_\alpha/d_\alpha$.

to make a connection with real systems, in the following we focus on systems of long and short hard spherocylinders labeled A and B for convenience [see Fig. (5.1)].

Hard spherocylinders are characterized by two geometrical parameters, their length l_α and their diameter d_α, defining their aspect ratio $\kappa_\alpha = l_\alpha/d_\alpha$. The resulting particle volume is

$$v_\alpha = \frac{\pi}{12}(3\kappa_\alpha + 2)d_\alpha^3 \,.$$

Between a couple of spherocylinders the excluded volume $V_{exc}(\gamma)$ [defined in (3.50)] is given by

$$\begin{aligned} V_{exc}(\gamma) = \frac{\pi}{4}(\kappa_\alpha d_\alpha^3 + \kappa_\beta d_\beta^3) + \frac{\pi}{4} d_\alpha d_\beta (d_\alpha + d_\beta)\sin\gamma + \frac{\pi}{4}(\kappa_\alpha d_\alpha d_\beta^2 + \kappa_\beta d_\beta d_\alpha^2)|\cos\gamma| \\ + \kappa_\alpha\kappa_\beta d_\alpha d_\beta (d_\alpha + d_\beta)\sin\gamma + (\kappa_\alpha d_\alpha + \kappa_\beta d_\beta) d_\alpha d_\beta E(\sin\gamma)\,, \end{aligned} \tag{5.1}$$

where $E(\sin\gamma)$ denotes the complete elliptic integral of the second kind. Within the original Onsager theory, only terms up to linear order in $\sin\gamma$ are considered; that is, the terms involving $|\cos\gamma|$ and $E(\sin\gamma)$ are neglected. In the present work we keep the *full* expression (5.1).

5.1.1 Orientational free energy

To calculate the resulting expansion coefficients $V_k^{\alpha\beta}$ which are defined in (4.5) and which determine the coefficients appearing in the free energy [see (4.13–4.15)], we derive the following analytic expressions for the coefficients $V_k^{\alpha\beta}$, $k = 0, 2, 4$, appearing in the expansion of $V_{exc}(\gamma)$ in Legendre polynomials [see equations (4.4–4.5)]. To this end we

expand the functions $|\cos\gamma|$ and $E(\sin\gamma)$ in Eq. (5.18) up to fourth order in $\sin\gamma$, yielding

$$|\cos\gamma| = (1-\sin\gamma)^{1/2} = 1 - \frac{1}{2}\sin^2\gamma - \frac{1}{8}\sin^4\gamma + \mathcal{O}(6)\,, \tag{5.2}$$

and

$$E(\sin\gamma) = \frac{\pi}{2} - \frac{\pi}{8}\sin^2\gamma - \frac{3\pi}{128}\sin^4\gamma + \mathcal{O}(6)\,. \tag{5.3}$$

Neglecting the term $\mathcal{O}(6)$, the excluded volume becomes

$$\begin{aligned} V_{exc}^{O(4)}(\gamma) =& \frac{\pi}{4}c_1 + \frac{\pi}{4}c_2\sin\gamma + \frac{\pi}{4}c_3\left(1 - \frac{1}{2}\sin^2\gamma - \frac{1}{8}\sin^4\gamma\right) \\ &+ c_4\left(\frac{\pi}{2} - \frac{\pi}{8}\sin^2\gamma - \frac{3\pi}{128}\sin^4\gamma\right) + c_5\sin\gamma\,, \end{aligned} \tag{5.4}$$

where the constants c_i depend on the aspect ratio and diameters of the particles and are

$$\begin{aligned} c_1 &= \kappa_\alpha d_\alpha^3 + \kappa_\beta d_\beta^3\,, & c_2 &= d_\alpha d_\beta(d_\alpha + d_\beta\,, \\ c_3 &= \kappa_\alpha d_\alpha d_\beta^2 + \kappa_\beta d_\beta d_\alpha^2\,, & c_4 &= (\kappa_\alpha d_\alpha + \kappa_\beta d_\beta) d_\alpha d_\beta \\ c_5 &= \kappa_\alpha\kappa_\beta d_\alpha d_\beta(d_\alpha + d_\beta)\,. \end{aligned} \tag{5.5}$$

We note that the coefficients c_3 and c_4 vanish within the original Onsager approach [24].

Starting from Eq. (5.4), we can now employ Eq. (4.5) to calculate the expansion coefficients of interest ($k = 0, 2, 4$):

$$V_k^{\alpha\beta} = \frac{2k+1}{2}\int_0^\pi d\gamma\; V_{exc}^{O(4)}(\gamma) P_k(\cos\gamma)\sin\gamma\,. \tag{5.6}$$

Using $P_0(\cos\gamma) = 1$ and performing the angular integral, we obtain the zero–order coefficient

$$V_0^{\alpha\beta} = \frac{\pi}{4}c_1 + \frac{\pi^2}{16}c_2 + \frac{3\pi}{20}c_3 + \frac{97\pi}{240}c_4 + \frac{\pi}{4}c_5\,. \tag{5.7}$$

To calculate $V_2^{\alpha\beta}$ we use that $P_2(\cos\gamma) = \frac{1}{2}(3\cos^2\gamma - 1)$. Since

$$\int_0^\pi d\gamma\; P_2(\cos\gamma)\sin\gamma = 0\,, \tag{5.8}$$

all linear functions of $\sin\gamma$ do not contribute to the coefficient. However, powers of $\sin\gamma$ do contribute since

$$\int_0^\pi d\gamma\;\; \sin\gamma\, P_2(\cos\gamma)\sin\gamma = -\frac{\pi}{16}\,, \tag{5.9}$$

$$\int_0^\pi d\gamma\;\; \sin^2\gamma\, P_2(\cos\gamma)\sin\gamma = -\frac{4}{15}\,, \tag{5.10}$$

$$\int_0^\pi d\gamma\;\; \sin^4\gamma\, P_2(\cos\gamma)\sin\gamma = -\frac{32}{105}\,. \tag{5.11}$$

Inserting these results into (5.6) with $k = 2$ we obtain

$$V_2^{\alpha\beta} = -\frac{5\pi^2}{128}c_2 + \frac{3\pi}{28}c_3 + \frac{17\pi}{168}c_4 - \frac{5\pi}{32}c_5. \tag{5.12}$$

The coefficients $V_4^{\alpha\beta}$ involve the Legendre polynomial $P_4(\cos\gamma) = \frac{1}{8}(35\cos^4\gamma - 30\cos^2\gamma + 3)$. We find that integrals involving linear and cubic terms in $\sin\gamma$ vanish whereas the other integrals give non-zero results. Specifically,

$$\int_0^\pi d\gamma \;\sin\gamma\, P_4(\cos\gamma)\sin\gamma = -\frac{\pi}{128}\,, \tag{5.13}$$

$$\int_0^\pi d\gamma \;\sin^4\gamma\, P_4(\cos\gamma)\sin\gamma = \frac{16}{315}\,. \tag{5.14}$$

With this we finally obtain

$$V_4^{\alpha\beta} = -\frac{9\pi^2}{1024}c_2 - \frac{\pi}{140}c_3 - \frac{3\pi}{560}c_4 - \frac{9\pi}{256}c_5\,. \tag{5.15}$$

It is worth noting that, since the aspect ratio and the diameter are always positive, the coefficients c_i must be positive as well. It follows that $V_4^{\alpha\beta}$ is always negative, whereas the sign of $V_2^{\alpha\beta}$ depends on the combination of sizes. This is different from standard Onsager theory where $c_3 = c_4 = 0$ and thus, $V_2^{\alpha\beta}$ is always negative.

Focusing only on the binary mixture (where the components are labeled A and B) and on the part of the free energy which depends on the orientational order parameters, that is,

$$\frac{\beta\mathcal{F}^{or}}{V} = \beta\mathcal{F}[\mathbf{Q}]/V - (\mathcal{F}_0^A + \mathcal{F}_0^B + \mathcal{F}_0^{AB})\,, \tag{5.16}$$

where the terms on the right side are defined in equations (4.12 and (4.13), respectively. We further specialize on situations where the hard spherocylinders have equal diameters, i.e., $d_A = d_B = d$, but different aspect ratios, $\kappa_A \neq \kappa_B$. This allows to introduce a dimensionless form of the orientational free energy, $\mathscr{F}^{or} = \beta\mathcal{F}^{or}d^3/V$, and the reduced densities $\rho_\alpha^* = \rho_\alpha d^3$. With these assumptions, the orientational free energy of a binary mixture of hard spherocylinders becomes

$$\begin{aligned}\mathscr{F}^{or} &= \mathscr{F}^{or}[\rho^*, \kappa; \mathbf{Q}] \\ &= \sum_{\alpha=A,B}\Big\{A_\alpha(\mathbf{Q}^\alpha : \mathbf{Q}^\alpha) - B_\alpha \mathsf{Tr}(\mathbf{Q}^\alpha\cdot\mathbf{Q}^\alpha\cdot\mathbf{Q}^\alpha) + C_\alpha(\mathbf{Q}^\alpha : \mathbf{Q}^\alpha)^2\Big\} \\ &\quad - A_{AB}(\mathbf{Q}^A : \mathbf{Q}^B) - C_{AB}(\mathbf{Q}^A : \mathbf{Q}^B)^2\,,\end{aligned} \tag{5.17}$$

where the coefficients A_α, B_α, ρ_α, A_{AB} and C_{AB}, depend on $\{\rho_\alpha^*\}, \{\kappa_\alpha\}$ and are

$$A_\alpha = \frac{1}{2}\rho_\alpha^* - \frac{1}{10}\rho_\alpha^{*2}\left(\frac{5\pi^2}{64} - \frac{5\pi}{12}\kappa_\alpha + \frac{5\pi}{16}\kappa_\alpha^2\right) G_{\alpha\alpha}\,, \tag{5.18}$$

$$B_\alpha = \frac{\sqrt{30}}{21}\rho_\alpha^* \tag{5.19}$$

$$C_\alpha = \frac{19}{28}\rho_\alpha^* - \frac{1}{18}\rho_\alpha^{*2}\left(\frac{9\pi^2}{512} + \frac{\pi}{40}\kappa_\alpha + \frac{9\pi}{128}\kappa_\alpha^2\right) G_{\alpha\alpha}\,, \tag{5.20}$$

$$A_{AB} = \frac{1}{5}\rho_A^*\rho_B^*\left(\frac{5\pi^2}{64} - \frac{5\pi}{24}(\kappa_A + \kappa_B) + \frac{5\pi}{32}\kappa_A\kappa_B\right) G_{AB}\,, \tag{5.21}$$

$$C_{AB} = \frac{1}{9}\rho_A^*\rho_B^*\left(\frac{9\pi^2}{512} + \frac{\pi}{80}(\kappa_A + \kappa_B) + \frac{9\pi}{256}\kappa_A\kappa_B\right) G_{AB}\,. \tag{5.22}$$

An explicit expression for the quantities $G_{\alpha\beta}$ in equations (5.18–5.22) results from a generalization of the Carnahan–Starling theory for HS systems to mixtures [125, 126], yielding [35]

$$G_{\alpha\beta} = \frac{4 - 3(\rho_\alpha^*\nu_\alpha + \rho_\beta^*\nu_\beta)}{4(1 - \rho_\alpha^*\nu_\alpha - \rho_\beta^*\nu_\beta)^2}\,, \tag{5.23}$$

where $\nu_\alpha = v_\alpha/d^3$.

5.2 Isotropic–Nematic transition

As a background for our later discussion of mixtures under shear we first investigate the isotropic–nematic transition in equilibrium. Specifically, we are interested in the stability of the two phases in dependence of the densities and aspect ratios.

As mentioned in detail in Chapter 2, in equilibrium one expects a *uniaxial* nematic phase described by a single director, $\mathbf{n}$, characterizing the preferred alignment of the rods [82, 127].For uniaxial alignment, the second rank tensor reduces to $\mathbf{Q}^\alpha = \sqrt{\frac{3}{2}}q^\alpha\langle\,\overline{\mathbf{nn}}\,\rangle$, where q_α is the eigenvalue related to $\mathbf{n}$. An important remark is that the products appearing in (5.17) become

$$\mathrm{Tr}(\mathbf{Q}^\alpha\cdot\mathbf{Q}^\beta) = q^\alpha q^\beta \quad \text{and} \quad \mathrm{Tr}(\mathbf{Q}^\alpha\cdot\mathbf{Q}^\alpha\cdot\mathbf{Q}^\alpha) = q^{\alpha^3}/\sqrt{6}\,.$$

By definition of the second rank tensor [see Eq. (4.1) with $k = 2$] the eigenvalues q^α are related to the well known Maier–Saupe order parameter S_2 via $q^\alpha = \sqrt{5}S_2$ [22].

As a further simplification, we focus on the *semi–dilute* regime corresponding to low densities. Physically, this implies that the particles have few contacts [128] and that long–range hydrodynamic interactions are negligible [129]. On a more formal level, the low–density limit implies that the contact values of the pair correlation functions tend to one, and the same holds for their density averages.

Mathematically, this limit corresponds to $G_{\alpha\beta} \to 1$. Still, even for this simplification, the mesoscopic theory we develop provides reliable results (in comparison to particle–based simulations [108]) in the range $\kappa = 20$–40 (as we will demonstrate below for the case of a one–component system). Although the choice $G_{\alpha\beta} = 1$ corresponds to that in the original Onsager theory [24], the present orientational free energy functional is different due to the treatment of the coefficients in the excluded volume.

5.2.1 Single component system

To compare our approach against literature results, we initially consider the case of a one–component system. The orientational free energy then reduces to the well–known Landau free energy [19]

$$\mathscr{F}^{or} = A(\rho^*, \kappa) q^2 - \frac{B(\rho^*)}{\sqrt{6}} q^3 + C(\rho^*, \kappa) q^4 \,, \tag{5.24}$$

where the coefficients now depend on the aspect ratio and the density. From Eq. (5.24), we find the three stationary solutions (determined by $d\mathscr{F}^{or}/dq = 0$)

$$q^0 = 0 \,, \tag{5.25}$$

$$q^{\pm} = \frac{\sqrt{6}B}{16C} \left(1 \pm \sqrt{1 - \frac{64AC}{3B^2}} \right) . \tag{5.26}$$

As usual, the isotropic phase becomes globally unstable (i.e., $d^2\mathscr{F}^{or}/dq^2|_{q^0} < 0$) when the second–order coefficient $A(\rho^*, \kappa)$ changes sign from positive and negative. In terms of the density, this implies that within the stable or meta stable isotropic phase,

$$\rho^* < 5 \left(\frac{5\pi^2}{64} - \frac{5\pi}{12}\kappa + \frac{5\pi}{16}\kappa^2 \right)^{-1} . \tag{5.27}$$

Directly at $A = 0$, the nematic state already exists as a meta stable state. The corresponding value of the order parameter follows from Eq. (5.26) as $q^c = \sqrt{6}B/8C$. Further, from the second derivative evaluated at q^+ one finds that the nematic state becomes globally unstable ($d^2\mathscr{F}^{or}/dq^2|_{q^\pm} < 0$) when $A > 3B^2/64C$. The free energies $\mathscr{F}^{or}(q^0)$ and $\mathscr{F}^{or}(q^+)$ become equal at

$$A_{IN} = \frac{B^2}{24C} \,, \tag{5.28}$$

The resulting order parameter at isotropic–nematic coexistence is given by

$$q_0 = \frac{\sqrt{6}B}{12C} \,. \tag{5.29}$$

This simple analysis provides straightforward relations between the density, ρ^*, and the aspect ratio, κ. In Fig. 5.2 we visualize the stability ranges following from the above

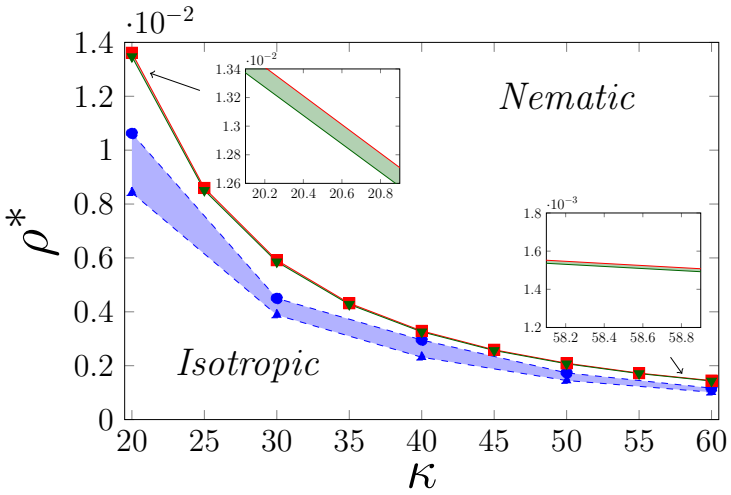

Figure 5.2: Isotropic–nematic transition of a system of hard spherocylinders with aspect ratios between 20 and 60. The (red) squares correspond to the lower limit of the density ρ^* given by inequality (5.30), while (green) down–triangles are the numerical solutions of the relation $A = 3B^2/64C$. For comparison, the (blue) circles and up–triangles correspond to data for the isotropic–nematic phase coexistence from Gibbs ensemble simulations of Bolhuis et al, see [108].

analysis where the axes are given by the density and the aspect ratio. In Fig. 5.2, the (red) ■ line represents the boundary of (meta–)stability of the isotropic state, determined by the maximal density fulfilling the inequality (5.27), as function of κ. On the other hand, the (green) ▼ line indicates the solutions of the relation $A = 3B^2/64C$ for a given value of κ. This line can be seen as the upper boundary of the stable isotropic state.

For smaller aspect ratios, we compare the stability limits with the coexistence densities of isotropic and nematic phases (plotted in (blue) • and ▲) obtained by Bolhuis *et al* in Ref. [108]. We find that two sets of data agree reasonably well. Analytically, in the limit of very large aspect ratios, $\kappa > 80$, our theoretical description is consistent with Onsager's second virial theory [24]. However, for smaller aspect ratios $(10 < \kappa < 20)$ the analytic calculations are very dissimilar, as we can see when they are compared to the Gibbs ensemble simulations [see Ref. [108]]. A very important remark is that the orientational free energy Eq. (5.24) can, by definition, not predict the coexistence *densities*, since we neglected the densities ρ_α as order parameters.

5.2.2 Binary mixture

Depending on the overall density and concentrations, binary mixtures of particles with different aspect ratios can exhibit a very rich phase behavior [16, 33]. As mentioned

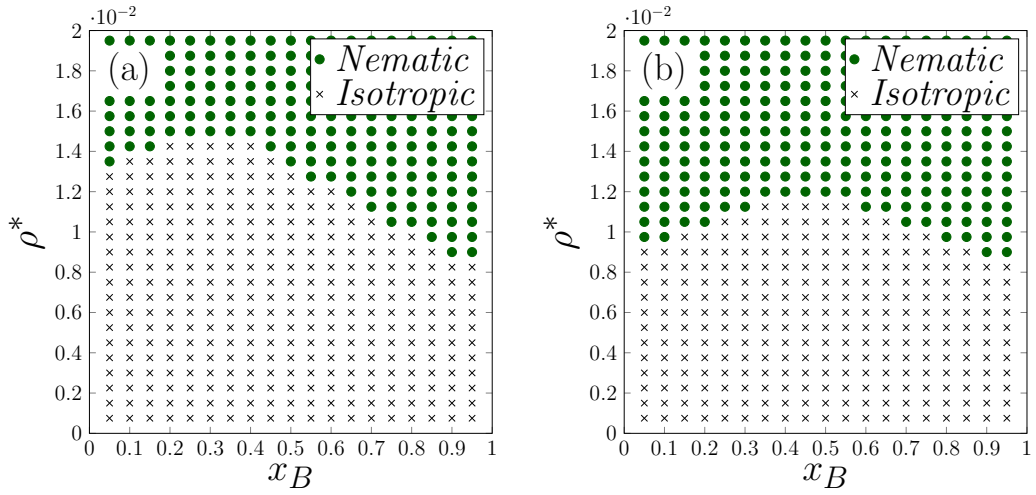

(a) $\kappa_A = 20\,, \quad \kappa_B = 25\,.$ (b) $\kappa_A = 24\,, \quad \kappa_B = 25\,.$

Figure 5.3: State diagrams for a mixture of long and short hard spherocylinders with uniaxial ordering. The nematic ordering is marked with (•), whereas $(\times)$ denotes an isotropic state. In the limit where $x_B = 0$ these diagrams coincide with the one component results portrayed in Fig, (5.2).

before, in order to calculate full phase diagrams, including first–order coexistence regions in density space, one would have to consider the full free energy given in equations (3.47–3.50). Here we restricted ourselves to computing orientational state diagrams of the binary mixture by minimizing the orientational part of the free energy, $\mathscr{F}^{or}$, with respect to the uniaxial order parameters q^A and q^B. The *state* diagrams hereby presented are evaluated in the plane spanned by the total density $\rho^* = Nd^3/V$ and concentration $x_\alpha = N_\alpha/\mathcal{N}$ (such that $\rho^*_\alpha = \mathcal{N}d^3x_\alpha/V = \rho^* x_\alpha$ is the density of component α). We focus on two mixtures characterized by aspect ratios also occurring in real systems [16].

The methodology is the following. Using a standard Newton–Raphson minimization algorithm, we search for values of q^A and q^B corresponding to minima of $\mathscr{F}^{or}$. We then evaluate the orientational free energy at these points and determine the minimum value, $\min\{\mathscr{F}^{or}\}$. In the case that $\min\{\mathscr{F}^{or}\} = 0$ the isotropic phase is stable whereas if $\min\{\mathscr{F}^{or}\} \neq 0$ a nematic state exists. The result of this procedure is shown in Fig. 5.3.

In both diagrams, Figs. 5.3.(a) and (5.3.(b), we see that for relatively low densities, $\rho^* \sim 0.005$, the isotropic state is stable for all concentrations. As the total density of the system increases, the isotropic phase becomes unstable with respect to the nematic, and for sufficiently high densities, $\rho^* \sim 0.020$, the system is in the nematic state irrespective of the concentration.

As expected, the mole fraction of long spherocylinders plays an important role for the location of the transition. This is observed by focusing on a constant density value, $\rho^* \sim 0.010$ in Fig. 5.3.(b). For $x_B = 0.2$ the nematic phase does not exist, but as x_B increases, $x_B = 0.8$, the nematic state appears. In the limiting case where $x_B = 0$ the results coincide with the one component system presented in Fig. 5.2.

Clearly, it would be very interesting to compare the equilibrium behavior found here to that of real systems. However, to our knowledge, experimental results have only be reported on binary mixtures of fd–viruses with *equal* length and *different* diameters [16]. This is different from the mixture of rods with different lengths and equal diameters considered in Fig. 5.3. One could apply the present theory also to the case of hard spherocylinders of equal length and different diameters only by re-scaling the number densities by the length (instead of the diameter) of the particles and recalculating the excluded volume coefficients in equations (5.21–5.25).

5.2.3 Scaled free energy

Here we make emphasis on the case of different length with the final motivation of analyze and characterize of the non–equilibrium behavior of rod–disk mixtures such as (models of) blood [44]. However, for the subsequent analysis of sheared systems it is convenient to re–write Eq. (5.17) into a dimensionless form using an appropriate scaling of the free energy. In principle, different scalings are possible. Here we follow the strategy used in earlier studies [57, 80, 23, 22] of one–component systems.

To develop a proper scaling, let us introduce the scaled alignment tensors, $\tilde{\mathbf{Q}}^\alpha$ and the scaled free energy, $\mathscr{F}^{or}_{ref}$, given by

$$\tilde{\mathbf{Q}}^\alpha = \frac{\mathbf{Q}^\alpha}{q_0^\alpha} \quad \text{and} \quad \tilde{\mathscr{F}}^{or} = \frac{\mathscr{F}^{or}}{\mathscr{F}^{or}_{ref}} \tag{5.30}$$

where q_0^α is the coexistence value of the uniaxial order parameter of the corresponding one–component system given in Eq. (5.29), and $\mathscr{F}^{or}_{ref} = 2\,C_{AB}\left(q_0^A q_0^B\right)^2$. In the latter expression, C_{AB} is the coupling coefficient of the fourth–order term $(\mathbf{Q}^A : \mathbf{Q}^B)^2$ of the free energy (5.17).

To simplify the expression for the scaled free energy resulting from inserting Eq. (5.30) into Eq. (5.17), we make the following assumptions. First, we set the coefficients B_α and C_α [see equations (5.19) and (5.20), respectively] equal to their (positive) values at I–N coexistence of the one–component system, that is,

$$B_\alpha = B_\alpha(\rho^*_{\alpha_{IN}}) \quad \text{and} \quad C_\alpha = C_\alpha(\rho^*_{\alpha_{IN}}, \kappa_\alpha)\,, \tag{5.31}$$

where the densities $\rho^*_{\alpha_{IN}}$ are calculated by solving Eq. (5.31). Thus, we henceforth neglect changes of B_α and C_α with ρ_α. We further suppose that the fourth–order

coefficient of the one–component system, C_A and C_B, are related to C_{AB} via

$$C_{AB} = C_A \left(\frac{q_0^A}{q_0^B}\right)^2 = C_B \left(\frac{q_0^B}{q_0^A}\right)^2 . \tag{5.32}$$

Equation (5.32) implies that for given values of κ_α and ρ_α^*, $|C_{AB}^2 - C_A C_B| = 0$. To test this assumption for a representative example, we consider a binary mixture in the nematic state ($\rho^* = 0.002$) where 30% of the particles have an aspect ratio $\kappa_A = 20$ and the others have an aspect ratio $\kappa_B = 25$. In this case we find $|C_{AB}^2 - C_A C_B| \approx 3.79 \times 10^{-7}$, which makes our ansatz plausible.

With the simplifications (5.31–5.32), the scaled version of the orientational free energy [see Eq. (5.17)] becomes

$$\begin{aligned}\tilde{\mathscr{F}}^{or}[\tilde{\mathbf{Q}}^A, \tilde{\mathbf{Q}}^B] = \sum_{\alpha=A}^{B} \Big\{ \frac{\Theta_\alpha}{2}(\tilde{\mathbf{Q}}^\alpha : \tilde{\mathbf{Q}}^\alpha) - \sqrt{6}\,\mathrm{Tr}(\tilde{\mathbf{Q}}^\alpha \cdot \tilde{\mathbf{Q}}^\alpha \cdot \tilde{\mathbf{Q}}^\alpha) + \frac{1}{2}(\tilde{\mathbf{Q}}^\alpha : \tilde{\mathbf{Q}}^\alpha)^2 \Big\} \\ - \frac{\Theta_{AB}}{2}(\tilde{\mathbf{Q}}^A : \tilde{\mathbf{Q}}^B) - \frac{1}{2}(\tilde{\mathbf{Q}}^A : \tilde{\mathbf{Q}}^B)^2 .\end{aligned} \tag{5.33}$$

In Eq. (5.33), the coefficients Θ_α of the second–orders term are given by

$$\Theta_\alpha = 24 \frac{A_\alpha(\rho_\alpha^*, \kappa_\alpha) C_\alpha(\rho_{\alpha_{IN}}^*, \kappa_\alpha)}{B_\alpha(\rho_{\alpha_{IN}}^*)^2} = \frac{A_\alpha(\rho_\alpha^*, \kappa_\alpha)}{A_{IN}(\rho_{\alpha_{IN}}^*, \kappa_\alpha)} , \tag{5.34}$$

which shows the explicit dependence of Θ_α on the composition (that is, on ρ_α) and κ. The remaining coefficient Θ_{AB} is a positive quantity which is depends not on the composition, but only on the aspect ratios. Explicitly,

$$\Theta_{AB} = \frac{9\left[\frac{5\pi^2}{64} - \frac{5\pi}{24}(\kappa_A + \kappa_B) + \frac{5\pi}{32}\kappa_A\kappa_B\right]}{5\left[\frac{9\pi^2}{512} + \frac{\pi}{80}(\kappa_A + \kappa_B) + \frac{9\pi}{256}\kappa_A\kappa_B\right] q_0^A q_0^B} . \tag{5.35}$$

In the limiting case of the one–component system, the scaled free energy (5.33) reduces to the corresponding expression given in [57, 80, 23, 22].

Analysis of the scaled free energy

To better understand the properties of the scaled free energy we consider, first, the explicit density dependence of the coefficients Θ_α appearing in front of the quadratic powers of $\tilde{\mathbf{Q}}^\alpha$ [see Eq. (5.34)]. As an illustration, we show in 5.4 numerical results for an equimolar binary mixture and three values of the aspect ratio (note that each Θ_α depends only on κ_α).

In Fig. 5.4, one observes the same qualitative behavior irrespective of the actual value of κ: the coefficient Θ_α first increases with density and then reaches a maximum, after which it monotonically decreases and changes sign from positive to negative. This change of sign is expected (within the Landau picture) for a system displaying a phase transition. The corresponding density is the smaller, the larger κ.

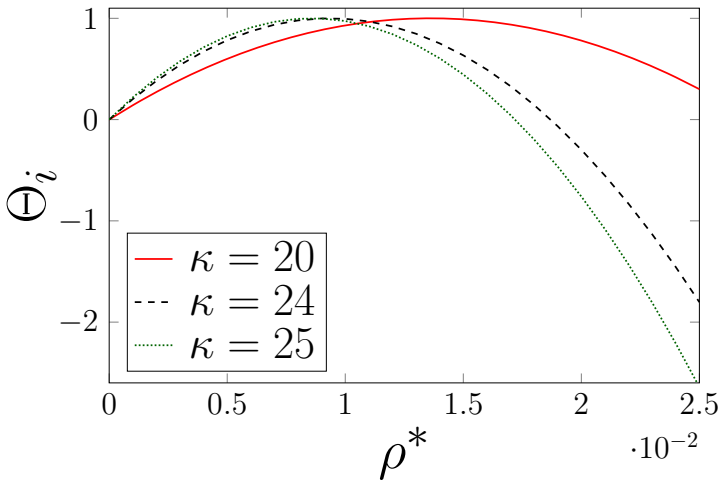

Figure 5.4: Relation of Θ_α versus the reduced density, given by Eq. (5.34), for equimolar binary mixtures ($x_A = x_B = 0.5$) and different aspect ratio. The coexistence densities $\rho^*_{\alpha_{IN}}$ are given by the roots of Eq. (5.31).

To examine the relation between the sign of Θ_α and the mixture's stability, we consider the case of uniaxial order. In this case 5.33 reduces to

$$\tilde{\mathscr{F}}^{or}_{uni} = \sum_{\alpha=A}^{B} \{\frac{\Theta_\alpha}{2}\tilde{q}_\alpha^2 - \tilde{q}_\alpha^3 + \frac{1}{2}\tilde{q}_\alpha^4\} - \frac{\Theta_{AB}}{2}\tilde{q}_A\tilde{q}_B - \frac{1}{2}\tilde{q}_A^2\tilde{q}_B^2\,, \tag{5.36}$$

where $\tilde{q}_\alpha = q_\alpha/q_0^\alpha$. The stability of a minimum $\tilde{\mathbf{q}}$ can be determined using the Hessian matrix [122, 130] given by

$$H(\tilde{q}_A, \tilde{q}_B) = \begin{pmatrix} \Theta_A - 6\tilde{q}_A + 6\tilde{q}_A^2 - \tilde{q}_B^2 & -\frac{\Theta_{AB}}{2} - 2\tilde{q}_A\tilde{q}_B \\ -\frac{\Theta_{AB}}{2} - 2\tilde{q}_A\tilde{q}_B & \Theta_B - 6\tilde{q}_B + 6\tilde{q}_B^2 - \tilde{q}_A^2 \end{pmatrix} \tag{5.37}$$

evaluated of the minimum. We now focus on the stability of the isotropic state, $\tilde{\mathbf{q}}_t = (0,0)$. Stability then requires that the two eigenvalues or, alternatively, the two diagonal elements Θ_α and the determinant

$$\det[H(\tilde{\mathbf{q}}_t)] = \Theta_A\Theta_B - \frac{\Theta_{AB}^2}{4} > 0, \tag{5.38}$$

are positive (where we recall that Θ_{AB} is a positive quantity). An illustration of the regions of stability of the isotropic phase in the Θ_A–Θ_B plane at fixed Θ_{AB} is portrayed in Fig. 5.5.

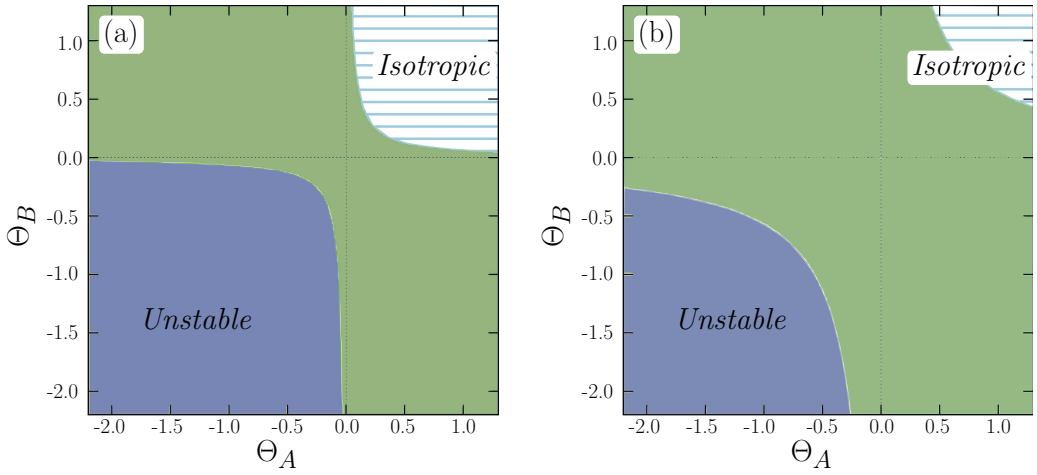

Figure 5.5: Stability regions of the isotropic state ($\tilde{\mathbf{q}}_t = (0,0)$) according to (5.38). The values of Θ_{AB} are (a) $\Theta_{AB} = 0.50$ and (b) $\Theta_{AB} = 1.50$.

From Fig. 5.5 we notice that $\tilde{\mathbf{q}}_t$ is locally stable for $\Theta_A, \Theta_B \gtrsim 0.5$ and locally unstable for $\Theta_A, \Theta_B \lesssim 0.5$. This areas are marked by the white striped and solid blue portions, respectively. The center solid green area denotes values where (5.38) is negative and thus $\tilde{\mathbf{q}}_t$ is locally meta stable. The larger Θ_{AB}, the smaller is the region where the isotropic state is a minimum of the free energy.

It seems straightforward to repeat the same analysis for free energy minima corresponding to nematic states ($q_A \neq 0$, $q_B \neq 0$). However, in that context we face a problem already discussed in the context of one–component systems [63, 61], which concerns the *bounds* of possible values. This can be seen as follows: The order parameters q_A and q_B are related to the Maier–Saupe order parameter S_2 by $q_\alpha = \sqrt{5} S_2$ [22].

Since S_2 is defined within the range $-1/2 \leq S_2 \leq 1$. The bounds of the corresponding scaled order parameters, q_A and q_B, involve the factor $1/q_0^\alpha$. Using Eq. (5.32) and the values of the coexisting densities $\rho^*_{\alpha_{IN}}$ given by the roots of Eq. (5.31), we find that the scaled order parameters are defined in the range

$$-1.30 \lesssim q_\alpha \lesssim 2.60\,. \tag{5.39}$$

However, free minimization of the scaled free energy Eq. (5.33) does not automatically respect these bounds; rather it yields, for a range of parameters, nematic minima outside the allowed domain. To solve this problem, one could consider an "amended" version of the free energy, similar to what has been done for one–component systems [63, 61]. However, this would go beyond the scope of the present work.

Given the simplifications involved in our scaling of the free energy, another question that arises is to which extent the stability conditions for the isotropic phase found here

ρ^* (10^{-2})	Fig. 5.3.(a) Θ_α $\kappa_A = 20$	$\kappa_B = 25$	Fig. 5.3.(b) Θ_α $\kappa_A = 24$	$\kappa_B = 25$	Eq. (5.38) $det[H(\tilde{\mathbf{q}}_t)]$	
0.50	0.599	0.825	0.783	0.825	+	*Isotropic*
1.00	0.929	0.973	0.995	0.973	+	*Isotropic*
1.75	0.918	-0.073	0.239	-0.073	-	*Unstable*
2.00	0.779	-0.759	-0.298	-0.759	-	*Unstable*
	$\Theta_{AB} = 1.203$		$\Theta_{AB} = 1.223$			

Table 5.1: Numerical values of the constants Θ_A, Θ_B and Θ_{AB} for equimolar binary mixtures ($x_A = x_B = 0.5$). This values correspond to different points in the phase diagrams in figures 5.3(a–b) and are calculated using Eq. (5.34) and Eq. (5.35).

are consistent with our earlier results obtained by minimization of the unscaled free energy [see Fig. 5.3]. To solve this, in Table (5.1) we summarize a simple evaluation of the quantities Θ_α for several state points in the diagrams plotted in Fig. 5.3, which shows consistency of unscaled and scaled free energy.

5.3 Elastic energy

In this section we turn to the elastic energy of the binary mixture. As mentioned at the end of Chapter 4 the difference between the mesoscopic free energy for homogeneous systems (4.64) and the one for inhomogeneous systems (4.65) is that in the later terms of gradients of the alignment tensor $\mathbf{Q}$ are taken into account. These additional terms correspond to the so–called elastic free energy or distortion free energy, $\mathcal{F}_e^{or}[\nabla \boldsymbol{Q}]$. Focusing on this contribution we have

$$\mathcal{F}_e^{or} = \mathcal{D}_{AA}\big(\nabla \boldsymbol{Q}^A \odot \nabla \boldsymbol{Q}^A\big) + \mathcal{D}_{BB}\big(\nabla \boldsymbol{Q}^B \odot \nabla \boldsymbol{Q}^B\big) + \mathcal{D}_{AB}\big(\nabla \boldsymbol{Q}^A \odot \nabla \boldsymbol{Q}^B\big)\,, \quad (5.40)$$

where the $\mathcal{D}_{\alpha\beta}$ coefficients are given by

$$\mathcal{D}_{AA} = \frac{\rho_A^2}{4\pi}\mathcal{M}_2^{AA}\,, \quad \mathcal{D}_{BB} = \frac{\rho_B^2}{4\pi}\mathcal{M}_2^{BB} \quad \text{and} \quad \mathcal{D}_{AB} = \frac{\rho_A \rho_B}{4\pi}\mathcal{M}_2^{AB}\,. \quad (5.41)$$

and $\mathcal{M}_2^{\alpha\beta}$ are the moments of the direct pair correlation function [see Chapter 4]:

$$\mathcal{M}_2^{\alpha\beta} = \frac{1}{(2\pi)^{3/2}} \int_V d\mathbf{x}\; \bar{c}_{\alpha\beta}^{(2)}(\mathbf{x})\,|\mathbf{x}|^2\,.$$

5.3.1 Oseen–Frank theory

As mentioned in Chapter 2, the Landau–de Gennes theory [19] couples phenomenological elastic coefficients L with the well known Frank elastic constants K_{ij}. In the one–constant approximation [19] this relation is given by

$$L = \frac{1}{2S_{eq}^2} K \,, \tag{5.42}$$

where S_{eq} is the equilibrium uniaxial order parameter of the single component fluid [81]. In analogy with this we propose that

$$\mathcal{D}_{\alpha\beta} = \frac{1}{4\, q_0^{\alpha}\, q_0^{\beta}} K^{\alpha\beta} \,, \tag{5.43}$$

where q_0^{α} is the coexistence value of the uniaxial order parameter in Eq. (5.29). Substitution of Eq. (5.41) in Eq. (5.43) leads to

$$K^{\alpha\beta} = \frac{\rho_\alpha \rho_\beta}{4\pi} \frac{q_0^{\alpha}\, q_0^{\beta}}{(2\pi)^{3/2}} \int\limits_V d\mathbf{x}\; \bar{c}^{(2)}_{\alpha\beta}(\mathbf{x})\, |\mathbf{x}|^2 \,, \tag{5.44}$$

Doing so, we obtained the Frank elastic constants $K^{\alpha\beta}$ of the binary mixture in the one–constant approximation. Comparing to previous studies (see e.g. Refs. [41, 32] and references therein) the aforementioned elastic constants are given in terms of the direct pair correlation function measured in the isotropic phase and the coexistence values of the uniaxial order parameter of the one component fluid, instead of the direct pair correlation function of the undistorted nematic phase [41, 32]. As it is, Eq. (5.44) is an approximation that relates weak distortions of the nematic phase to the the isotropic fluid.

As a further simplification, as before, we may assume that the diameter of the molecules is such that $d_\alpha = d_\beta = d$, we may write the dimensionless elastic energy $\mathscr{F}_e^{or}$ in terms of the reduced densities $\rho_\alpha^* = \rho_\alpha d^3$ viz:

$$\mathscr{F}_e^{or} = \frac{\xi_{AA}^2}{2}\left(\nabla \boldsymbol{Q}^A \odot \nabla \boldsymbol{Q}^A\right) + \frac{\xi_{BB}^2}{2}\left(\nabla \boldsymbol{Q}^B \odot \nabla \boldsymbol{Q}^B\right) + \frac{\xi_{AB}^2}{2}\left(\nabla \boldsymbol{Q}^A \odot \nabla \boldsymbol{Q}^B\right), \tag{5.45}$$

where $\xi_{\alpha\beta}$ are the elastic correlation length coefficients given in terms of the Frank elastic constants as

$$\xi_{\alpha\beta}^2 = \frac{K^{\alpha\beta}}{2 q_0^{\alpha}\, q_0^{\beta}\, d^3} \,. \tag{5.46}$$

In general $\xi_{\alpha\beta}$ is given in terms of the *pitch* of the cholesteric which determines the typical length scale associated to the helical periodicity. The pitch length is normally on the order of hundreds or thousands times the particle length. However, a unified picture which links microscopic and macroscopic chirality is still to be achieved since it is clear that the relation between pitch and elastic constants depends on both the single-particle properties and the thermodynamic state of the system [131].

5.4 Summary

In this chapter we developed a theory suitable for the description of isotropic and nematic phases of binary mixtures of hard spherocylinders in thermodynamic equilibrium. We started from the general expressions of the mesoscopic theory obtained in Chapter 4 and specialize our description to the semi–dilute regime reaching similar expressions to the well–known Landau–de Gennes theory. The resulting expression for the orientational free energy is then:

$$\begin{aligned}\mathscr{F}^{or} = &\sum_{\alpha=A}^{B}\Big\{A_\alpha(\mathbf{Q}^\alpha:\mathbf{Q}^\alpha) - B_\alpha \mathsf{Tr}(\mathbf{Q}^\alpha\cdot\mathbf{Q}^\alpha\cdot\mathbf{Q}^\alpha) + C_\alpha(\mathbf{Q}^\alpha:\mathbf{Q}^\alpha)^2\Big\}\\ &- A_{AB}(\mathbf{Q}^A:\mathbf{Q}^B) - C_{AB}(\mathbf{Q}^A:\mathbf{Q}^B)^2\,,\end{aligned}$$

where the coefficients A_α, B_α, ρ_α, A_{AB} and C_{AB} are

$$\begin{aligned}A_\alpha &= \frac{1}{2}\rho_\alpha^* - \frac{1}{10}\rho_\alpha^{*2}\left(\frac{5\pi^2}{64} - \frac{5\pi}{12}\kappa_\alpha + \frac{5\pi}{16}\kappa_\alpha^2\right)G_{\alpha\alpha}\,,\\ B_\alpha &= \frac{\sqrt{30}}{21}\rho_\alpha^*\\ C_\alpha &= \frac{19}{28}\rho_\alpha^* - \frac{1}{18}\rho_\alpha^{*2}\left(\frac{9\pi^2}{512} + \frac{\pi}{40}\kappa_\alpha + \frac{9\pi}{128}\kappa_\alpha^2\right)G_{\alpha\alpha}\,,\\ A_{AB} &= \frac{1}{5}\rho_A^*\rho_B^*\left(\frac{5\pi^2}{64} - \frac{5\pi}{24}(\kappa_A+\kappa_B) + \frac{5\pi}{32}\kappa_A\kappa_B\right)G_{AB}\,,\\ C_{AB} &= \frac{1}{9}\rho_A^*\rho_B^*\left(\frac{9\pi^2}{512} + \frac{\pi}{80}(\kappa_A+\kappa_B) + \frac{9\pi}{256}\kappa_A\kappa_B\right)G_{AB}\,.\end{aligned}$$

To validate our theory, we further analyze mixtures characterized by molecules having equal diameters and different length as in Ref. [14] (opposed to the experimental realizations of "thick–thin" mixtures of *fd*–viruses having equal length and different diameters [16]). Our numerical calculations show that even for the one–component system, there is an reasonable agreement with the coexistence densities obtained by Gibbs ensemble simulations [108]. In case of binary mixtures we did not resolve a full phase diagram of the system. However, we calculate a state diagram which can be use to give some predictions of the overall behavior of the mixture.

At the end of this chapter we briefly discuss the Oseen–Frank elastic theory and its relation with the mesoscopic free energy density of distortion for a binary mixture. We show how after a simple assumption it is possible to write an expression similar to the well–known Frank elastic constants in terms of the direct correlation function. The resulting expression is given in of gradients of $\mathbf{Q}$ viz

$$\mathscr{F}_e^{or}[\nabla\boldsymbol{Q}] = \frac{\xi_{AA}^2}{2}\big(\nabla\boldsymbol{Q}^A\odot\nabla\boldsymbol{Q}^A\big) + \frac{\xi_{BB}^2}{2}\big(\nabla\boldsymbol{Q}^B\odot\nabla\boldsymbol{Q}^B\big) + \frac{\xi_{AB}^2}{2}\big(\nabla\boldsymbol{Q}^A\odot\nabla\boldsymbol{Q}^B\big)\,,$$

where $\xi_{\alpha\beta}$ are the elastic correlation lengths

$$\xi^2_{\alpha\beta} = \frac{K^{\alpha\beta}}{2q_0^\alpha\, q_0^\beta\, d^3} \quad \text{where} \quad K^{\alpha\beta} = \frac{\rho^*_\alpha \rho^*_\beta}{4\pi} \frac{q_0^\alpha\, q_0^\beta}{(2\pi)^{3/2}} \int\limits_V d\mathbf{x}\; \bar{c}^{(2)}_{\alpha\beta}(\mathbf{x})\, |\mathbf{x}|^2$$

where $K^{\alpha\beta}$ are the Frank elastic coefficients of the weakly distorted nematic phase. As in the case of homogeneous systems, this relation may be used to further characterize the material and to provide a first approximation to link between microscopic and macroscopic chirality. However, we should point out that at this level of simplification the material is only defined by a small number of quantities which may not be enough to fully parametrize any material.

Chapter 6

Dynamic equations and constitutive relations for binary mixtures

The non–equilibrium phenomena associated with the molecular orientation of anisotropic fluids is coupled with the exchange of mass, energy and momentum. However, due to its molecular structure, a proper description of their dynamic properties requires a measure of the rotational degrees of freedom of the molecules. Such description can be done in different levels: in terms of single–particle models where each particle is described by the set $\{\mathbf{r}_i(t), \phi_i(t)\}$ (Jeffery orbits [132]); in terms of probability distribution functions $p(\mathbf{r}, \phi, t)$ (Fokker–Planck equation [80, 133], Dynamical Density Functional theory [100, 134]); or, in terms of the evolution of macroscopic variables, like the nematic director $\mathbf{n}(\mathbf{r}, t)$ (Ericksen–Leslie theory [135, 136]) or the alignment tensor $\mathbf{Q}(\mathbf{r}, t)$ (Doi–Hess theory [57, 137]). In this chapter we aim to extend the later description for binary mixtures employing our equilibrium theory and the basic concepts of linear irreversible thermodynamics.

6.1 General remarks

The Doi–Hess theory [57, 80] of irreversible processes in liquid crystals is based on the local equilibrium hypothesis. This hypothesis states that all equilibrium thermodynamic relations are valid for the thermodynamic variables assigned to an elemental volume [138]. Thus, individual molecules are ignored and the fluid consists of continuous matter. Hence, all thermodynamic variables like temperature, internal energy U and

entropy S are given in terms of *field variables*, *i.e.*,

$$T = T(\vec{r},t)\,, \quad U(t) = \int_V \varrho\, u(\vec{r},t) dV\,, \quad S(t) = \int_V \varrho\, s(\vec{r},t) dV\,, \tag{6.1}$$

where ϱ is the mass density of the fluid and the field variables $u(\vec{r},t)$, $s(\vec{r},t)$ are the specific internal energy and entropy, respectively. Consequently, the thermodynamics of irreversible processes is a continuum theory treating the state parameters of the system as field variables [105, 139].

For fluids with internal degrees of freedom the general assumption of the Doi–Hess theory [57, 80] is that the thermodynamic functions, such as specific internal energy, specific volume and specific entropy, depend on the alignment. Further, these quantities may be decomposed in two parts: one that is independent on the alignment (0) and the other which vanishes in the absence of it (a). Thus,

$$u = u_0 + u_a(\mathbf{Q})\,, \quad \varrho^{-1} = \varrho_0^{-1} + \varrho_a^{-1}(\mathbf{Q})\,, \quad s = s_0 + s_a(\mathbf{Q})\,. \tag{6.2}$$

Under this assumption the Gibbs fundamental relation [57] is

$$Tds = du + pd\varrho^{-1} - \left(\frac{\partial\, g_a(\mathbf{Q})}{\partial \mathbf{Q}}\right) d\mathbf{Q}\,, \tag{6.3}$$

where $g_a(\mathbf{Q})$ is the specific Gibbs free energy associated with the alignment

$$g_a = u_a + p\varrho_a^{-1} - Ts_a\,. \tag{6.4}$$

Commonly, g_a is associated with the alignment tensor and its gradients [57],

$$g_a = g_a(\mathbf{Q}, \nabla\mathbf{Q})\,. \tag{6.5}$$

6.2 Extension to binary mixtures

In order to extend the treatment of irreversible thermodynamics to a binary mixture several modifications of the standard theory are needed [1]. First, we assume that we have an homogeneously mixed system, *i.e.* every element of volume has the same mass density $\varrho = m/V$ where m is the mass of the mixture.

Firstly, in the standard theory [57, 23], the Gibbs free energy of alignment is given by a dimensionless form of the sum of the Landau–de Gennes potential (2.17) with the energy of distortion (2.23) [see Chapter 2] with a proportionality factor. For the binary mixture we assume that $g_a(\mathbf{Q}, \nabla\mathbf{Q})$ is given in terms of the free energy density functional $\mathscr{F}^{or}[\mathbf{Q}, \nabla\mathbf{Q}] = \mathscr{F}^{or}[\mathbf{Q}] + \mathscr{F}_e^{or}[\nabla\mathbf{Q}]$,

$$g_a(\mathbf{Q}, \nabla\mathbf{Q}) = \frac{k_B T}{m} \mathscr{F}^{or}[\mathbf{Q}, \nabla\mathbf{Q}]\,. \tag{6.6}$$

[1] For an alternative derivation, please refer to Henning Reinken's Master's thesis [71].

where $\mathscr{F}^{or}$ and $\mathscr{F}_e^{or}$ are given by

$$\mathscr{F}^{or}[\boldsymbol{Q}] = \sum_{\alpha=A}^{B}\Big\{A_\alpha(\mathbf{Q}^\alpha:\mathbf{Q}^\alpha) - B_\alpha \mathsf{Tr}(\mathbf{Q}^\alpha\cdot\mathbf{Q}^\alpha\cdot\mathbf{Q}^\alpha) + C_(\mathbf{Q}^\alpha:\mathbf{Q}^\alpha)^2\Big\} - A_{AB}(\mathbf{Q}^A:\mathbf{Q}^B) - C_{AB}(\mathbf{Q}^A:\mathbf{Q}^B)^2\,, \tag{6.7}$$

$$\mathscr{F}_e^{or}[\nabla\boldsymbol{Q}] = \frac{\xi_{AA}^2}{2}\left(\nabla\boldsymbol{Q}^A\odot\nabla\boldsymbol{Q}^A\right) + \frac{\xi_{BB}^2}{2}\left(\nabla\boldsymbol{Q}^B\odot\nabla\boldsymbol{Q}^B\right), \tag{6.8}$$

where A_α, B_α, ρ_α, A_{AB} and C_{AB} are given by Eqs. (5.18)–(5.22) in the semi–dilute regime [see Chapter 5 Sect. 5.2] and $\xi_{\alpha\alpha}^2$ by Eq. (5.46). Notice that in Eq. (6.8) terms carrying the coupling $\left(\nabla\boldsymbol{Q}^A\odot\nabla\boldsymbol{Q}^B\right)$ are not taken into account. This might corresponds to weak distortions of the coexisting nematic state. This assumption is similar to the one adopted in Ref. [133] which is based in the mean field potential approximation. Thus, the coupling between component A and component B is only carried out through terms containing the products $(\mathbf{Q}^A:\mathbf{Q}^B)$ appearing in Eq. (6.7).

Finally, from Eq. (6.6), taking into account the concentration x_α (μ_α chemical potential) of the components in the mixture, the Gibbs fundamental relation (6.3) for the binary mixture is

$$Tds = du + pd\varrho^{-1} + \sum_{\alpha=A}^{B}\mu_\alpha dx_\alpha - \frac{k_BT}{m}\sum_{\alpha=A}^{B}\frac{\partial\mathscr{F}^{or}[\mathbf{Q},\nabla\mathbf{Q}]}{\partial\mathbf{Q}^\alpha}d\mathbf{Q}^\alpha\,. \tag{6.9}$$

6.2.1 Gibbs fundamental relation

In the non–equilibrium situation, the thermodynamic variables are functions of time and thus the Gibbs fundamental relation becomes [57]

$$T\frac{ds}{dt} = \frac{du}{dt} + p\frac{d\varrho^{-1}}{dt} + \sum_{\alpha=A}^{B}\mu_\alpha\frac{dx_\alpha}{dt} - \frac{k_BT}{m}\sum_{\alpha=A}^{B}\frac{\partial\mathscr{F}^{or}}{\partial\mathbf{Q}^\alpha}\frac{d\mathbf{Q}^\alpha}{dt}\,. \tag{6.10}$$

The quantities $d\mathcal{A}/dt$ are known as *thermodynamic fluxes* and measure the rate of change of $\mathcal{A}$ due to the different transport processes occurring in the system. To link transport processes with thermodynamic fluxes a set of constitutive equations is needed. For example, disregarding spatial inhomogeneities, one of the simplest (non–trivial) constitutive equations for the alignment tensors is

$$\frac{d\mathbf{Q}^\alpha}{dt} = -\tau_\alpha\mathbf{Q}^\alpha\,, \tag{6.11}$$

where τ_α is the relaxation time of the alignment of the system towards equilibrium. This equation describes the simple exponential relaxation of the alignment of component α in the absence of orienting fields or flows. However, Eq. (6.11) is an oversimplified assumption and in reality it may be more complicated depending on the effects of flow or external fields.

6.2.2 Conservation laws and balance equation

From the standpoint of the theory of irreversible processes, the constitutive equations are obtained from local conservation laws, particularly conservation of mass, momentum, internal energy and angular momentum). In isothermal conditions the conservation of mass, momentum and internal energy for the mixture are:

$$\varrho \frac{dx_\alpha}{dt} + \nabla \cdot \mathbf{J}_\alpha = 0\,, \tag{6.12}$$

$$\varrho \frac{d\mathbf{v}}{dt} - \nabla \cdot \mathbf{T}^{tot} = 0\,, \tag{6.13}$$

$$\varrho \frac{du}{dt} - \mathbf{T}^{tot} : \nabla \mathbf{v} = 0\,. \tag{6.14}$$

As it is common in continuum theories, d/dt denotes the material derivative given by

$$\frac{d}{dt} \equiv \frac{\partial}{\partial t} + \mathbf{v} \cdot \nabla\,. \tag{6.15}$$

In Eqs. (6.12)–(6.14) $\mathbf{v}(\mathbf{r}, t)$ is the flow velocity, $\mathbf{T}^{tot}$ is the total stress tensor and $\mathbf{J}_\alpha$ is the diffusion flux of the component α with concentration x_α.

A key quantity used for the study of the hydrodynamic properties of the mixture is the stress tensor $\mathbf{T}^{tot}$. The total stress tensor can be written as

$$\mathbf{T}^{tot} = -p\,\alpha + \mathbf{T}^{asy} + \overline{\mathbf{T}}\,, \tag{6.16}$$

where the first term represents the (isotropic) hydrostatic pressure and the two other terms describe flow–induced effects [57]. The antisymmetric part of the stress tensor, $\mathbf{T}^{asy}$, relates the angular momentum of the particles with the velocity field $\mathbf{v}$. For liquid crystals (and other colloidal systems) the angular relaxation times are much smaller than the collective orientational order relaxation rate [140] and therefore $\mathbf{T}^{asy}$ is usually set to zero. In fact, in Newtonian flow regimes $\mathbf{T}^{asy}$ naturally vanishes [22, 63]. However, as we will see in the following section, the remaining contribution of the stress tensor $\overline{\mathbf{T}}$ does not vanish and in fact is associated with the alignment tensors $\mathbf{Q}^\alpha$.

The time dependence of the alignment tensors $\mathbf{Q}^\alpha$ is described by balance equations which couple the dynamics of the alignment with the velocity field $\mathbf{v}$. Following the ansatz of Hess–Pereira [57, 58] and disregarding non–convective flow of alignment we assume

$$\frac{d\mathbf{Q}^\alpha}{dt} = 2\,\overline{\Omega \cdot \mathbf{Q}^\alpha} + 2\sigma\,\overline{\Gamma \cdot \mathbf{Q}^\alpha} + \left(\frac{\delta \mathbf{Q}^\alpha}{\delta t}\right)_{\text{irr}}\,, \tag{6.17}$$

where $\mathbf{\Omega} = (1/2)(\nabla \mathbf{v}^T - \nabla \mathbf{v})$ and $\mathbf{\Gamma} = (1/2)(\nabla \mathbf{v}^T + \nabla \mathbf{v})$ are the flow vorticity and deformation, respectively. In Eq. (6.17), $(\delta \mathbf{Q}^\alpha / \delta t)_{\text{irr}}$ represents the production and decay of alignment due to irreversible processes [57, 23, 58].

Finally, for the theory of non–equilibrium thermodynamics the so–called balance equation for the entropy plays a central role. This equation reads:

$$\varrho \frac{ds}{dt} + \nabla \cdot \mathbf{J}_s = \left(\frac{\delta s}{\delta t}\right)_{\text{irr}} \geq 0\,. \tag{6.18}$$

Equation (6.18) expresses the fact that the entropy of a volume element changes in time for two reasons: it changes because entropy flows into the volume element with a rate $\mathbf{J}_s$; and because there is an entropy source due to irreversible phenomena inside the volume element, $(\delta s/\delta t)_{\text{irr}}$. The entropy production, $(\delta s/\delta t)_{\text{irr}}$, is always non–negative (Second law of thermodynamics) [139].

6.2.3 Entropy production and phenomenological equations

In order to find an explicit form of the entropy production in the volume element due to the hydrodynamic interactions and the decay or production of alignment we have to insert Eqs. (6.12)–(6.18) into the Gibbs fundamental relation (6.8). This yields

$$T\left(\frac{\delta s}{\delta t}\right)_{\text{irr}} = \left(\overline{\mathbf{T}} - 2\frac{\varrho}{m}k_B T\sigma \sum_{\alpha=A}^{B} \overline{\mathbf{Q}^\alpha \cdot \mathbf{\Psi}^\alpha}\right) : \mathbf{\Gamma} - \frac{\varrho}{m}k_B T \sum_{\alpha=A}^{B} \mathbf{\Psi}^\alpha : \left(\frac{\delta \mathbf{Q}^\alpha}{\delta t}\right)_{\text{irr}}, \tag{6.19}$$

where the second rank tensor $\mathbf{\Psi}^\alpha$ is given by [see Eqs. (6.7) and (6.8)]. The entropy production in (6.19) takes into account two processes which correspond to dissipative processes: viscous flow and production (decay) of alignment. Moreover, each of these terms contains a thermodynamic force–flux pair. In general, the choice of which quantity is a thermodynamic flux or force depends on their spatial and temporal symmetry. Considering that $\mathbf{\Gamma}$ and $(\delta \mathbf{Q}^\alpha/\delta t)_{\text{irr}}$ are not independent under time reversal it is convention to choose them as thermodynamic forces [58].

In the linear approximation [139] fluxes are proportional to the thermodynamic forces and thus, the entropy production (6.19) is a bi–linear expression in the fluxes and thermodynamic forces. Within this approximation we write the relation between fluxes and forces for the binary mixture as:

$$-\mathbf{\Psi}^A = \tau_A \left(\frac{\delta \mathbf{Q}^A}{\delta t}\right)_{\text{irr}} + \tau_{AB}\left(\frac{\delta \mathbf{Q}^B}{\delta t}\right)_{\text{irr}} + \sqrt{2}\tau_{Ap}\mathbf{\Gamma}\,, \tag{6.20}$$

$$-\mathbf{\Psi}^B = \tau_B \left(\frac{\delta \mathbf{Q}^B}{\delta t}\right)_{\text{irr}} + \tau_{AB}\left(\frac{\delta \mathbf{Q}^A}{\delta t}\right)_{\text{irr}} + \sqrt{2}\tau_{Bp}\mathbf{\Gamma}\,, \tag{6.21}$$

$$\left(\overline{\mathbf{T}} - 2\frac{\varrho}{m}k_B T\sigma \sum_{\alpha=A}^{B} \overline{\mathbf{Q}^\alpha \cdot \mathbf{\Psi}^\alpha}\right) = \left(\sqrt{2}\frac{\varrho}{m}k_B T\right)\left(\tau_{pA}\left(\frac{\delta \mathbf{Q}^B}{\delta t}\right)_{\text{irr}} + \tau_{pB}\left(\frac{\delta \mathbf{Q}^A}{\delta t}\right)_{\text{irr}} + \sqrt{2}\tau_p\mathbf{\Gamma}\right)\,. \tag{6.22}$$

In Eqs. (6.20)–(6.22) the phenomenological coefficients τ_x and have units of time. It is possible to write Eqs. (6.20)–(6.22) in a somewhat more transparent form as:

$$\begin{pmatrix} -\boldsymbol{\Psi}^A \\ -\boldsymbol{\Psi}^B \\ \overline{\mathbf{T}} - 2\frac{\varrho}{m}k_BT\sigma\sum_{\alpha=A}^{B}\overline{\mathbf{Q}^\alpha\cdot\boldsymbol{\Psi}^\alpha} \end{pmatrix} = \begin{pmatrix} \tau_A & \tau_{AB} & \tau_{Ap} \\ \tau_{BA} & \tau_B & \tau_{Bp} \\ \tau_{pA} & \tau_{pB} & \tau_p \end{pmatrix} \begin{pmatrix} \left(\frac{\delta\mathbf{Q}^A}{\delta t}\right)_{\text{irr}} \\ \left(\frac{\delta\mathbf{Q}^B}{\delta t}\right)_{\text{irr}} \\ 2\frac{\varrho}{m}k_BT\,\boldsymbol{\Gamma} \end{pmatrix}, \tag{6.23}$$

where we identify Onsager's matrix of phenomenological coefficients $\mathbb{L}$ which is

$$\mathbb{L} = \begin{pmatrix} \tau_A & \tau_{AB} & \tau_{Ap} \\ \tau_{BA} & \tau_B & \tau_{Bp} \\ \tau_{pA} & \tau_{pB} & \tau_p \end{pmatrix}. \tag{6.24}$$

According to Onsager's theorem $\mathbb{L}$ is a symmetric matrix [141] and thus the cross coupling coefficients obey the so–called Onsager's reciprocal relations

$$\tau_{Ap} = \tau_{pA}, \quad \tau_{Bp} = \tau_{pB} \quad \text{and} \quad \tau_{AB} = \tau_{BA}\,. \tag{6.25}$$

Since the production of entropy is always a non–negative quantity, a by–product of Onsager's theorem is that $\mathbb{L}$ should always be positive semi–definite matrix [141]. Thus the following relations exist between the coefficients of the phenomenological laws in Eqs. (6.20)–(6.22):

$$\tau_A > 0\,, \qquad \tau_B > 0\,, \qquad \tau_p > 0\,, \tag{6.26}$$

$$\tau_A\tau_B > \tau_{Ap}^2\,, \qquad \tau_B\tau_p > \tau_{Bp}^2\,, \qquad \tau_A\tau_B > \tau_{AB}^2\,, \tag{6.27}$$

$$\tau_A\tau_B\tau_p + 2\tau_{AB}\tau_{Ap}\tau_{Bp} > \tau_A\tau_{Bp}^2 + \tau_B\tau_{Ap}^2 + \tau_p\tau_{AB}^2\,. \tag{6.28}$$

As expected making $\tau_B = \tau_{AB} = \tau_{Bp} = 0$ results in the original phenomenological laws set by the standard Doi–Hess theory [57].

6.2.4 Complete dynamic equations

Using the subtraction method, the set of equations for the thermodynamic fluxes of alignment (6.20) and (6.21) can be written into

$$\left(\frac{\delta\mathbf{Q}^A}{\delta t}\right)_{\text{irr}} = \pi_A\boldsymbol{\Psi}^A + \pi_{AB}\boldsymbol{\Psi}^B + \pi_{Ap}\sqrt{2}\boldsymbol{\Gamma}\,, \tag{6.29}$$

$$\left(\frac{\delta\mathbf{Q}^B}{\delta t}\right)_{\text{irr}} = \pi_{AB}\boldsymbol{\Psi}^A + \pi_B\boldsymbol{\Psi}^B + \pi_{Bp}\sqrt{2}\boldsymbol{\Gamma}\,, \tag{6.30}$$

where the coupling coefficients π_x have units of time^{-1} and are given in terms of the relaxation times τ_x viz

$$\pi_A = -\frac{\tau_B}{\tau_A\tau_B - \tau_{AB}^2}\,, \qquad \pi_{AB} = \frac{\tau_{AB}}{\tau_A\tau_B - \tau_{AB}^2}\,, \qquad \pi_B = -\frac{\tau_A}{\tau_A\tau_B - \tau_{AB}^2}\,, \tag{6.31}$$

$$\pi_{Ap} = \frac{\tau_{AB}\tau_{Bp} - \tau_{Ap}\tau_B}{\tau_A\tau_B - \tau_{AB}^2}\,, \qquad \pi_{Bp} = \frac{\tau_{AB}\tau_{Ap} - \tau_{Bp}\tau_A}{\tau_A\tau_B - \tau_{AB}^2}\,. \tag{6.32}$$

Finally, inserting Eqs. (6.29) and (6.30) into Eq. (6.17) results into the equations that describe the dynamical behavior of a binary mixture in the presence of a velocity field $\mathbf{v}(\mathbf{r},t)$, which are,

$$\frac{d\mathbf{Q}^A}{dt} = 2\,\overline{\Omega\cdot\mathbf{Q}^A} + 2\sigma\,\overline{\Gamma\cdot\mathbf{Q}^A} + \pi_{Ap}\sqrt{2}\mathbf{\Gamma} + \pi_A\mathbf{\Psi}^A + \pi_{AB}\mathbf{\Psi}^B\,, \tag{6.33}$$

$$\frac{d\mathbf{Q}^B}{dt} = 2\,\overline{\Omega\cdot\mathbf{Q}^B} + 2\sigma\,\overline{\Gamma\cdot\mathbf{Q}^B} + \pi_{Bp}\sqrt{2}\mathbf{\Gamma} + \pi_{AB}\mathbf{\Psi}^A + \pi_B\mathbf{\Psi}^B\,. \tag{6.34}$$

where $\mathbf{\Psi}^\alpha$ takes into account the relaxation of the alignment towards equilibrium via

$$\mathbf{\Psi}^A = \frac{\partial\mathscr{F}^{or}[\mathbf{Q}]}{\partial\mathbf{Q}^A} - \xi_{AA}^2\nabla^2\mathbf{Q}^A\,, \tag{6.35}$$

$$\mathbf{\Psi}^B = \frac{\partial\mathscr{F}^{or}[\mathbf{Q}]}{\partial\mathbf{Q}^B} - \xi_{BB}^2\nabla^2\mathbf{Q}^B\,. \tag{6.36}$$

6.2.5 Equation for the stress tensor

Before further discussion and applications of the dynamic equations of the alignment tensors [Eqs. (6.33) and (6.36)] some implications of the phenomenological laws (6.20)–(6.22) have to view reviewed. Particularly the viscous flow of the binary mixture.

Inserting Eqs. (6.29) and (6.30) into the phenomenological law of the stress tensor (6.22) results into the relation

$$\overline{\mathbf{T}} = 2\eta_{\text{iso}}\mathbf{\Gamma} + \overline{\mathbf{T}}_{\text{al}}\,. \tag{6.37}$$

According to Eq. (6.37), $\overline{\mathbf{T}}$ splits into a *Newtonian* contribution (already present in fluids with vanishing orientational order) and a contribution depending explicitly on the alignment. The Newtonian viscosity η_{iso} is modified viz

$$\eta_{\text{iso}} = \frac{\varrho}{m}k_BT\tau_p\left(1 - \frac{\tau_{Ap}^2\tau_B + \tau_{Bp}^2\tau_A - 2\tau_{AB}\tau_{Ap}\tau_{Bp}}{\tau_A\tau_B\tau_p - \tau_{AB}^2\tau_p}\right)\,. \tag{6.38}$$

The first term of Eq. (6.38) corresponds to the viscosity of the mixture when $\mathbf{Q}^A$ and $\mathbf{Q}^B$ and consequently $\mathbf{\Psi}^A(\mathbf{\Psi}^B)$ completely vanish. The second term characterizes the

coupling between the stress tensor and the alignment when $\mathbf{Q}^A$ and $\mathbf{Q}^B$ are non–zero. Lastly, the contribution depending explicitly on $\mathbf{Q}^A$ and $\mathbf{Q}^B$ is given by

$$\overline{\mathbf{T}}_{\text{al}} = \frac{\varrho}{m} k_B T \left(\sqrt{2} \sum_{\alpha=A}^{B} \pi_{\alpha p} \mathbf{\Psi}^{\alpha} + 2\sigma \sum_{\alpha=A}^{B} \overline{\mathbf{Q}^{\alpha} \cdot \mathbf{\Psi}^{\alpha}} \right) , \tag{6.39}$$

where the coefficients $\pi_{\alpha p}$ are given by Eq. (6.32). Equation (6.39) is known as the stress tensor of alignment and is this contribution which allows us to study the hydrodynamic properties of the fluid.

Finally, to measure the hydrodynamic effects arising in the binary mixture due to the alignment $\mathbf{Q}^A$ and $\mathbf{Q}^B$ the momentum balance equation reads

$$\varrho \frac{d\mathbf{v}}{dt} - \nabla \cdot \overline{\mathbf{T}} = 0 , \tag{6.40}$$

6.3 Relaxation of the alignment

In the absence of flow ($\mathbf{v} = 0$) and disregarding spatial inhomogeneities Eqs. (6.33)–(6.34) read

$$\frac{d\mathbf{Q}^A}{dt} = \pi_A \frac{\partial \mathscr{F}^{or}[\mathbf{Q}]}{\partial \mathbf{Q}^A} + \pi_{AB} \frac{\partial \mathscr{F}^{or}[\mathbf{Q}]}{\partial \mathbf{Q}^B} , \tag{6.41}$$

$$\frac{d\mathbf{Q}^B}{dt} = \pi_{AB} \frac{\partial \mathscr{F}^{or}[\mathbf{Q}]}{\partial \mathbf{Q}^A} + \pi_B \frac{\partial \mathscr{F}^{or}[\mathbf{Q}]}{\partial \mathbf{Q}^B} . \tag{6.42}$$

Notice that (6.41)–(6.42) are non–linear relaxation equations since $\mathscr{F}^{or}[\mathbf{Q}]$ as given in (6.7) is non–linear with respect to $\mathbf{Q}^A$ and $\mathbf{Q}^B$. The full relaxation of the order parameters is governed by Eqs. (6.41) and (6.42). Though this non linear system can solved in general, only some special features are discussed in the following. In particular, we study the linear decay of the alignment.

If $\mathscr{F}^{or}[\mathbf{Q}]$ is replaced by its linear approximation, Eqs. (6.41)–(6.42) reduce to the system of coupled linear equations

$$\frac{d\mathbf{Q}^A}{dt} = \pi_A (A_A \mathbf{Q}^A - A_{AB} \mathbf{Q}^B) + \pi_{AB} (A_B \mathbf{Q}^B - A_{AB} \mathbf{Q}^A) , \tag{6.43}$$

$$\frac{d\mathbf{Q}^B}{dt} = \pi_{AB} (A_A \mathbf{Q}^A - A_{AB} \mathbf{Q}^B) + \pi_B (A_B \mathbf{Q}^B - A_{AB} \mathbf{Q}^A) , \tag{6.44}$$

which can be written as the system

$$\dot{\mathbf{Q}} = \mathbb{M} \mathbf{Q} , \tag{6.45}$$

where $\mathbf{Q} = (\mathbf{Q}^A, \mathbf{Q}^B)^T$ and the matrix $\mathbb{M}$ is given by

$$\mathbb{M} = \begin{pmatrix} \pi_A A_A - \pi_{AB} A_{AB} & \pi_{AB} A_B - \pi_A A_{AB} \\ \\ \pi_{AB} A_A - \pi_B A_{AB} & \pi_B A_B - \pi_{AB} A_{AB} \end{pmatrix} . \tag{6.46}$$

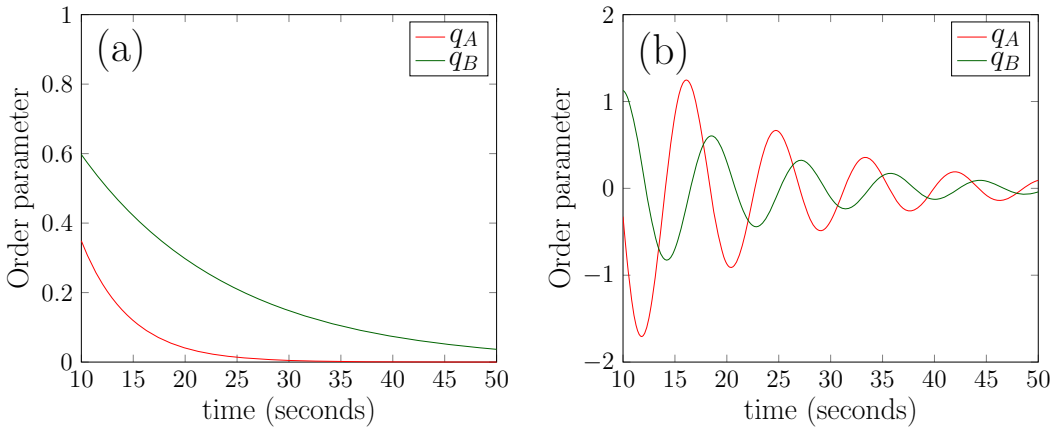

Figure 6.1: Relaxation towards equilibrium of the binary mixture given in Eq. (6.51): (a) Non coupled system $A_{AB} = 0$, (b) Coupled system $A_{AB} \neq 0$.

This approximation is applicable for small alignment and low concentrations. Since the relaxation times τ_x and for small concentrations the coefficients A_x are always positive, then $\mathbb{M}$ is a positive definite matrix. Hence, Eq. (6.45) shows that the alignment of the binary mixture relaxes to zero. This feature is common in liquid crystals with concentrations above the isotropic–nematic coexistence characteristic value [19].

6.3.1 Vanishing cross–coupling of the entropy production

When the system relaxes towards its equilibrium value it is possible to track the relaxation of the full alignment tensors $\mathbf{Q}^A$ and $\mathbf{Q}^B$ by only looking at the uniaxial alignment with a constant director [57]. The coupling between the true relaxation times in the full non–linear equations (6.41)) and (6.42)) is more complicated and requires further analysis by its own. In order to simplify the analysis, in the following we will assume *vanishing cross–coupling*.

The assumption of vanishing cross–coupling implies that the production of entropy of component A and the production of entropy of component B are completely independent. Thus, the relaxation time τ_{AB} vanishes and consequently $\pi_{AB} = 0$. Under this approximations Eq. (6.45) reduces to

$$\begin{pmatrix} d_t q^A(t) \\ \\ d_t q^B(t) \end{pmatrix} = \begin{pmatrix} -\tau_A^{-1} A_A & \tau_A^{-1} A_{AB} \\ \\ \tau_B^{-1} A_{AB} & -\tau_B^{-1} A_B \end{pmatrix} \begin{pmatrix} q^A(t) \\ \\ q^B(t) \end{pmatrix} , \tag{6.47}$$

where $q^A(t)$ and $q^B(t)$ are the uniaxial order parameters of the corresponding alignment tensors and d_t denotes the material derivative (6.15). The quantities $\tau_A A_A^{-1}$ and $\tau_B A_B^{-1}$

are known as the *true* relaxation time of alignment of the single component system [80]. Thus, the true relaxation times of alignment for the binary mixture are $\tau_A A_{AB}^{-1}$ and $\tau_B A_{AB}^{-1}$

In general, the solutions of the system (6.47) have the form

$$\mathbf{q}(t) = C_1 \mathbf{x}_1 \exp(\lambda_1 t) + C_2 \mathbf{x}_2 \exp(\lambda_2 t) \tag{6.48}$$

where C_i (with $i = 1, 2$) are constants that depend on the initial conditions, and $\mathbf{x}_i$ and λ_i are the eigenvectors and eigenvalues of $\mathbb{M}$. The simplest solution of (6.47) is obtained when the relaxation towards equilibrium of A is independent of the relaxation of B, *i.e.* there is no inter–component coupling, thus, $A_{AB} = 0$ [see Fig. 6.1.(a)]. However, the *real* solution is obtained after solving the eigenvalue equation

$$\det |\mathbb{M} - \lambda \alpha| = 0 \,. \tag{6.49}$$

Before solving Eq. (6.49) it is important to make some general remarks on the phenomenological relaxation times τ_A and τ_B. In Ref. [80] the single particle relaxation times τ_α are

$$\tau_\alpha = \frac{8\pi\eta R_g^3}{6 k_B T} \,, \tag{6.50}$$

where η is the viscosity of the solvent (usually water for colloidal suspensions) and R_g is the radius of gyration of the rigid molecule. Considering *fd*–viruses with a radius of gyration $\sim 11nm$ embedded in a aqueous solution at room temperature ($\eta \approx 0.79 mPa{\cdot}s$ at $300K$) [142, 143] we get $\tau_{\textit{fd}\text{–virus}} \approx 10^{-2} - 10^{-3} s$.

Considering a binary mixture of short and long *fd*–viruses with aspect ratios $\kappa_A = 20$ and $\kappa_B = 25$ and phenomenological relaxation times $\tau_A = 7.5{\times}10^{-3}$ and $\tau_b = 2.5{\times}10^{-3}$ in the isotropic state [see Fig. 5.3], Eq. (6.47) reads:

$$\begin{pmatrix} d_t q^A(t) \\ \\ d_t q^B(t) \end{pmatrix} = \begin{pmatrix} -0.215 & -1.286 \\ \\ -0.428 & -0.069 \end{pmatrix} \begin{pmatrix} q^A(t) \\ \\ q^B(t) \end{pmatrix} \,, \tag{6.51}$$

Given an initial value different form zero, the analytic solutions of (6.51) may be obtained straightforwardly from Eq. (6.47). The behavior of these solutions in time is showed in Fig. 6.1.(b). As expected, even for the simplest inter–component coupling the mixture relaxes towards the values $q_A = q_B = 0$. Here, the alignment presents a regular oscillatory decay of the type $\sin(t)\exp(-t)$ showing that even for a simple linear approximation the coupling coefficient A_{AB} plays a very important role.

In the same manner, it is possible to study the relaxation of uniaxial order parameters towards its equilibrium nematic values. This task is in general more complicated since (at least) terms of second order in q_A and q_B (*i.e.* $q_\alpha^2(t)$) should be included. Thus we

have to consider the full system

$$\frac{d\mathbf{Q}^A}{dt} = -\frac{1}{\tau_A}\frac{\partial \mathscr{F}^{or}[\mathbf{Q}]}{\partial \mathbf{Q}^A}\,, \tag{6.52}$$

$$\frac{d\mathbf{Q}^B}{dt} = -\frac{1}{\tau_B}\frac{\partial \mathscr{F}^{or}[\mathbf{Q}]}{\partial \mathbf{Q}^B}\,. \tag{6.53}$$

Trivially, for the uncoupled system ($A_{AB} = C_{AB} = 0$), the uniaxial order parameters q_A and q_B must decay uniformly [23] at a rate $\tau_\alpha^{-1}A_\alpha$ to the equilibrium value of the corresponding one–component system (q_A^c and q_B^c) [see above Eq. (5.28) in Sec. 5.2.1]. However, depending on the degree of *nematicity* of the system the dynamic behavior may be sensitive to the values of A_α, B_α and C_α or even to the initial conditions of the system. On the other hand, when the coupling coefficients does not vanish, *i.e.* $A_{AB} \neq 0$ and $C_{AB} \neq 0$, this analysis is even more complex and further studies in this direction are needed.

In this work we assume that in the nematic state both components of the mixture decay uniformly at a same rate τ_{ref}. As it is the case for the one component system [80] this rate is supposed to be modulated by the ratio of the coefficients B_α and C_α

$$\tau_{ref} = \tau_A\frac{24C_A}{B_A^2} = \tau_B\frac{24C_B}{B_B^2}\,. \tag{6.54}$$

The ratio $B_\alpha^2/24C_\alpha$ corresponds to the isotropic–nematic coexistence value of A_α [see Eq. (5.28)]. Equation (6.54) indicates that the solutions of Eqs. (6.52) and (6.53) decay uniformly at the same rate towards the value of q_A and q_B in the stationary state.

6.3.2 Final dynamic equations

Under the vanishing cross–coupling approximation ($\pi_{AB} = 0$), Eqs. (6.33) and (6.34) simplify to the set of equations:

$$\frac{d\mathbf{Q}^A}{dt} = 2\overline{\Omega\cdot\mathbf{Q}^A} + 2\sigma\overline{\Gamma\cdot\mathbf{Q}^A} - \sqrt{2}\frac{\tau_{Ap}}{\tau_A}\mathbf{\Gamma} - \frac{1}{\tau_A}\frac{\partial \mathscr{F}^{or}[\mathbf{Q}]}{\partial \mathbf{Q}^A} + \xi_{AA}^2\nabla^2\mathbf{Q}^A\,, \tag{6.55}$$

$$\frac{d\mathbf{Q}^B}{dt} = 2\overline{\Omega\cdot\mathbf{Q}^B} + 2\sigma\overline{\Gamma\cdot\mathbf{Q}^B} - \sqrt{2}\frac{\tau_{Bp}}{\tau_B}\mathbf{\Gamma} - \frac{1}{\tau_B}\frac{\partial \mathscr{F}^{or}[\mathbf{Q}]}{\partial \mathbf{Q}^B} + \xi_{BB}^2\nabla^2\mathbf{Q}^B\,. \tag{6.56}$$

where $\mathbf{\Omega} = \frac{1}{2}(\nabla\mathbf{v}^T - \nabla\mathbf{v})$ and $\mathbf{\Gamma} = \frac{1}{2}(\nabla\mathbf{v}^T + \nabla\mathbf{v})$ describe the effect of flow vorticity and its deformation on the average alignment of the particles, respectively. The ratio τ_{ip}/τ_α in the third term of Eqs. (6.55–6.56) measures the impact of external perturbations. It defines the tumbling parameter λ_α a quantity related to the aspect ratio κ_α viz

$$\lambda_\alpha = -\frac{\tau_{\alpha p}}{\tau_\alpha} = \sqrt{\frac{3}{5}}\frac{\kappa_\alpha^2 - 1}{\kappa_\alpha^2 + 1}\,. \tag{6.57}$$

For spherical particles $\lambda = 0$, whereas for prolate and oblate particles, $\lambda > 0$ and $\lambda < 0$, respectively.

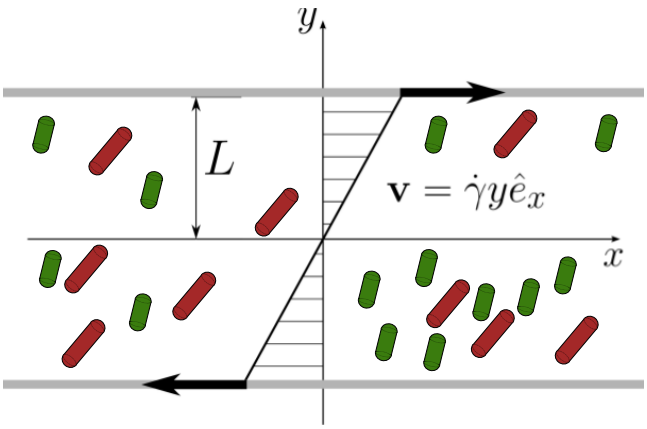

Figure 6.2: Sketch of a binary mixture in a planar Couette flow. Here, the mixture of rod–like molecules is enclosed between two infinite parallel plates at $y = \pm L$ moving along the x–axis with velocities $v_x = \pm L\dot{\gamma}$.

6.4 Simple Couette geometry

In the following we specialize to a planar Couette flow (see Fig. 6.2) where the fluid is confined between two infinitely extended, parallel plates (separated by a distance $2L$ along the y–direction) moving in opposite directions. The flow profile (for a Newtonian fluid) is then given by $\mathbf{v}(\mathbf{r}) = \dot{\gamma} y \hat{\mathbf{e}}_x$, with $\dot{\gamma}$ the shear rate.

6.4.1 Scaled dynamic equations

Reintroducing the scaled alignment tensors $\tilde{\mathbf{Q}}^\alpha$ and the scaled free energy according to Eq, (5.30) and the definition of λ_α in Eq. (6.54), equations (6.55) and (6.56) become

$$\frac{d\tilde{\mathbf{Q}}^A}{d\tilde{t}} = 2\tilde{\dot{\gamma}}\overline{\tilde{\mathbf{\Omega}} \cdot \tilde{\mathbf{Q}}^A} + 2\sigma\tilde{\dot{\gamma}}\overline{\tilde{\mathbf{\Gamma}} \cdot \tilde{\mathbf{Q}}^A} - \tilde{\Phi}'_A + \sqrt{2}\tilde{\lambda}_A\tilde{\dot{\gamma}}\tilde{\mathbf{\Gamma}} + \tilde{\xi}_A^2\tilde{\nabla}^2\tilde{\mathbf{Q}}^A\,, \tag{6.58}$$

$$\frac{d\tilde{\mathbf{Q}}^B}{d\tilde{t}} = 2\tilde{\dot{\gamma}}\overline{\tilde{\mathbf{\Omega}} \cdot \tilde{\mathbf{Q}}^B} + 2\sigma\tilde{\dot{\gamma}}\overline{\tilde{\mathbf{\Gamma}} \cdot \tilde{\mathbf{Q}}^B} - \tilde{\Phi}'_B + \sqrt{2}\tilde{\lambda}_B\tilde{\dot{\gamma}}\tilde{\mathbf{\Gamma}} + \tilde{\xi}_B^2\tilde{\nabla}^2\tilde{\mathbf{Q}}^B\,, \tag{6.59}$$

where $\tilde{t} = t/t_{ref}$ and $\tilde{\dot{\gamma}} = \dot{\gamma} t_{ref}$ are the re-scaled time and shear rate, $\tilde{\nabla}^2 = \nabla^2 L^2$, and the reference time t_{ref} is given by

$$t_{ref} = \frac{\tau_\alpha (q_0^\alpha)^2}{\mathscr{F}_{ref}^{or}}\,. \tag{6.60}$$

The scaled vorticity and deformation tensors are $\tilde{\mathbf{\Omega}} = (1/2)(\hat{e}^x\hat{e}^y - \hat{e}^y\hat{e}^x)$ and $\tilde{\mathbf{\Gamma}} = (1/2)(\hat{e}^x\hat{e}^y + \hat{e}^y\hat{e}^x)$, respectively. Further, the scaled tumbling parameters and correlation

lengths are

$$\tilde{\lambda}_\alpha = \frac{\lambda_\alpha}{q_0^\alpha} = \sqrt{\frac{3}{5}}\frac{1}{q_0^\alpha}\frac{\kappa_\alpha^2-1}{\kappa_\alpha^2+1}\,, \qquad \tilde{\xi}^2 = \frac{(q_0^\alpha)^2}{L^2\mathscr{F}_{ref}^{or}}\xi_{ii}^2\,. \tag{6.61}$$

An example of typical values of the scaled tumbling parameters, we consider systems involving the PEG–coated *fd*–virus, like the ones used in the experiments of thick and thin colloidal rods of Purdy *et al.* [16]. For these systems, the Maier-Saupe order parameter at coexistence is $S_0 = \langle P_2\rangle \approx 0.5 - 0.8$ [143] . Using $q_0^\alpha = \sqrt{5}S_0$ [22] one obtains $\tilde{\lambda}_\alpha \sim 0.43 - 0.69$. Finally, the derivative of the scaled free energy [see Eq. (5.33)] is given by

$$\begin{aligned}\tilde{\Phi}'_\alpha &= \frac{\partial\tilde{\mathscr{F}}^{or}(\tilde{\mathbf{Q}}^A,\tilde{\mathbf{Q}}^B)}{\partial\tilde{\mathbf{Q}}^\alpha}\,,\\ \tilde{\Phi}'_\alpha &= \Theta_\alpha\tilde{\mathbf{Q}}^\alpha - 2\sqrt{6}\,\overline{\tilde{\mathbf{Q}}^\alpha\cdot\tilde{\mathbf{Q}}^\alpha} + 2(\tilde{\mathbf{Q}}^\alpha:\tilde{\mathbf{Q}}^\alpha)\cdot\tilde{\mathbf{Q}}^\alpha - \frac{1}{2}\Theta_{AB}\tilde{\mathbf{Q}}^\beta - (\tilde{\mathbf{Q}}^A:\tilde{\mathbf{Q}}^B)\cdot\tilde{\mathbf{Q}}^\beta\,.\end{aligned} \tag{6.62}$$

6.4.2 Scaled momentum balance equation

Using the above definitions it is possible to write the scaled momentum balance equation

$$\frac{d\tilde{\mathbf{v}}}{d\tilde{t}} = \frac{1}{\beta}\tilde{\nabla}\cdot\tilde{\mathbf{T}}\,, \tag{6.63}$$

where we introduced the definition of the scaled stress tensor $\mathbf{T} = \varrho m^{-1}\mathscr{F}_{ref}^{or}\tilde{\mathbf{T}}$ and the additional parameter β is defined as

$$\beta = \frac{\dot{\gamma}L^2 m}{k_B T\mathscr{F}_{ref}^{or}t_{ref}}\,. \tag{6.64}$$

This coefficient, or rather the ratio between β and the scaled viscosity $\tilde{\eta}_{iso} = \eta_{iso}\tilde{\dot{\gamma}}$ defines the Reynolds number of the solvent

$$Re = \frac{\beta}{\tilde{\eta}_{iso}} = \frac{\dot{\gamma}L^2\rho}{\eta_{iso}}\,. \tag{6.65}$$

Experiments of shear–induced instabilities are typically performed in the low Reynolds number limit (Stokesian limit), $Re \ll 1$ [144, 145]. In this limit the momentum balance equation (6.63) reduces to

$$\tilde{\nabla}\cdot\tilde{\mathbf{T}} = 0\,. \tag{6.66}$$

We note that due to the time dependence of $\tilde{\mathbf{Q}}(t)$, the total stress $\tilde{\mathbf{T}}$ generally depends on time, however, at each time the total stress has to fulfill Eq. (6.66). The resulting velocity profile may deviate from the linear profile assumed initially. This feature is essential for

the description of spatial symmetry–breaking such as shear banding. Finally, the scaled contribution to the stress tensor is

$$\tilde{\mathbf{T}} = -\tilde{p}\mathbb{I} + 2\tilde{\eta}_{iso}\tilde{\mathbf{\Gamma}} + \overbrace{\tilde{\mathbf{T}}}^{}_{\text{al}} \tag{6.67}$$

where $\tilde{p} = p/\varrho m^{-1}\mathscr{F}^{or}_{ref}$ and the contribution to the stress tensor due to the changes in the alignment of the binary mixture is

$$\overbrace{\tilde{\mathbf{T}}}^{}_{\text{al}} = \sum_{\alpha=A}^{B}\left(\sqrt{2}\tilde{\lambda}_\alpha\tilde{\Phi}_\alpha - \sqrt{2}\tilde{\lambda}_\alpha\tilde{\xi}^2_\alpha\tilde{\nabla}^2\tilde{\mathbf{Q}}^\alpha + 2\sigma\overbrace{\tilde{\mathbf{Q}}^\alpha\cdot\tilde{\Phi}_\alpha}^{} - 2\sigma\tilde{\xi}^2\overbrace{\tilde{\mathbf{Q}}^\alpha\cdot\tilde{\Phi}_\alpha}^{}\right). \tag{6.68}$$

Remarks: In the following, we drop the tilde $(\sim)$ on all variables appearing in Eqs. (6.55–6.68). Thus, all quantities are identified with the same symbols as originally unless vagueness could arise. Following previous studies of one–component systems [146, 147] we set $\sigma = 0$ since this parameter has minor effect on the dynamics of the system for planar Couette flow geometry.

6.5 Explicit equations of motion

All together, the set of equations (6.58)–(6.68) represent the spatiotemporal evolution of second rank tensors. In fact, this set of equations can not be solved analytically beyond the uniaxial approximation (introduced to study the relaxation of the alignment in Sect. 6.3). Therefore, in order to study the *full* non–linear evolution of the alignment and the stress, $\mathbf{Q}^\alpha$ and $\mathbf{T}$ may be expanded in terms of a standard tensor basis $\mathbf{B}_i$ with five independent elements [see Appendix A]. In this basis

$$\mathbf{Q}^\alpha = \sum_{i=0}^{4} q_i^\alpha\mathbf{B}_i \quad \text{and} \quad \mathbf{T} = \sum_{i=0}^{4} T_i\mathbf{B}_i \tag{6.69}$$

where the coefficients x_i (where $x = q, T$) are determined using the relation $x_i = \mathbf{X} : \mathbf{B}_i$ [79].

Using the basis (6.69) in the Stokesian limit ($Re \ll 1$), Eqs. (6.58), (6.59) and (6.66) reduce to

$$\frac{d\mathbf{Q}^A}{dt} = \xi_A^2\nabla^2\mathbf{Q}^A + 2\dot{\gamma}\overbrace{\mathbf{\Omega}\cdot\mathbf{Q}^A}^{} + \sqrt{2}\lambda\mathbf{\Gamma} - \mathbf{\Phi}'_A\,, \tag{6.70}$$

$$\frac{d\mathbf{Q}^B}{dt} = \xi_B^2\nabla^2\mathbf{Q}^B + 2\dot{\gamma}\overbrace{\mathbf{\Omega}\cdot\mathbf{Q}^B}^{} + \sqrt{2}\lambda\mathbf{\Gamma} - \mathbf{\Phi}'_B\,, \tag{6.71}$$

$$\nabla\cdot\mathbf{T} = 0\,, \tag{6.72}$$

where $\mathbf{\Phi}'_\alpha$ is the derivative of the one component orientational free energy [see Eq. (6.62)]

$$\Phi'_\alpha = \Theta_\alpha\mathbf{Q}^\alpha - 2\sqrt{6}\overbrace{\mathbf{Q}^\alpha\cdot\mathbf{Q}^\alpha}^{} + 2(\mathbf{Q}^\alpha:\mathbf{Q}^\alpha)\cdot\mathbf{Q}^\alpha - \frac{1}{2}\Theta_{AB}\mathbf{Q}^\beta - (\mathbf{Q}^A:\mathbf{Q}^B)\cdot\mathbf{Q}^\beta\,. \tag{6.73}$$

Further, we assume that the spatial variation of $\mathbf{Q}$ and $\mathbf{T}$, is restricted to a one–dimensional investigation along the y–axis (the direction of the shear gradient [see Fig. 6.2]). This assumption reduces the degrees of freedom of the solution and implies that the possibility of banding in vorticity (z–) direction is excluded.

Using the tensor basis (6.69), Eq. (6.70) transforms into the set of equations:

$$\begin{aligned}
\frac{dq_0^\alpha}{dt} &= -(\phi_0^\alpha + \varphi_0^\beta) + \xi^2 \frac{\partial^2 q_0^\alpha}{\partial y^2}\,, \\
\frac{dq_1^\alpha}{dt} &= -(\phi_1^\alpha + \varphi_1^\beta) + \dot\gamma \frac{\partial v}{\partial y} q_2^\alpha + \xi^2 \frac{\partial^2 q_1^\alpha}{\partial y^2}\,, \\
\frac{dq_2^\alpha}{dt} &= -(\phi_2^\alpha + \varphi_2^\beta) - \dot\gamma \frac{\partial v}{\partial y} q_1^\alpha + \xi^2 \frac{\partial q_2^\alpha}{\partial y^2} + \dot\gamma\lambda \frac{\partial v}{\partial y}\,, \\
\frac{dq_3^\alpha}{dt} &= -(\phi_3^\alpha + \varphi_3^\beta) + \frac{1}{2}\dot\gamma \frac{\partial v}{\partial y} q_4^\alpha + \xi^2 \frac{\partial^2 q_3^\alpha}{\partial y^2},, \\
\frac{dq_4^\alpha}{dt} &= -(\phi_4^\alpha + \varphi_4^\beta) - \frac{1}{2}\dot\gamma \frac{\partial v}{\partial y} q_3^\alpha + \xi^2 \frac{\partial^2 q_4^\alpha}{\partial y^2}\,.
\end{aligned} \tag{6.74}$$

Here the quantities ϕ_i^α describe the relaxation of the particles towards equilibrium and are

$$\begin{aligned}
\phi_0^\alpha &= q_0^\alpha\big(\Theta_i - 3q_0^\alpha + 2\mathfrak{q}_\alpha^2\big) + 3(q_1^{\alpha\,2} + q_2^{\alpha\,2}) - \frac{3}{2}(q_3^{\alpha\,2} + q_4^{\alpha\,2})\,, \\
\phi_1^\alpha &= q_1^\alpha\big(\Theta_i + 6q_0^\alpha + 2\mathfrak{q}_\alpha^2\big) - \frac{3}{2}\sqrt{3}\,(q_3^{\alpha\,2} - q_4^{\alpha\,2})\,, \\
\phi_2^\alpha &= q_2^\alpha\big(\Theta_i + 6q_0^\alpha + 2\mathfrak{q}_\alpha^2\big) - 3\sqrt{3}\,q_3^\alpha q_4^\alpha\,, \\
\phi_3^\alpha &= q_3^\alpha\big(\Theta_i - 3q_0^\alpha + 2\mathfrak{q}_\alpha^2\big) - 3\sqrt{3}\,(q_1^\alpha q_3^\alpha + q_2^\alpha q_4^\alpha)\,, \\
\phi_4^\alpha &= q_4^\alpha\big(\Theta_i - 3q_0^\alpha + 2\mathfrak{q}_\alpha^2\big) + 3\sqrt{3}\,(q_1^\alpha q_4^\alpha - q_2^\alpha q_3^\alpha)\,.
\end{aligned} \tag{6.75}$$

while the quantities φ_i^β display the inter–component interaction within the mixture and are

$$\varphi_i^\beta = -q_i^\beta(\Theta_{AB} + \mathfrak{q}_{AB}^2)\,, \tag{6.76}$$

where $i = 0, \cdots, 4$. In equations (6.74)–(6.75), $\mathfrak{q}_\alpha^2 = \sum q_i^{\alpha\,2}$ and $\mathfrak{q}_{AB}^2 = \sum q_i^\alpha q_i^\beta$. For one–component systems, it can be shown by general arguments [50] (and has been demonstrated numerically [48, 49]) that the structure of equations (6.74)–(6.75) leads to various types of oscillatory solutions as long as that the shear rate $\dot\gamma \neq 0$.

Finally, the divergence of the stress tensor in Eq. (6.72) is now rewritten as

$$\frac{\partial T_2}{\partial y} = \sqrt{2}\eta_{iso}\dot\gamma \frac{\partial^2 v}{\partial y^2} + \sum_{\alpha=A}^{B}\left(\sqrt{2}\lambda_\alpha \frac{\partial(\phi_2^\alpha + \varphi_2^\beta)}{\partial y} - \sqrt{2}\lambda_\alpha \xi_\alpha^2 \frac{\partial^3 q_2^\alpha}{\partial y^3}\right). \tag{6.77}$$

The surviving component of the stress tensor T_2 refers to the in–shear plane stress (T_{xy}) exerted on the system due to the velocity field.

6.6 Summary

In this chapter we present a natural extension of the theory of non–equilibrium alignment phenomena to a system composed of a binary mixture of rigid anisotropic particles. We achieved this combining the equilibrium theory developed in Chapter 5 with the theory of irreversible processes for liquid crystals.

Following standard calculations of the theory of linear irreversible thermodynamics we obtained a set of phenomenological laws which relate the hydrodynamic behavior of the fluid and the thermodynamic fluxes and forces of alignment. Further, employing Onsager's theorem we get a complete set of hydrodynamic equations where the alignment tensors $\mathbf{Q}^A$ and $\mathbf{Q}^B$ are coupled with the flow velocity $\mathbf{v}$. The final hydrodynamic equations for the mixture are:

$$\frac{d\mathbf{Q}^A}{dt} = 2\overbrace{\Omega\cdot\mathbf{Q}^A}^{} + 2\sigma\overbrace{\Gamma\cdot\mathbf{Q}^A}^{} + \pi_{Ap}\sqrt{2}\mathbf{\Gamma} + \pi_A\mathbf{\Psi}^A + \pi_{AB}\mathbf{\Psi}^B\,,$$
$$\frac{d\mathbf{Q}^B}{dt} = 2\overbrace{\Omega\cdot\mathbf{Q}^B}^{} + 2\sigma\overbrace{\Gamma\cdot\mathbf{Q}^B}^{} + \pi_{Bp}\sqrt{2}\mathbf{\Gamma} + \pi_{AB}\mathbf{\Psi}^A + \pi_B\mathbf{\Psi}^B\,.$$

where π_x are related to phenomenological times and the terms $\mathbf{\Psi}^\alpha$ (given by the derivatives of the scaled free energy densities derived in Chapter 5) account for the relaxation of the alignment towards equilibrium. Here $\mathbf{\Omega} = \frac{1}{2}(\nabla\mathbf{v}^T - \nabla\mathbf{v})$ and $\mathbf{\Gamma} = \frac{1}{2}(\nabla\mathbf{v}^T + \nabla\mathbf{v})$ describe the effect of flow vorticity and its deformation on the average alignment of the particles, respectively.

We analyze these equations in the limit when the entropy production of component A and B are completely independent and study the relaxation of the mixture towards equilibrium in the absence of flow. We show that even with the simplest inter–component coupling (entering through the free energy of alignment) the dynamics of the decay of alignment are very complicated. Thus we conclude that the vanishing cross–coupling approximation is suitable as a first approach to study the full dynamics of the system.

Finally, specializing to a planar Couette shear flow geometry, we introduce the scaled alignment tensors $\mathbf{Q}^A$ and $\mathbf{Q}^B$ and re–write the hydrodynamic equations (for the alignment and the stress tensors) into a dimensionless form which are used in the subsequent chapter to analyze the shear–induced instabilities.

Chapter 7

Shear induced instabilities and oscillatory states in binary mixtures

In this chapter we study the dynamic behavior of binary mixtures under shear. However, to provide a systematic approach we subdivide this chapter in two parts: On the first part, we review the well–known oscillatory orientational dynamics of an homogeneous single component system [49]. However, we expand this analysis to study the spatiotemporal behavior of the alignment order parameter and its impact on the underlying relations between stress and shear rate. On the second part we turn to the analysis of the orientational dynamics of a spatially homogeneous binary mixture. This chapter includes the main results of the publications: *Binary mixtures of rod-like colloids under shear: microscopically-based equilibrium theory and order–parameter dynamics* [111] and *Shear banding in nematogenic fluids with oscillating orientational dynamics* [148].

7.1 General Remarks

The shear induced behavior of nematogenic fluids has been intensely studied for the one component system on the basis of equations (6.74)–(6.75) (see e.g. [149, 49, 50]). In these studies it has been proven that nematogenic fluids present a wide variety of orientational dynamics depending on the initial equilibrium state (isotropic or nematic).

The dynamics of the full alignment tensor are characterized by the dynamics of the corresponding nematic director. Thus, in average, the particles in the fluid perform a variety of shear induced oscillatory states. The different types of regular oscillatory states are: wagging (W), tumbling (T), kayaking–wagging (KW), kayaking–tumbling (KT), and (flow–)alignment states (A). Moreover, under certain conditions chaotic dynamics may be present [48, 51, 49, 150]. All these states are characterized by the time–dependent

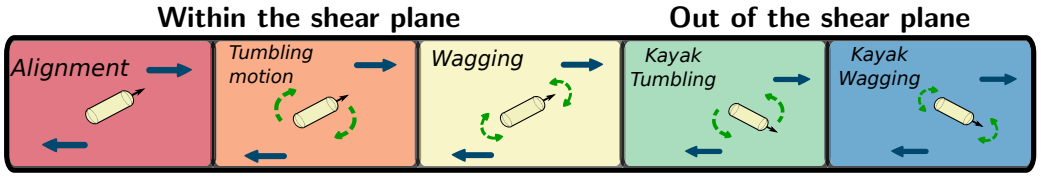

Figure 7.1: Sketch of the different types shear induced regular oscillatory states. The blue arrows show the direction in which the Couette walls are moving whereas the green arrows indicate the motion of the nematic director.

behavior $\mathbf{Q}(t)$ (and conversely of the coefficients $q_i(t)$) and it is possible to set one particular oscillatory state depending on the shear rate and the tumbling parameters [see Eqs. (6.74)–(6.75)].

Excluding chaotic dynamics, the regular time–dependent states can be classified in two groups: states lying *within* the shear plane (A, T, W) and states lying *out of* the shear plane (KT, KW). Trivially, the A state corresponds to a fixed point of the system (6.74)–(6.75) and therefore the dynamics of the $q_i(t)$ coefficients are "frozen" as a function of time. In contrast, the regular states W and T are characterized by full in–plane rotations of nematic director and $q_3(t) = q_4(t) = 0$. Finally, the out of the shear plane oscillatory states (KW, KT) are named after their in–shear plane counterparts with the difference that here $q_i(t) \neq 0 \, \forall i \in [0, 1, 2, 3, 4]$.

7.1.1 Dynamical state diagram

All the different steady oscillatory states can be summarized in a *dynamical state diagram* [49]. In Fig. 7.2, we show the dynamical state diagram spanned in the plane $\dot{\gamma} - \lambda$ for a one component system characterized by $\Theta = -1.0$. The colored areas are computed via direct numerical integration and each one corresponds to different dynamical behavior: A = Alignment, W = Wagging, T = Tumbling, KW = Kayak–Wagging and KT = Kayak–Tumbling (see Fig. 7.1). We should note that because of our choice of scaling (see Chapter 6) the values of λ differ from those in earlier studies (e.g. [49]) by a constant factor.

In earlier studies [51, 50] investigating similar values of Θ, the authors reported the occurrence of an important region characterized by irregular and even chaotic motion of the nematic director. This chaotic region is located around the point where the KT, KW and A states meet. Here we do not detect such region because our algorithm does not resolve Lyapunov exponents.

The boundaries between the colored regions in Fig. 7.2 correspond to different types of dynamical bifurcations. The simplest one is a (supercritical) Hopf bifurcations occur-

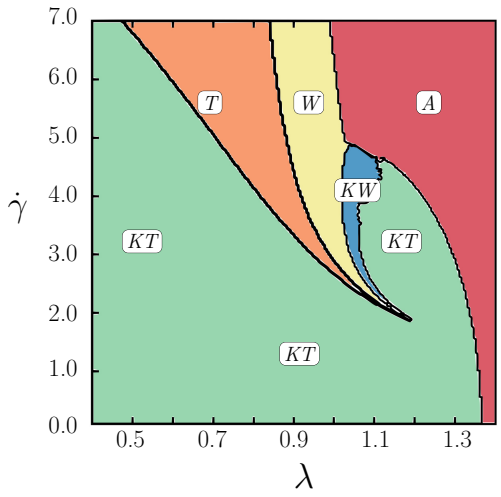

Figure 7.2: Dynamical state diagram for a one component system characterized by $\Theta = -1.0$. The colored areas are computed via direct numerical integration and each one corresponds to different dynamical behavior: A = Alignment, W = Wagging, T = Tumbling, KW = Kayak–Wagging and KT = Kayak–Tumbling.

ring at the boundary between alignment (A) and wagging (W). In Ref. [50] a complete continuation analysis is presented which reveals the complexity of the dynamical behavior already in the one component case (where one has already five dynamical variables).

In order to study the shear induced instabilities occurring in binary mixtures, it is necessary to provide a systematic approach containing a deep analysis of the one component case. Thus, in the following section (Section 7.2) we investigate systems composed of only one component, *i.e.*, in the limit $\rho_b \to 0$. Further, in Section 7.3 we continue our analysis with the investigations of binary mixtures of rod–like colloids

7.2 Shear banding with oscillating orientational dynamics

In recent years, several theoretical approximations have explored the spatial inhomogeneities of the alignment $\mathbf{Q}$ and the stress $\mathbf{T}$, yielding shear banding between different steady states. In some cases, the unsheared system is close to the isotropic–nematic transition [59] and in others the dynamics of the sheared homogeneous system is irregular or chaotic [52, 75]. In this section, our purpose is to extend the work in Refs. [52, 75] to parameter values where the homogeneous system exhibits *regular* oscillatory dynamics.

7.2.1 Numerical calculations and boundary conditions

For the study of inhomogeneous systems the gradient terms appearing in (6.74)–(6.77) should be discretized. To this end we use a central finite difference scheme of fourth order

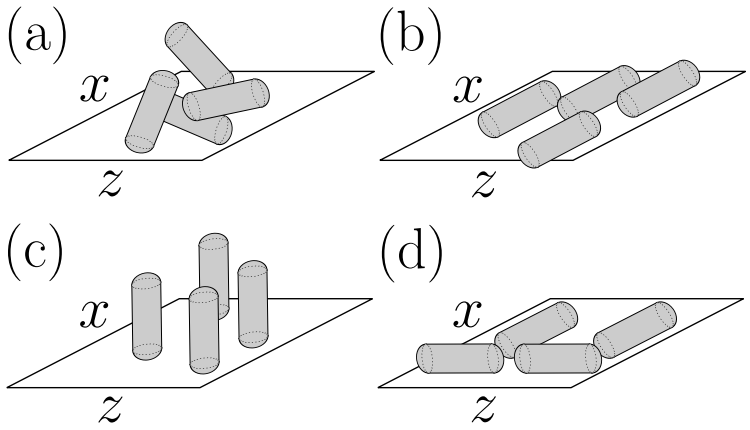

Figure 7.3: Sketch of the boundary conditions applied to the tensor $\mathbf{Q}$ at the plates: (a) Isotropic [see Eq. (7.1)] (b) Planar nematic [Eq. (7.2)] (c) Vertical nematic [Eq. (7.3)] and (d) Planar degenerate [Eq. (7.4)].

where asymmetric stencils (using only available grid points) are implemented [151]. The calculations are initialized with values of $q_0, \cdots, q_4$ matching the boundary conditions, with a small random perturbation. The steady configurations of the system are found by monitoring the evolution of $q_0, \cdots, q_4$ and T_2, disregarding transient initial behavior. The resulting dynamical states are characterized employing an algorithm that recognizes the periodicity as in the previous section. For further details, please refer to Henning Reinken's Master's thesis [71].

Regarding the boundary conditions at the plates ($y = \pm L$), we assume strong anchoring conditions, *i.e.*, the value of $\mathbf{Q}$ at the plates is constant in time, but may have different symmetries. From an experimental point of view, strong anchoring conditions are possible by chemical or mechanical treatment of the plates [83, 84, 85, 86]. Here we focus on the following idealized cases:

$$\mathbf{Q}\Big|_{y=-L}^{y=L} = 0 \qquad \text{(Isotropic)}\,, \tag{7.1}$$

$$\mathbf{Q}\Big|_{y=-L}^{y=L} = \sqrt{\frac{3}{2}}\,\tilde{\mu}_3^{eq}\,\overline{\hat{\mathbf{e}}_x\hat{\mathbf{e}}_x} \qquad \text{(Planar nematic)}\,, \tag{7.2}$$

$$\mathbf{Q}\Big|_{y=-L}^{y=L} = \sqrt{\frac{3}{2}}\,\tilde{\mu}_3^{eq}\,\overline{\hat{\mathbf{e}}_y\hat{\mathbf{e}}_y} \qquad \text{(Vertical nematic)}\,, \tag{7.3}$$

$$\mathbf{Q}\Big|_{y=-L}^{y=L} = -\sqrt{\frac{3}{2}}\,\tilde{\mu}_3^{eq}\,\overline{\hat{\mathbf{e}}_y\hat{\mathbf{e}}_y} \qquad \text{(Planar degenerate)}\,, \tag{7.4}$$

where $\tilde{\mu}_3^{eq}$ is the equilibrium value of the alignment tensor in the nematic phase. Equations (7.1) and (7.4) describe disordered states where the particle orientations are distributed, either in all three directions ("isotropic") or within the plane of the plates, i.e.,

in the x–z plane ("planar degenerate") (see Fig. 7.3). The other two boundary conditions correspond to nematic states, with the director lying either in the plane of the plates ("planar nematic") or along the gradient (y–) direction ("vertical nematic") (see Fig. 7.3). For the velocity field usual no–slip boundary conditions, $v_x(y = \pm 1) = \pm 1$ (in reduced units), are implemented [63].

7.2.2 Homogeneous solutions

Here we consider spatially homogeneous systems far away from the boundaries in the limit of infinite plate separation, *i.e.*, $L \to \infty$. In this limit, the correlation length appearing in Eq. (6.77) is zero and thus, all gradient terms vanish. In particular, the stress T_2 takes the form

$$T_2(t) = \sqrt{2}\eta_{iso}\dot{\gamma} + \sqrt{2}\lambda\Phi_2\,. \tag{7.5}$$

Homogeneous systems sheared from the isotropic state

We start considering systems whose equilibrium state is isotropic ($\Theta = 1.20$). Increasing the shear rate from zero, the system develops a paranematic (PN) state[1]; this is illustrated in Fig. 7.4(a). The behavior upon further increase of $\dot{\gamma}$ depends on the value of the chosen tumbling parameter λ (a measure of the aspect ratio).

For $\lambda \gtrsim 0.62$ one observes a transition from paranematic to shear–aligned (A) state. The PN–A transition is accompanied by a narrow region of bistability (not visible in Fig. 7.4) where the degree of ordering of the system is highly dependent on the initial condition. For smaller values of the tumbling parameter ($\lambda \lesssim 0.62$) the A state is unstable and the system develops wagging (W) motion. Overall, the behavior found in the present calculations agrees qualitatively with that reported in ref. [50], however, the quantitative data for the boundary lines differ due to the different scaling of the free energy.

For each of the parameter sets $(\dot{\gamma}, \lambda)$ we calculated the stress T_2 (in the W state, averaging $T_2(t)$ over one period of time). Remarkably, we observe that different parameter sets may lead to the same value of T_2. To illustrate this point, Fig. 7.4(a) includes dashed (blue) lines and solid (green) lines corresponding to two constant values of T_2. Moreover, there are several regions of λ where T_2 assumes the same value for different shear rates. For example, at $\lambda = 0.55$ there are three values of $\dot{\gamma}$ with $T_2 = 0.6$, and for $\lambda \geq 0.7$ one finds two solutions with $T_2 = 0.4$.

Due to this multivalued behavior, it is interesting to consider the corresponding flow curves, $T_2(\dot{\gamma})$. The results for $\lambda = 0.55$ and $\lambda = 1.25$ are plotted in Figs. (7.4(b) and (7.4(c), respectively. The flow curve for $\lambda = 0.55$ [see Fig. 7.4(b)] displays a region with a negative slope between $\dot{\gamma} \approx 0.357$ and $\dot{\gamma} \approx 0.365$. Within this region the homogeneous flow is mechanically unstable, and as one might expect, the system forms a

[1] The paranematic state PN is similar to the AA state but it is characterized by weak nematic order.

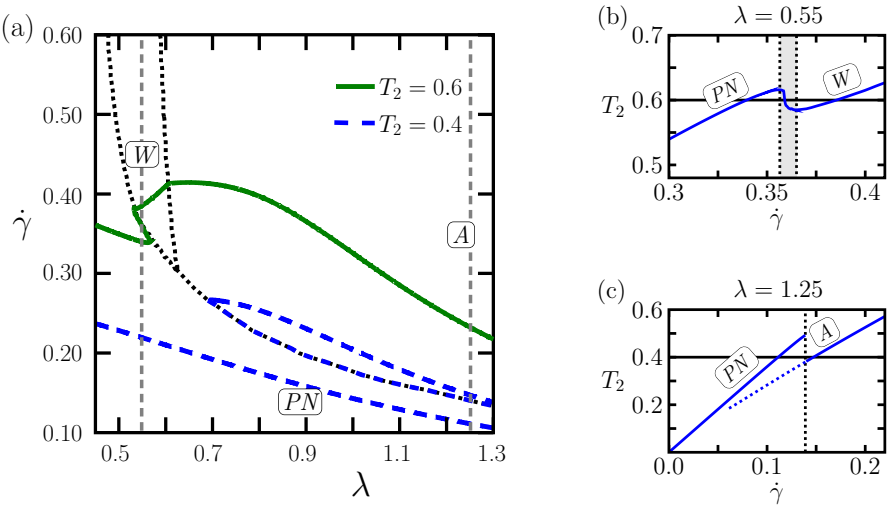

Figure 7.4: a) State diagram in the plane spanned by tumbling parameter (λ) and shear rate ($\dot{\gamma}$) at $\Theta = 1.20$ (isotropic equilibrium system). The dotted gray lines indicate the boundaries between three different states: paranematic (PN), shear–aligned (A) and wagging (W). The dashed (blue) and solid (green) lines connect points with constant stress $T_2 = 0.4$ and $T_2 = 0.6$, respectively. (Second row) Homogeneous flow curves $T_2(\dot{\gamma})$ for (b) $\lambda = 0.55$ and (c) $\lambda = 1.25$.

spatially inhomogeneous, shear banded state. We also note that the shear rate $\dot{\gamma} \approx 0.359$ characterized by $T_2 = 0.6$ and $dT_2/d\dot{\gamma} < 0$ agrees roughly with the corresponding point on the boundary line PN–W in Fig. 7.4(a). This indicates that the orientational transition from the PN state to the (oscillatory) W state, on the one side, and the shear banding instability, on the other side, are closely correlated.

In contrast, for $\lambda = 1.25$ [see Fig. 7.4(c)] the flow curve does not display a region with negative slope. Rather one observes a discontinuity and, associated with this, hysteretic behavior. Upon increase of $\dot{\gamma}$ from the small values, *i.e.*, from the paranematic (PN) state, the systems discontinuously "jumps" to the aligned (A) state only at $\dot{\gamma} \approx 0.14$ [which is above the upper blue dashed line in Fig. 7.4(a)]. However, decreasing $\dot{\gamma}$ starting from the large shear rates characterizing the A state, the jump occurs at the much smaller shear rate $\dot{\gamma} \approx 0.06$. As we will show at the end of this section, the formation of shear bands in this case ($\lambda = 1.25$) strongly depends on the boundary conditions.

Homogeneous systems sheared from the nematic state

We now turn to systems deep in the nematic phase. Specifically, we set $\Theta = -0.25$ in Eq. (6.75). The dashed (blue) and solid (green) lines in Fig. 7.5(a) indicate parameter

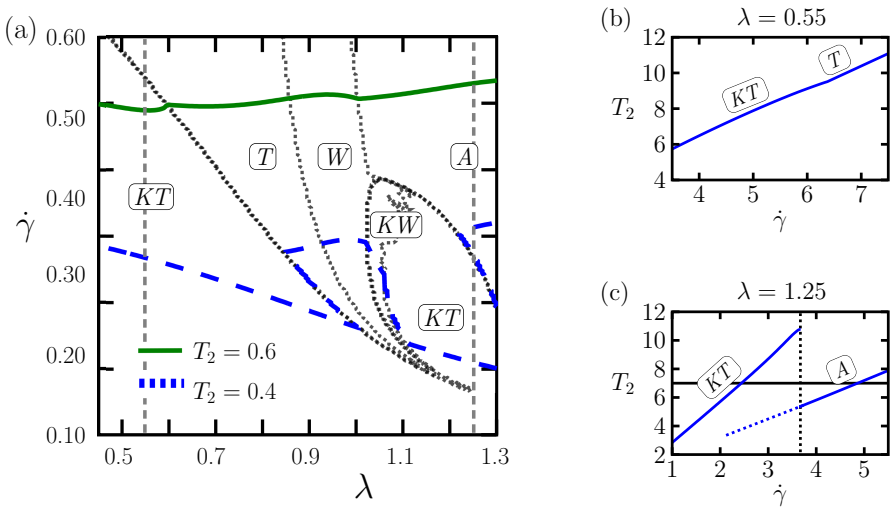

Figure 7.5: (a) State diagram at $\Theta = -0.25$. The dotted gray lines indicate the boundaries between the different dynamical states: wagging (W), tumbling (T), kayaking–tumbling (KT), kayaking–wagging (KW), and shear–alignment (A). The dashed (blue) and solid (green) lines connect points with constant stress $T_2 = 7.0$ and $T_2 = 9.0$, respectively. (Second row) Homogeneous flow curves $T_2(\dot\gamma)$ for (b) $\lambda = 0.55$ and (c) $\lambda = 1.25$.

sets at which the orientational dynamics yield the constant stress–values $T_2 = 9.0$ and $T_2 = 7.0$, respectively. In the first case, the line provides a unique relation in the sense that an increase of $\dot\gamma$ at fixed λ yields only one crossing with this line. This is different for the case $T_2 = 7.0$ where, depending on λ, one or two crossings can be observed.

Exemplary flow curves for two values of the tumbling parameter are shown in the right hand side of Fig. 7.5. At $\lambda \approx 0.55$ [see Fig. 7.5(b)], where each of the constant–pressure lines is crossed only once, one observes a monotonic increase of T_2 with $\dot\gamma$. In particular, there is no discontinuity even at $\dot\gamma \approx 6.5$, where the underlying orientational dynamics changes from the KT to the T states. In fact, a systematic bifurcation analysis (such as the one in Ref. [50]) would reveal a *bistable* region characterized by the presence of (at least) two attractors between the pure KT and the pure T state. In such a situation, the stress T_2 would not be uniquely defined. This aspect certainly deserves more attention in a future study.

In contrast, in the case $\lambda = 1.25$ showed in Fig. 7.5(a), an increase of $\dot\gamma$ from small values yields two crossings with the constant–stress curve $T_2 = 7.0$. As seen from Fig. 7.5(c), the flow curve exhibits a pronounced discontinuity related to the transformation of the (out–of–plane) oscillating KT state into the shear–aligned (A) steady state at $\dot\gamma \approx 3.67$. One also recognizes a strong dependence on initial conditions (hysteresis), similar to the situation discussed in Fig. 7.4(c).

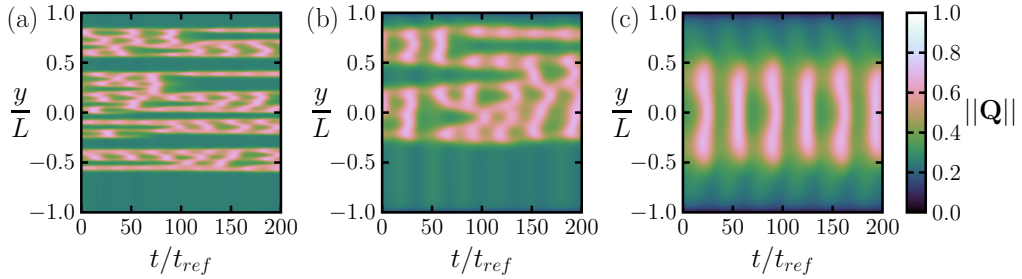

Figure 7.6: Spatiotemporal behavior of the norm of $\mathbf{Q}$ at $\dot{\gamma} = 3.65$, $\lambda = 1.25$ and different correlation lengths (a) $\xi^2 = 10^{-5}$, (b) $\xi^2 = 10^{-4}$ and (c) $\xi^2 = 10^{-3}$. The equilibrium state $(\dot{\gamma} = 0)$ is isotropic $(\Theta = 1.20)$.

7.2.3 Spatiotemporal behavior and shear banding

In the preceding discussion we found indications of the formation of inhomogeneous states in both, systems sheared from the isotropic and systems sheared from the nematic phase. Now, we turn to the analysis of the corresponding systems (characterized by certain values of the tumbling parameter) calculating the full spatiotemporal behavior of the $\mathbf{Q}$ and the resulting shear stress T_2. To this end we have solved numerically Eqs. (6.74)–(6.77) using the methodology described in Sect. 7.2.1.

Our discussion in this section is divided into two parts: First, we focus on the correlation length ξ, which appears as a prefactor of the gradient term in the orientational free energy density [see Eqs. (6.74)–(6.75)]; later we turn our attention to the boundary condition for $\mathbf{Q}$ at the plates [see Eqs. (7.1)–(7.4)].

Impact of the correlation length

Initially isotropic system We first consider the system at $\Theta = 1.20$ and $\lambda = 0.55$ [see Fig. 7.4(b)] focusing on a shear rate $\dot{\gamma} = 0.365$. In Figs. 7.6(a)–(c) we show the spatiotemporal evolution of $||\mathbf{Q}||$ (the norm of $\mathbf{Q}$–tensor) at three different values of the correlation length. Since the equilibrium state is isotropic, we choose the boundary conditions according to Eq. (7.1), thus the boundaries do not support any orientational ordering.

As seen from Fig. 7.6(a) the system forms spatiotemporal structures with locally large values of $||\mathbf{Q}||$ already at the smallest correlation length considered, $\xi = 10^{-5}$. The observed pattern is rather "loose" with its width changing in time. We can also observe that, within the inhomogeneous regions, $||\mathbf{Q}||$ is oscillating in time. The oscillations in these regions are consistent with a wagging (W) state and outside $||\mathbf{Q}||$ takes values typical of a paranematic (PN) state. This behavior is expected since the value of $\dot{\gamma}$ considered in Fig. 7.6 is very close to the boundary between the PN and W state (see Fig. 7.4).

Upon increasing the correlation length, ξ, we observe from Figs. 7.6(b) and 7.6(c)

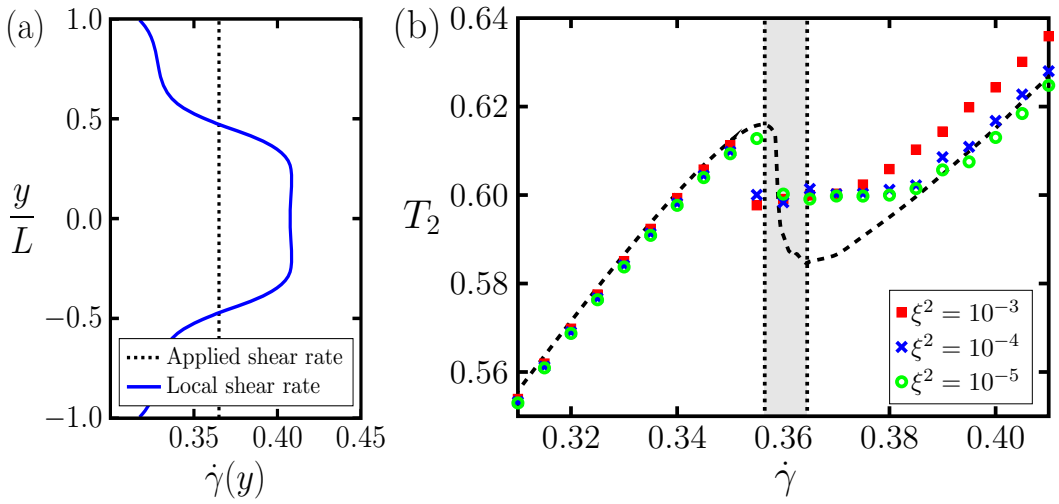

Figure 7.7: (a) Local shear rate within the banded state of the initially isotropic system ($\Theta = 1.20$, $\lambda = 0.55$, average (applied) shear rate $\dot{\gamma} = 0.365$). (b) Inhomogeneous flow curves at different correlation lengths. The symbols ■ (red), × (blue) and ○ (green) correspond to $\xi^2 = 10^{-5}$, $\xi^2 = 10^{-4}$ and $\xi^2 = 10^{-3}$, respectively. As a reference the homogeneous flow curve is included (black dashed line).

that the regions characterized by W motion become more defined, in terms of the shape and oscillatory motion of the order parameter. At the same time the interface between the W and PN region broadens. As a consequence, the W oscillations are transferred to some extent into the outer region, however, with a very small amplitude.

A further illustration of the presence of shear bands is plotted in Fig. 7.7(a), where we present a snapshot of the *local* shear rate, $\dot{\gamma}(y)$, for the system at $\xi^2 = 10^{-3}$. Here, we see that the band in the middle of the system has a significantly higher shear rate than the PN state close to the boundaries. On the other hand, Fig. 7.7(b) shows the flow curves obtained for the inhomogeneous (initially isotropic) systems for different correlation length. We obtained these curves by calculating the mean value of T_2 increasing gradually from lower to larger values of $\dot{\gamma}$ (see Ref. [152]). As a reference, the corresponding homogeneous flow curve [see Fig. 7.4(b)] is included.

Interestingly, the value of T_2 corresponding to the banded state is essentially independent of ξ; in other words, the value of T_2 appears to be unique. This observation is consistent with previous studies on the basis of both, a $\mathbf{Q}$–tensor model [59] and the DJS model [74]. We further observe from Fig. 7.7(b) that there is a slight dependence on the value of T_2 on ξ at high shear rates beyond the banded state. This is an effect stemming from the inhomogeneities induced by the confining walls: the larger ξ, the larger is the extent of these inhomogeneities into the bulk–like region between the plates. In fact, excluding these regions from the calculations the results for T_2 completely agree for different ξ.

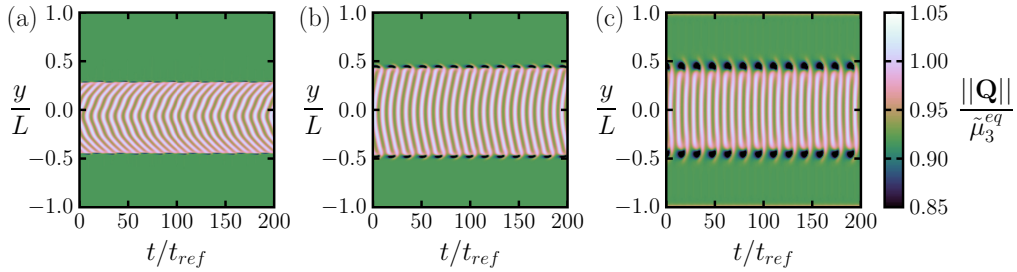

Figure 7.8: Spatiotemporal behavior of the norm of $\mathbf{Q}$ at $\dot{\gamma} = 3.65$, $\lambda = 1.25$ and different correlation lengths (a) $\xi^2 = 10^{-5}$, (b) $\xi^2 = 10^{-4}$ and (c) $\xi^2 = 10^{-3}$. The equilibrium state ($\dot{\gamma} = 0$) is nematic ($\Theta = -0.25$).

Initially nematic system We now turn to the system at $\Theta = -0.25$ and $\lambda = 1.25$, where the homogeneous flow curve [see Fig. 7.5(c)] is discontinuous. Results for the norm of $\mathbf{Q}$ as function of space and time are shown in Fig. 7.8, where we assumed equivalent planar nematic boundary conditions [see Eq. (7.2)], but different correlation lengths.

In all exemplary cases showed in Fig. 7.8, there is a a clear spatial separation of the system into an inner band, where the orientational behavior corresponds to the kayak–tumbling (KT) state, and an outer region where the system is in a shear–aligned (A) state. Upon increase of ξ the width of the KT band widens, while the oscillations within the band become more and more regular.

Corresponding results for the local shear rate and the inhomogeneous flow curves are given in Fig. 7.9. Compared to the initially isotropic system, we see from Fig. 7.9(a) that the oscillatory (KT) band is characterized by a *smaller* shear rate than the regions close to the boundaries. A further difference comes up when we consider in Fig. 7.9(b) the values of the stress plateau in the inhomogeneous flow curve. Here we find a dependence on the correlation length; that is, the value of T_2 at the plateau increases with ξ. This contrasts with our corresponding results for the initially isotropic system.

Role of the boundary conditions

In this final subsection we will address the role of the boundary conditions [see eqs. (7.1)–(7.4)]. For the following analysis we set the correlation length to a constant value of $\xi^2 = 10^{-5}$. However, higher values yield very similar results. In Fig. 7.10 we present numerical results for the resulting flow curves of the inhomogeneous systems previously discussed.

As before, we first consider systems sheared from the isotropic state at $\lambda = 0.55$ where clear shear banding instabilities are found even for isotropic boundary conditions [see figs. 7.6 and 7.7]. As indicated by the flow curves in Fig. 7.10(a), similar behavior occurs for other (including nematic) boundary conditions. Indeed, all of the systems

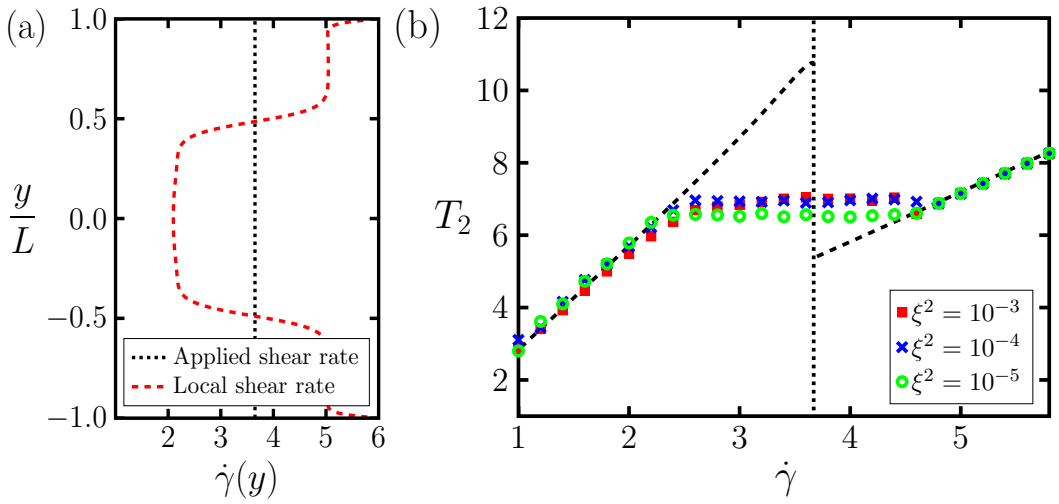

Figure 7.9: (a) Local shear rate within the banded state of the initially nematic system ($\Theta = -0.25$, $\lambda = 1.25$, average (applied) shear rate $\dot{\gamma} = 3.65$). (b) Inhomogeneous flow curves at different correlation lengths. The symbols ■ (red), × (blue) and ○ (green) correspond to $\xi^2 = 10^{-5}$, $\xi^2 = 10^{-4}$ and $\xi^2 = 10^{-3}$, respectively. As a reference the homogeneous flow curve is included (black dashed line).

form bands (within a range of shear rates $\dot{\gamma} \approx 0.355$ – $\dot{\gamma} = 0.385$) with wagging–like oscillations within PN regimes at the plates. Outside the banding region, the systems are characterized by the same value of T_2.

We observe that the value of the "selected" stress within the banding region, $T_2^{sel} \approx 0.59$, is essentially independent of the boundary conditions. Specifically, for the two types of isotropic boundary conditions, as well as for nematic ordering within the plane of the plates, the system stays in the homogeneous PN state for all $\dot{\gamma}$ up to the maximum of the flow curve. In contrast, the system with vertical alignment at the plates, *i.e.*, alignment in the shear gradient (y–) direction, forms bands once the value of T_2^{sel} is reached (at $\dot{\gamma} \approx 0.34$). In this sense, the vertical nematic ordering favors the occurrence of the W state characterized by oscillations in the gradient direction. For completeness we also note that upon decreasing $\dot{\gamma}$ from high values, the system goes without hysteresis into the banded state (with the same stress), irrespective of the boundary conditions.

In the initially nematic case [see Fig. 7.10(b)], upon increasing $\dot{\gamma}$ from lower values all systems, irrespective of boundary conditions, display shear band formation at shear rates in the range $\dot{\gamma} \approx 3.0$ – $\dot{\gamma} \approx 4.5$. After this critical values they break up into a band with kayaking–tumbling dynamics (*i.e.*, oscillations out of the shear plane) surrounded by regions of shear–alignment at the boundaries. The stress T_2 characterizing the banded state seems to be unique, and the boundary conditions only affect the onset of shear banding (upon starting from the low–shear rate branch, where the system is in the KT state). Moreover, from Fig. 7.10(b) we see that the onset of banding is "delayed" when

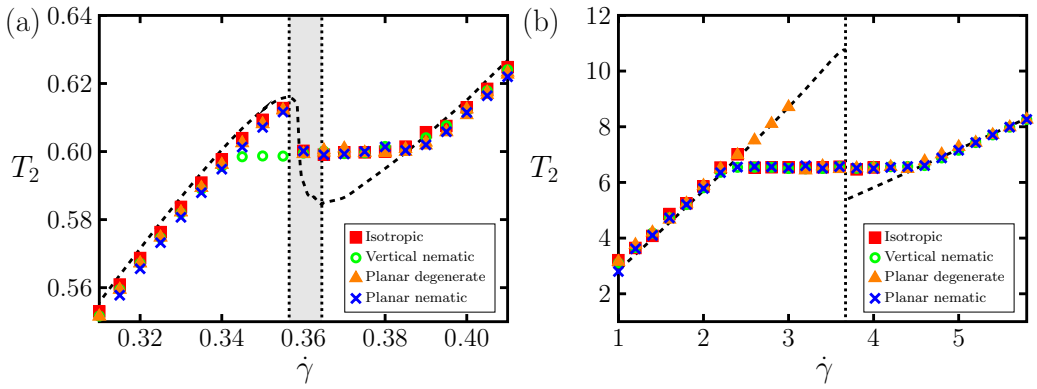

Figure 7.10: Influence of the boundary conditions on the inhomogeneous flow curves for (a) initially isotropic systems at $\Theta = 1.20$, $\lambda = 0.55$ and (b) initially nematic systems at $\Theta = -0.25$, $\lambda = 1.25$. The correlation length is set to $\xi^2 = 10^{-5}$. As a reference the homogeneous flow curves have been included.

planar degenerate boundaries are used. This is because these boundary conditions seem to support the KT state. Interestingly, the behavior upon decreasing the shear rate from the aligned state is different: in that case, all systems stay in the aligned state until the lower end of the high–shear rate branch is reached; then they directly jump into the KT state without an intermediate shear banded state.

Finally, both systems considered in Fig. 7.10 display shear banding irrespective of the detailed nature of the boundary conditions, if the shear rate is increased from low values. The boundary conditions then only influence the "critical" shear rate at which the homogeneous state observed at small $\dot{\gamma}$ breaks up into bands. On the contrary, shear banding upon decreasing $\dot{\gamma}$ from high values is only seen in the initially isotropic system. The behavior in the initially nematic system thus depends on the initial conditions, similar to what has been found in the DJS model [153].

7.3 Binary mixtures of rod–like colloids

After the analysis of the spatiotemporal behavior, in this section we turn to the analysis of binary mixtures. In the following we assume spatially homogeneous systems where the boundaries of the system do not play a role. Thus, we numerically solve Eqs (6.74)–(6.77) in the limit where $L \to \infty$.

To perform the numerical integration we employ a standard Runge-Kutta algorithm with adaptive step size control [151]. As in the case of the one component system, the starting values of the tensor components $q_0^\alpha, \cdots, q_4^\alpha$ (where $\alpha = A, B$) are chosen randomly in the interval $[0, 1]$, using a uniform distribution. We note that due to the high non–linearity of the problem at hand the choice of initial values and the overall number of time–steps required to obtain reliable results (disregarding transient initial behavior)

strongly depends on the chosen parameters. Therefore, all numerical integrations have been repeated several times. Finally, to characterize the resulting dynamical states, we use an algorithm that recognizes the periodicity and sign change of the calculated time–dependent order parameters $q_i^\alpha(t)$ (see e.g. Refs. [149, 49, 146]).

7.4 Orientational dynamics of binary mixtures

In the following we investigate sheared systems whose equilibrium state ($\dot{\gamma} = 0$) is nematic. Specifically, we set $\Theta_A = \Theta_B = -0.25$. According to the stability analysis in Chapter 5, in this case the isotropic phase is unstable irrespective to the value of Θ_{AB}.

The section is divided into two parts. First, we discuss the effect of varying the shear rate, $\dot{\gamma}$, and the tumbling parameter of species B, λ_B, while λ_A is fixed. We note that in real experiments, variation of the tumbling parameter is somewhat difficult since each value of this parameter corresponds to a different aspect ratio (and thus, particle type), see Eq. (6.74). However, in the framework of our dynamical equations $\lambda_{B(A)}$ is the crucial parameter measuring the impact of the shear induced perturbation, thus it seems worth to explore its role. Specifically, we set $\lambda_A = 1.2$ and consider a range of values $\lambda_B > \lambda_A$, implying that the B–particles have larger aspect ratios. The second part of the section addresses the role of the "cross–coupling" parameter Θ_{AB}.

7.4.1 Variation of the tumbling parameter and the shear rate

The numerical integration leads to dynamical state diagrams for each of the two species which we present in Fig. 7.11. As in Fig. 7.2, each colored region corresponds to a different dynamical state characterized by a specific behavior of the respective nematic director, related to the largest eigenvalue of the alignment tensor $\mathbf{Q}^{A(B)}$. Specifically, we observe wagging states (W), tumbling states (T), kayaking–wagging states (KW), kayaking–tumbling states (KT), and (flow–)alignment states (A). The boundaries between these colored regions correspond to different types of dynamical bifurcations and an analysis for the mixture would have been beyond the scope for this work. However, we note that the shape of each state diagram in Fig. 7.11 is qualitatively similar to that of one component systems (see Fig. 7.2). As in the one component system, we expect that a chaotic or irregular also occurs in the mixture (for both species) at values of $\dot{\gamma}$, λ_B where the regions A, KW and KT meet.

While the overall behavior of the two species is very similar, there are interesting differences for specific values of $\dot{\gamma}$ and λ_B. For example, consider the shear rate $\dot{\gamma} = 7.5$ and $\lambda_B = 3.0$. At these parameters, the long rods are in the W state while the short rods are in a tumbling (T) state. In other words, both directors display oscillatory behavior in the shear plane, but with different characteristics: Tumbling is characterized by full in–plane rotations of nematic director, whereas wagging just implies finite back–and–forth–motion in angular space.

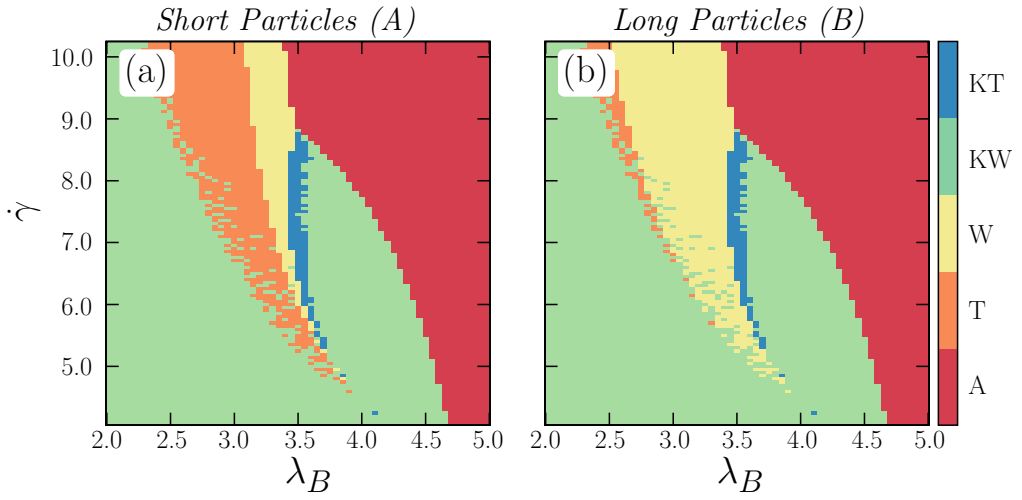

Figure 7.11: Dynamical state diagram for a binary mixtures characterized by $\Theta_A = -0.25$, $\Theta_B = -0.25$, $\Theta_{AB} = 1.50$, and $\lambda_A = 1.2$. Parts a) and b) illustrate the behavior of the short and long particles, respectively. Color bar on the right side: A = Alignment, W = Wagging, T = Tumbling, KW = Kayak–Wagging, KT = Kayak–Tumbling.

The tumbling and wagging states are characterized by in shear plane periodic motion of the nematic director, but the T state is characterized by full rotations of nematic director. Therefore, it is of interest to compare the angle between both nematic directors. Since in the T and W states $q_3^\alpha = q_4^\alpha = 0$, in terms of the components $q_0^\alpha, q_1^\alpha, q_2^\alpha$, $\vartheta(t)$ the angle between directors is given by

$$\vartheta(t) = \arccos\left(\frac{q_j^A q_j^B}{\sqrt{q_j^A q_j^A}\sqrt{q_j^B q_j^B}}\right), \tag{7.6}$$

where $j = 0, 1, 2$ and we used the Einstein convention. The angle between nematic directors is showed in Fig. 7.12(a) where we choose a constant shear rate $\dot{\gamma} = 7.5$ and three different values of λ_B.

As it can be seen form Fig. 7.12(a), at the largest λ_B considered, both species are in a shear aligned state. For single–component systems, it is well known that the shear aligned state is characterized by a finite angle between the (stationary) director and shear direction, and that this "flow angle" depends on the tumbling parameter. Therefore, one would expect the two directors of the mixture to have different (stationary) flow angles with respect to the shear direction, and consequently, enclose a finite angle in between. This is exactly what we see from the corresponding curve in Fig. 7.12(a). At $\lambda_B = 3.25$, both species are in the tumbling state (see Fig. 7.12), with the directors displaying

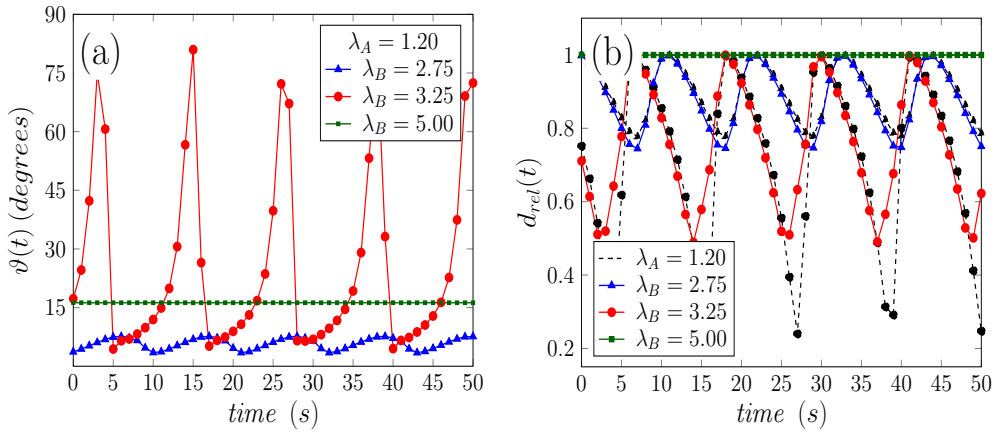

Figure 7.12: (a) Angle between the nematic directors as function of time at $\dot{\gamma} = 7.5$ and three values of λ_B. The green solid line (■) corresponds to shear–aligned states of both species ($\lambda_B = 5.0$), whereas the blue line (▲) corresponds to synchronized tumbling states ($\lambda_B = 2.75$). Finally, the red line (●) represents a case where the A–species (B–species) is in a tumbling (wagging) state ($\lambda_B = 2.75$). (b) Relative alignment of the nematic directors as a function of time at $\dot{\gamma} = 7.5$. The dashed black lines and the solid lines correspond to the behavior of the A–species ($\lambda_A = 1.20$) and B–species (with varying λ_B), respectively. The (■) symbol correspond to shear–aligned states of both components ($\lambda_B = 5.0$) whereas the (▲) correspond to synchronized tumbling states ($\lambda_B = 3.25$). Finally, (●) represents the coexisting T/W state ($\lambda_B = 3.75$).

full rotations. Still, we observe from Fig. 7.12(a) that the angle *between* the tumbling directors is close to zero at all times considered. We interpret this behavior as (nearly) *synchronous* tumbling. At $\lambda_B = 2.75$, the behavior is markedly different: Here we observe a periodic variation of the angle between the directors, reaching values up to nearly 90 degree. This reflects the simultaneous appearance of tumbling (species A) and wagging (species B).

To further compare the in–plane oscillations of the nematic directors in the different regions of the state diagram (see Fig. 7.11) we also look at their relative amplitudes. To this end we introduce a quantity that compares, for each component of the mixture, the instantaneous magnitude $|\mathbf{Q}^\alpha|(t)$ with its maximum value $\max\{|\mathbf{Q}^\alpha|\}$ (we recall at this point that the tensors considered here are *not* normalized to one). In terms of the components q_0^i, q_1^i, q_2^i, the relative alignment is therefore given by

$$d_{rel}^{A(B)}(t) = \frac{\sqrt{q_j^{A(B)} q_j^{A(B)}}}{\max\left\{\sqrt{q_j^{A(B)} q_j^{A(B)}}\right\}}, \tag{7.7}$$

where $j = 0, 1, 2$ and we used the Einstein convention. This quantity is shown in

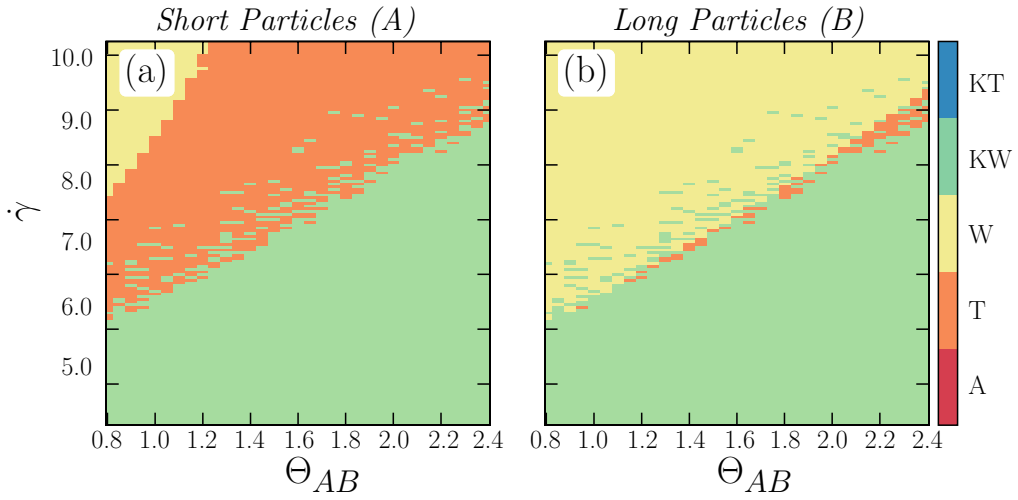

Figure 7.13: Dynamical state diagram in the plane spanned by shear rate and cross coupling parameter for a binary mixtures characterized by $\Theta_A = -0.25$, $\Theta_B = -0.25$, $\lambda_A = 1.2$ and $\lambda_B = 3.0$. Parts a) and b) illustrate the behavior of the short and long particles, respectively.

Fig. 7.12(b). As expected, in the shear aligned state ($\lambda_B = 5.0$) the relative alignment of both components does not oscillate in time. Further, when both nematic directors are tumbling (i.e., perform full rotations, here at $\lambda_B = 2.75$), the oscillations are in phase and also their magnitude is comparable. In contrast, in the coexisting T/W state ($\lambda_B = 3.25$), there is a marked difference between the amplitude of oscillations. Still, the oscillations are in phase. Therefore, we conclude that both, the T state and the coexisting T/W state are characterized by synchronous motion.

7.4.2 Variation of the cross coupling and the shear rate

In view of the variety of dynamical states at *fixed* cross coupling parameter Θ_{AB} it is interesting to further explore the impact of this parameter. To this end we present in Fig. 7.13 the state diagrams obtained at fixed tumbling parameters $\lambda_A = 1.20$ and $\lambda_B = 3.0$, in the plane spanned by Θ_{AB} and $\dot{\gamma}$. At $\dot{\gamma} = 0$ (equilibrium), all systems considered are in the (meta–)stable nematic phase.

At small shear rates $\dot{\gamma} \lesssim 5.0$, both species are in the out–of–plane KT state for all cross coupling parameters considered. At larger shear rates the out–of–plane oscillations then transform into in–plane oscillations of W or T type. As indicated from Fig. 7.13, an increase of Θ_{AB} shifts this boundary between KT and T or W towards larger shear rates for both components of the mixture. A further effect becomes apparent when we consider a fixed, high shear rate, e.g., $\dot{\gamma} = 8.0$. Here, an increase of Θ_{AB} can induce

profound changes of the dynamical state, such as a change from W to T to KT. Along this way, there a large regions where the two components display *different* dynamical behavior (coexistence of T and W), similar to what we have discussed before.

Finally, we notice the small "islands" of KT regions within the T state (A–species) or W–state (B–species). This indicates a bistability of the solutions which may be interpreted as a coexistence of in–shear plane and out–of–shear plane oscillations (as already mentioned in [50]). In fact, as we have previously showed for the one component system, any type of bistability may translate into spatially separated dynamical coexistence of different states (shear banding).

7.5 Summary

We present the shear induced instabilities occurring in systems of rod–like particles. We divide our discussion in two parts: the study of shear banding in one component systems and the analysis of oscillatory states in spatially homogeneous binary mixtures.

For one component systems, we focused on instabilities along the gradient direction. We saw that systems with different initial equilibrium states (isotropic or nematic), tumbling parameters (i.e., aspect ratios), and boundary conditions show complex shear banding behavior. Interestingly, the shear bands appearing in these systems are accompanied by oscillatory orientational motion in certain regions of space. We observe that band formation strongly depends on the orientational boundary conditions applied to the system. In this sense certain boundaries may enable or inhibit the formation of shear bands.

Similar to what occurs in one component systems, for a binary mixture we found a variety of oscillatory dynamical states of the nematic directors, either with in–plane or with out–of–plane symmetry. However, given an specific set of tumbling parameters, we observe symmetry breaking behavior for intermediate and high values of the shear rate. This behavior is characterized by the coexistence of simultaneous appearance of tumbling motion (short particles) and wagging motion (long particles). However, albeit the actual motion is different, there is an overall synchronization of the system.

We also observed that an additional control parameter of this oscillatory behavior is the coupling interaction Θ_{AB}. We show that by increasing Θ_{AB} at fixed shear rate, one can find transitions from in–plane oscillations to out–of–plane oscillations (kayaking–tumbling).

Chapter 8

Concluding remarks

8.1 Summary

In this thesis we investigated mixtures of rigid anisotropic colloidal particles under shear. In particular, we focused on binary mixtures of rod–like particles and developed a theoretical framework capable to describe their equilibrium behavior and the shear induced rheological response.

In Chapter 1, we give a general introduction to colloidal mixtures of rigid rod–like particles and addressed their basic equilibrium and shear induced behavior. Further, in Chapters 2 and 3, we continue this introductory remarks by presenting the phenomenological and microscopical descriptions of rod–like systems in equilibrium.

We begin our investigations in Chapter 4 where we cover the first goal of our research: to bridge microscopic and phenomenological theories. There, on the basis of the density functional theory, we construct a free energy functional given in terms of mesoscopic variables (the second rank alignment tensors and their derivatives). In addition, this functional contains both microscopic features of the system, namely, number density and aspect ratio of the particles. The combination of microscopic (DFT) and mesoscopic descriptions makes our approach a part of the theories contributing to a scale–bridging characterization of colloidal mixtures.

To validate our approach, we focus on binary mixtures characterized by molecules having equal diameters and different length in Chapter 5. Compared to previous experiments and particle based simulations our calculations show a reasonable agreement. In fact, the calculated state diagrams can be used to make predictions of the overall behavior of the mixture. At the end of this chapter, we discussed the relation between our theory and the Oseen–Frank elastic theory. In this regard, we obtained expressions for the Frank elastic constants (in the one constant approximation) in terms of the direct correlation function for the mixture. However, we should point out that at this level of simplification the material is only defined by a small number of quantities which may not be enough to fully parametrize any material.

We note that the biggest restriction of our equilibrium investigations (in general) is that we have focused on the orientational part of the free energy alone. Therefore, the stability analysis done in Chapter 5 does not give any information about phase transitions (or coupled phase transitions) involving the number densities as order parameters. This would clearly be an interesting extension of our work.

In Chapter 6, we presented a natural extension of the Doi–Hess description for binary mixtures. We achieved this by combining our equilibrium theory with the concepts of linear irreversible thermodynamics. By virtue of this, we got a pair of dynamic equations of motion which relate the alignment tensors of the particles (one for each component) with the hydrodynamic effects (through the stress tensor and the velocity field). Further, specializing to a planar Couette flow geometry and by expanding these tensor equations into an appropriate basis, we obtained an 11-dimensional coupled system of partial differential equations.

Finally, in Chapter 7, we focused on the shear induced instabilities occurring in binary mixtures. We divided our investigations in two parts: First, we analyzed the shear banding instabilities occurring in one component systems, and then, we focused on the shear induced orientational dynamics of binary mixtures.

In the case of shear banding instabilities, we focused on instabilities along the gradient direction and studied systems whose (un–sheared) equilibrium states were (stable) isotropic or nematic. We studied various tumbling parameters (aspect ratios) and different anchoring conditions. Our results reveal the appearance of shear banded states in the gradient direction accompanied by regions with oscillatory dynamics. This feature is not seen in other models (such as the non–local DJS model) and it is due to the coupling between alignment tensor and shear stress. Further, contrary to earlier studies [52, 75], we focused on parameters where the homogeneous systems exhibit regular oscillatory dynamics, and as a result the shear bands are characterized by regions of regular oscillatory orientational dynamics.

We noticed that the band formation is strongly dependent on two factors: the correlation length and the orientational boundary conditions. We observed that by changing these features the shear banded states (appearing in the middle of the sample see e.g. Fig. 7.8) become more defined in terms of width and *regularity* of the dynamics. This implies that the bands can be tuned, in principle, only by changing one of these parameters. Since the spatial correlation length is a property of the fluid, the obvious candidates are the boundary conditions. In fact, our observations prove that certain boundary conditions can support or hinder the formation of shear bands depending on the anchoring close to the plates.

We then turn to the analysis of binary mixtures. In this case, we showed that in a binary mixture deep in the nematic state there is a variety of synchronized oscillatory states of the nematic directors, either with in–plane or with out–of–plane symmetry. Strikingly, given a specific set of tumbling parameters (aspect ratios) in the mixture, we observe an area where two different in–plane oscillatory states coexist: tumbling motion for short particles and wagging motion for long particles. Interestingly, even though the

actual motion of the components is different, the oscillatory motion is still in synchrony. Additionally, we observed that as the coupling between the particles is increased, at a fixed shear rate, one can find transitions from in–plane oscillations to out–of–plane oscillations (kayaking–tumbling). However, these transitions are highly bistable and this can translate into an even more convoluted spatiotemporal behavior. At this point, it would be very interesting to extend the present analysis to spatially inhomogeneous systems.

8.2 Outlook and further investigations

Concerning the future development of our research, there are several directions that could be followed to extend our work; both for equilibrium and non–equilibrium phenomena.

Regarding the equilibrium theory, it would be very interesting to understand to what extent the mesoscopic free energy functionals are modified by coupling to density fluctuations. Therefore, the next logical step would be to improve our theory in order to take into account *full* spatial segregation. An idea is to the ansatz for the one body density:

$$\rho(\boldsymbol{r}, \hat{\boldsymbol{u}}) = \varrho(\boldsymbol{r}) f(\hat{\boldsymbol{u}}) \,,$$

where $\varrho(\boldsymbol{r})$ is an inhomogeneous density and $f(\hat{\boldsymbol{u}}(\mathbf{r}))$ is the usual orientational distribution function. In fact, with our investigations we prove that the ODF (under certain approximations) can always be written in terms of $\mathbf{Q}$–tensors, therefore the prospective free energy functional should be:

$$\mathcal{F}[\rho] \to \mathcal{F}[\varrho(\boldsymbol{r}), \mathbf{Q}(\boldsymbol{r})] \,.$$

Doing so, we could encounter some challenges. For example, because $\boldsymbol{r}$ and $\hat{\boldsymbol{u}}$ are not independent variables, even the normalization of $\rho(\boldsymbol{r}, \hat{\boldsymbol{u}})$ is not obvious. Another interesting complication arising from this ansatz has to do with a more general issue, the exact coupling between $\varrho(\boldsymbol{r})$ and the complete set of $\mathbf{Q}(\boldsymbol{r})$ tensors. This is a problem that has its roots on the closure approximation. Indeed changing the underlying assumption of the theory will necessarily change the way we cut the series expansion in the excess free energy [see Chapter 4].

Clearly, it would be interesting to extend the non–equilibrium investigations as well. First, the obvious candidate is to extend the analysis for the binary mixture towards spatially inhomogeneous systems. In fact, we ran some preliminary calculations for the homogeneous flow curves and the related spatiotemporal behavior. These calculations show that the region where the in–plane oscillatory states coexist is very unstable. The nature of these instabilities is not clear, thus, further analysis should be done in this direction.

Regarding the one component systems, it would also be interesting to study the shear induced instabilities in the direction perpendicular to the gradient. In fact, recent

publications [67, 68] show that *fd*–virus suspensions exhibit *vorticity* banding (where regularly stacked bands are formed along the vorticity direction). In this way it could be interesting to see if the Doi–Hess model is able to reproduce these phenomena.

To close this discussion, for industrial and technological applications it would be interesting to impose an additional control to the system in order to have a well–defined rheological response. One idea is to *tune* the system introducing an additional feedback. In fact, recent experimental studies [154, 155] use oscillatory rheometers to control the behavior of the viscosity and stress of the system. In view of this, an extension of our work would be to develop a theoretical approach that reproduces such behavior. In fact, earlier studies [156] showed that in the scope of the Doi–Hess theory, a feedback control strategy may lead to the stabilization of different dynamical states. The scheme used in these investigations is based on a single time delay τ in the alignment tensor, such that $\mathbf{Q} = \mathbf{Q}(t-\tau)$. However, considering our results for spatially inhomogeneous systems, an alternative approach would be to introduce a similar scheme to the stress tensor, *i.e.*, $\mathbf{T} = \mathbf{T}(t-\tau)$. This proposition would model the action of the oscillatory rheometer and would make it easier to compare the theoretical results with experimental measurements.

Appendices

Appendix A

Basic tensor concepts

Introduction

Tensor calculus came into prominence with the development of Einstein's general theory of relativity in 1916. Since then it can be seen as a universal language in mathematical physics [157]. Tensors not only enable us to write general equations in a very compact manner, but they also serve as a guide in the selection of physical laws by indicating invariance with respect to the transformation of coordinates.

The aim of this appendix is to serve as a short mathematical introduction to the use of Cartesian tensors and tensor calculus and to provide the necessary identities and relationships needed in the main text.

In physics it is usual to deal with real variables as functions represented by Cartesian coordinates of a point in a plane. If we are dealing with a quantity of three variables then the ordinary Euclidean space of three dimensions may be used. If the number of variables exceeds three, the geometrical representation is more complicated and a space of more than three dimensions is needed. For example, in the case of a rigid body in the Euclidean space, additional variables (Euler angles) are needed to describe its rotations around the fixed molecular axes.

In general, a tensor is a multidimensional array of numerical values. The rank (order) of a tensor is the dimensionality of the array needed to represent it. For example, a scalar is a zero rank tensor, whereas a linear map represented by a matrix is a 2nd order tensor. A more abstract definition is that of tensors being multilinear maps taking an element of a vector space into another vector space. Tensors do not change in any coordinate system and its components only depend on the relating transformed coordinate systems [158]. Some examples of tensor quantities commonly used by physicists are:

- **Scalar** $a \in \mathbb{R}$: 0–order tensor
- **Vector** $\mathbf{v} \in \mathbb{R}^n$: 1–order tensor
- **Matrix** $\mathbf{M} \in \mathbb{R}^n \times \mathbb{R}^n$: 2–order tensor

- **Levi–Civita symbols** $\epsilon_{ijk} \in \mathbb{R}^n \times \mathbb{R}^n \times \mathbb{R}^n$: 3–order tensor

A.1 General definitions and notations

Consider two right-handed coordinate systems V and V' in $\mathbb{R}^3$. The components of a vector $\mathbf{v} \in V$ are denoted by v_μ where $\mu = 1, 2, 3$, or $\mu = x, y, z$. If $\mathbf{v}'$ is the image of $\mathbf{v}$ in V' then

$$v'_\nu = D_{\mu\nu} v_\mu$$

where $\mathbf{D}$ is an orthogonal matrix describing the rotation $V \to V'$. The analogous transformation for a 2nd rank tensor $A_{\mu\nu}$ is

$$A'_{\lambda\gamma} = D_{\lambda\mu} D_{\gamma\nu} A_{\mu\nu} \,,$$

where $D_{kj} = D_{jk}$. This transformation between Cartesian tensors can be extended to k order tensors directly via [22]:

$$A'_{\mu_1\mu_2\cdots\mu_k} = D_{\mu_1\nu_1} D_{\mu_2\nu_2} \cdots D_{\mu_k\nu_k} A_{\mu_1\mu_2\cdots\mu_k} \,.$$

For many applications it is necessary to manipulate tensors in different ways. The multiplication of a tensor with a real number a means the multiplications of all its elements by this number, *i.e.* $aA_{\mu_1\mu_2\cdots\mu_k}$. On the other hand, the addition of two tensors can be done only when both have the same rank [22].

A.1.1 Scalar product

An important tensor manipulation is that of the tensor product. Between two vectors, the usual scalar product is

$$\mathbf{a} \cdot \mathbf{b} = a_\mu b_\mu \,,$$

where repeated indices are implicitly summed over (Einstein's convention). However, for second rank tensors the maximum contraction is done via the Frobenius inner product defined by,

$$\mathbf{A} : \mathbf{B} = A_{\mu\nu} B_{\mu\nu} \,.$$

The most general contraction between two k rank tensors always results in a scalar and it is denoted by $\odot$,

$$\mathbf{A}_{(k)} \odot \mathbf{B}_{(k)} = A_{\mu_1\mu_2\cdots\mu_k} B_{\mu_1\mu_2\cdots\mu_k} \,.$$

A.1.2 Tensor product

The cross product between two vectors in $\mathbb{R}^n$ results in a new vector in the same space, *i.e.*

$$\forall\ \mathbf{a}, \mathbf{b} \in \mathbb{R}^n \Rightarrow \mathbf{a} \times \mathbf{b} = \mathbf{c} \in \mathbb{R}^n \,.$$

However, the outer product, also known as tensor or dyadic product, between these pair of vectors results into a matrix, *i.e.*

$$\forall\ \mathbf{a},\mathbf{b}\in\mathbb{R}^n \Rightarrow \mathbf{a}\otimes\mathbf{b}=\mathbf{C}\in\mathbb{R}^{n\times n}\,.$$

In index notation the $\mu\nu$ element of the product $\mathbf{a}\otimes\mathbf{b}$ is

$$C_{\mu\nu}=(\mathbf{a}\mathbf{b}^T)_{\mu\nu}=a_\mu b_\nu \quad \text{where} \quad \mu,\nu=1,2,\cdots,n\,.$$

A tensor of rank k can be constructed as a hierarchy of outer products between a set of vectors. Let $\{\mathbf{a},\mathbf{b},\cdots\mathbf{k}\}$ be a set of vectors in $\mathbb{R}^n$ then, in terms of this set, the tensor $\mathbf{A}_{(k)}$ of order k is

$$\mathbf{A}_{(k)}=\mathbf{a}\otimes\mathbf{b}\otimes\cdots\otimes\mathbf{k} \quad \text{index notation} \quad A_{\mu_1\mu_2\cdots\mu_k}=a_{\mu_1}b_{\mu_2}\cdots k_{\mu_k}\,.$$

A.2 Decomposition of tensors

The decomposition of tensors is unique. For example, a second rank tensor, having 9 components can be decomposed into a sum of three tensors, one of each with 1, 3, and 5 linearly independent components [113]. The irreducible parts of a second rank tensor $\mathbf{A}$ are: an isotropic tensor $\mathbf{A}^{iso}$; an antisymmetric tensor $\mathbf{A}^{asy}$ and a symmetric traceless tensor $\overline{\mathbf{A}}$. Since $\mathbf{A}^{iso}=(\mathrm{Tr}\mathbf{A})\mathbb{I}/3$,

$$\mathbf{A}=\frac{1}{2}\mathrm{Tr}\mathbf{A}\mathbb{I}+\mathbf{A}^{asy}+\overline{\mathbf{A}}\,. \tag{A.1}$$

Tensors are classified by their behavior under rotations. Therefore, we can learn more about their representation by considering a decomposition of them in terms of the rotation group $SO(3)$. A Cartesian tensor of rank k has 3^k components and can be decomposed into a linear combination of its irreducible parts, each of which spans one of the irreducible representations of $SO(3)$ [113].

For an arbitrary Cartesian tensor of rank k, $\mathbf{A}_{(k)}$, the symmetric traceless part, $\overline{\mathbf{A}}_{(k)}$, is the only irreducible representation which is not reduced into a lower rank tensor [22].The number of independent components of an irreducible tensor of rank k is

$$2k+1\,.$$

A.2.1 Isotropic tensors

The symmetric traceless part of a tensor $\mathbf{A}_{(k)}$ can be written as a tensor contraction with another tensor which does not change its form when the Cartesian coordinate system is replaced by a rotated one, an isotropic tensor. Special cases are:

- Second rank (Kronecker delta):

$$\delta_{\mu\nu} = \begin{cases} 1 & \mu = \nu \\ 0 & \mu \neq \nu \end{cases} .$$

- Third rank (Levi–Civita symbol):

$$\epsilon_{\lambda\mu\nu} = \begin{cases} 1 & \lambda\mu\nu = 123; 312; 231 \\ -1 & \lambda\mu\nu = 213; 132; 321 \\ 0 & \text{otherwise} \end{cases} .$$

In terms of this tensors, the antisymmetric and isotropic parts of a second rank tensor $\mathbf{A}$ are:

$$\mathbf{A}^{asy} = -\frac{1}{2}\epsilon_{\lambda\mu\nu}\epsilon_{\gamma\eta\nu}A_{\mu\nu} , \tag{A.2}$$

$$\mathbf{A}^{iso} = \frac{1}{3}\delta_{\mu\eta}\delta_{\lambda\nu}A_{\mu\nu} . \tag{A.3}$$

A combination of second and third rank isotropic tensors can be constructed to give the projector of the symmetric traceless part:

$$\mathbf{\Delta}^{(2)} = \Delta_{\mu\lambda\eta\nu} = \frac{1}{2}(\delta_{\mu\eta}\delta_{\lambda\nu} + \delta_{\mu\nu}\delta_{\lambda\eta}) - \frac{1}{3}\delta_{\mu\lambda}\delta_{\eta\nu} . \tag{A.4}$$

This identity is such that for a arbitrary second rank tensor $\mathbf{A}$:

$$\overline{\mathbf{A}} = \mathbf{\Delta}^{(2)} : \mathbf{A} . \tag{A.5}$$

A generalization of the projection tensor $\mathbf{\Delta}^{(2)}$ is straightforward noticing that: the isotropic tensor of rank $2k$ should be symmetric and traceless in the first k indices and in the last k indices. This projection tensor is denoted by $\mathbf{\Delta}^{(k)}$ and is such that when applied to an arbitrary tensor $\mathbf{A}_{(k)}$ of rank k gives [113]:

$$\overline{\mathbf{A}}_{(k)} = \mathbf{\Delta}^{(k)} \odot \mathbf{A}_{(k)} . \tag{A.6}$$

A.3 Tensor operations

Restricting to second rank tensor quantities, in this section we list some basic identities and results of tensor analysis. For a more detailed discussion around this topic we refer the reader to *Tensor Calculus* by J. L. Synge *et al* [157] and *Tensor Analysis and Elementary Differential Geometry for Physicists and Engineers* by H. Nguyen-Schäfer *et al* [158].

A.3.1 First order derivatives

Gradient

The partial differentiation with respect to Cartesian components of the position vector $\mathbf{r}$ is frequently denoted by the operator

$$\nabla_\mu = \frac{\partial}{\partial r_\mu} \,. \tag{A.7}$$

The application of this operator to a 2nd rank tensor results in a $2+1$ rank tensor. The gradient of a second rank tensor $\mathbf{A}$ is

$$\nabla \mathbf{A} = \nabla_\lambda A_{\mu\nu} = B_{\lambda\mu\nu} = \mathbf{Q}_{(3)} \,. \tag{A.8}$$

A useful identity in terms of the Kronecker delta is

$$\nabla_\mu r_\nu = \delta_{\mu\nu} \,. \tag{A.9}$$

Divergence

The divergence of a tensor of rank k results on a tensor of rank $k-1$. The divergence of a second rank tensor is denoted by

$$\nabla \cdot \mathbf{A} = \nabla_\mu A_{\mu\nu} = B_\nu \,, \tag{A.10}$$

where B_μ is a vector.

Curl

The curl can operate on any tensor of rank k (higher than one) and results in a tensor of the same rank. For example, the curl of a second rank tensor is denoted

$$\nabla \times \mathbf{A} = \epsilon_{\lambda\mu\nu} \nabla_\mu A_{\nu\kappa} \,. \tag{A.11}$$

A.3.2 Integration theorems

Gauss' theorem

Let S be an open surface bounding a region Ω of volume V. Given the unit normal vector $\hat{\boldsymbol{n}}$ (pointing outwards) and $\mathbf{A}(\mathbf{x})$ a tensor field, then:

$$\int_V \mathbf{A} \cdot \nabla dV = \oint_S \mathbf{A} \cdot \hat{\boldsymbol{n}} dS \,. \tag{A.12}$$

Stoke's theorem:

Let S be an open surface bounded by a closed curve C. Given the unit normal vector $\hat{\boldsymbol{n}}$ (pointing outwards) and $\mathbf{A}(\mathbf{x})$ a tensor field, then:

$$\oint_C \mathbf{A} \cdot d\mathbf{x} = \int_S (\mathbf{A} \times \nabla) \cdot \hat{\boldsymbol{n}} dS \,. \tag{A.13}$$

A.3.3 Second order derivatives

Laplacian

The Laplacian refers to the special second derivative of a rank k tensor resulting on a tensor of rank k. It is the result of taking the divergence of a gradient and is denoted by

$$\nabla^2 \mathbf{A} = \nabla \cdot \nabla \mathbf{A} = \nabla_\lambda \nabla_\lambda A_{\mu\nu} \,. \tag{A.14}$$

An important identity related to the second order derivative $\nabla^2 \mathbf{A}$ is:

$$\nabla^2 \mathbf{A} = \nabla(\nabla \cdot \mathbf{A}) + \nabla \times (\nabla \times \mathbf{A}) \,. \tag{A.15}$$

Theorem

For a rank ($k = 2$) tensor field $\mathbf{A}$ the following identities for the second order derivative hold:

$$\nabla \times (\nabla \mathbf{A}) = 0 \qquad (\mathbf{A}\nabla) \times \nabla = 0 \tag{A.16}$$

$$\nabla \cdot (\nabla \times \mathbf{A}) = 0 \qquad (\mathbf{A} \times \nabla) \cdot \nabla = 0 \tag{A.17}$$

given that $\mathbf{A}$ is *smooth* enough. This theorem can be reformulated in the following way:

- The gradient of a tensor field is curl–free, *i.e.*, its curl vanishes.
- The curl of a tensor field is divergence–free, *i.e.*, its divergence vanishes.

This theorem may be proved applying Gauss' and Stoke's theorems to the tensor products $(\mathbf{A}\nabla)$ and $(\mathbf{A} \times \nabla)$ [157].

Green's identity for tensors

$$\nabla^2(\mathbf{A} : \mathbf{B}) = (\nabla^2 \mathbf{B}) : \mathbf{A} + 2(\nabla \mathbf{A}) \odot (\nabla \mathbf{B}) + \mathbf{B} : (\nabla(\nabla \cdot \mathbf{A})) - \mathbf{B} : (\nabla \times (\nabla \times \mathbf{A})) \,. \tag{A.18}$$

The fourth order derivative of a tensor field is often referred as "the Laplacian of the Laplacian" and is denoted by

$$\nabla^4 \mathbf{A} = \nabla^2 \nabla^2 \mathbf{A} \,.$$

The fourth order derivative of a tensor field is often used to stabilize an otherwise divergent partial differential equation [130].

A.3.4 Derivative with respect to second rank tensors

Given a scalar differentiable function $f(\mathbf{A})$ which maps the matrix $\mathbf{A} \in \mathbb{M}^{n\times m}$ to $\mathbb{R}$, the derivative of f with respect to $\mathbf{A}$ is

$$\mathbf{C} = \frac{\partial f(\mathbf{A})}{\partial \mathbf{A}} = \begin{pmatrix} \frac{\partial f}{\partial A_{11}} & \cdots & \frac{\partial f}{\partial A_{n1}} \\ \vdots & \ddots & \vdots \\ \frac{\partial f}{\partial A_{1n}} & \cdots & \frac{\partial f}{\partial A_{nm}} \end{pmatrix} . \tag{A.19}$$

where $\mathbf{C} \in \mathbb{M}^{n\times m}$. Some higher order derivatives referenced in the main text are:

$$\frac{\partial}{\partial \mathbf{A}} \mathsf{Tr}(\mathbf{A}^l) = l(\mathbf{A}^{l-1})^T , \tag{A.20}$$

$$\frac{\partial}{\partial \mathbf{A}} \mathsf{Tr}(\mathbf{A}^T\mathbf{B}\mathbf{A}) = \mathbf{B}\mathbf{A} + \mathbf{B}^T\mathbf{A} , \tag{A.21}$$

$$\frac{\partial}{\partial \mathbf{A}} \mathsf{Tr}(\mathbf{A}\mathbf{B}\mathbf{A}^T) = \mathbf{A}\mathbf{B}^T + \mathbf{A}\mathbf{B} . \tag{A.22}$$

All of this identities may be extended according to the specific type of matrix operator. Further information can be found in *The Matrix Cookbook* by K. B. Petersen *et al* [159].

A.4 Tensor basis

A symmetric traceless tensor $\mathbf{Q}$ has five independent components. Thus, it can be written in terms of these components using a standard orthonormal tensor basis [79]:

$$\begin{aligned} \mathbf{Q} &= \sum_{i=0}^{4} q_i \mathbf{B}_i , \qquad \text{where} & \mathbf{B}_0 &= \sqrt{\frac{3}{2}}\, \overline{\hat{\boldsymbol{e}}_z \hat{\boldsymbol{e}}_z} , \\ \mathbf{B}_1 &= \sqrt{\frac{1}{2}} \left(\overline{\hat{\boldsymbol{e}}_x \hat{\boldsymbol{e}}_x} - \overline{\hat{\boldsymbol{e}}_y \hat{\boldsymbol{e}}_y} \right) , & \mathbf{B}_2 &= \sqrt{2}\, \overline{\hat{\boldsymbol{e}}_x \hat{\boldsymbol{e}}_y} , \\ \mathbf{B}_3 &= \sqrt{2}\, \overline{\hat{\boldsymbol{e}}_x \hat{\boldsymbol{e}}_z} & \mathbf{B}_4 &= \sqrt{2}\, \overline{\hat{\boldsymbol{e}}_y \hat{\boldsymbol{e}}_z} . \end{aligned} \tag{A.23}$$

This tensor basis has the property $\mathbf{B}_i : \mathbf{B}_j = \delta_{ij}$, where δ_{ij} is the Kronecker symbol. The q_i components are given by the contraction $q_i = \mathbf{Q} : \mathbf{B}_i$. In matrix notation the

basis tensors are

$$\mathbf{B}_0 = \frac{1}{\sqrt{6}}\begin{pmatrix} -1 & 0 & 0 \\ 0 & -1 & 0 \\ 0 & 0 & 2 \end{pmatrix}, \qquad \mathbf{B}_1 = \frac{1}{\sqrt{2}}\begin{pmatrix} 1 & 0 & 0 \\ 0 & -1 & 0 \\ 0 & 0 & 0 \end{pmatrix},$$
$$\mathbf{B}_2 = \frac{1}{\sqrt{2}}\begin{pmatrix} 0 & 1 & 0 \\ 1 & 0 & 0 \\ 0 & 0 & 0 \end{pmatrix}, \qquad \mathbf{B}_3 = \frac{1}{\sqrt{2}}\begin{pmatrix} 0 & 0 & 1 \\ 0 & 0 & 0 \\ 1 & 0 & 0 \end{pmatrix}, \tag{A.24}$$
$$\mathbf{B}_4 = \frac{1}{\sqrt{2}}\begin{pmatrix} 0 & 0 & 0 \\ 0 & 0 & 1 \\ 0 & 1 & 0 \end{pmatrix}.$$

Explicitly the q_i components are related to the Cartesian components q_{ij} by

$$q_0 = -\frac{1}{\sqrt{6}}\left(q_{xx} + q_{yy} - 2q_{zz}\right), \qquad q_1 = \frac{1}{\sqrt{2}}\left(q_{xx} - q_{yy}\right),$$
$$q_2 = \frac{1}{\sqrt{2}}q_{xy}, \qquad q_3 = \frac{1}{\sqrt{2}}q_{xz}, \tag{A.25}$$
$$q_4 = \frac{1}{\sqrt{2}}q_{yz}.$$

These basis tensors have been used in a wide variety of tensor equations including flow alignment of liquid crystals [23, 79] and the non–linear behavior of gases, simple liquids and molecular fluids [80, 160, 161]. An equivalent set of basis tensors is used to study the Landau theory of blue phases and cholesterics [162, 163].

Appendix B

Spherical harmonics and their tensor representation

The rotation group $SO(3)$ is very relevant in fluid theory because it is used to represent physical quantities which are invariant under rotations, like tensors [see App. A], intermolecular potentials or pair correlation functions [99].

In this appendix we provide a compendium of the properties of the spherical harmonics and its relation with symmetric traceless tensors. For proofs of these relations we refer to standard references in group theory and its representations (e.g. *Introduction to group theory with applications* by G. Burns [164]).

B.1 Spherical harmonics

The spherical harmonic functions $\mathsf{Y}_{\mu\nu}(\hat{\boldsymbol{u}})$ employed in this study are

$$\mathsf{Y}_{\mu\nu}(\hat{\boldsymbol{u}}) \equiv \mathsf{Y}_{\mu\nu}(\theta,\phi) = (-1)^{\nu}\left[\frac{(2\mu+1)(\mu-\nu)!}{4\pi(\mu+\nu)!}\right]^{1/2} P_{\mu\nu}(\cos\theta)e^{i\nu\phi}\,, \tag{B.1}$$

where $\nu = 0,\cdots,\mu$ and $\mu = 0,1,2,\cdots$. Here $P_{\mu\nu}(\hat{\boldsymbol{u}}\cdot\hat{\boldsymbol{u}}')$ refers to the associated Legendre functions (for a short overview see Ref. [130]).The unit vector $\hat{\boldsymbol{u}}$ is such that $\hat{\boldsymbol{u}} = (\sin\theta\cos\phi, \sin\theta\sin\phi, \cos\theta)$. This definition may be extended to $\nu < 0$ using the identity

$$\mathsf{Y}_{\mu-\nu} = (-1)^{\nu} Y^{*}_{\mu\nu}\,, \tag{B.2}$$

where $Y^{*}_{\mu\nu}$ denotes the complex conjugate of $\mathsf{Y}_{\mu\nu}$. The spherical harmonics are orthogonalized functions such that:

$$\int_{\mathbb{S}^2} Y^{*}_{\mu\nu}(\hat{\boldsymbol{u}})\mathsf{Y}_{\mu'\nu'}(\hat{\boldsymbol{u}})d\hat{\boldsymbol{u}} = \delta_{\mu\mu'}\delta_{\nu\nu'}\,. \tag{B.3}$$

The integral over $\mathbb{S}^2$ denotes the solid angle integral where $\cos\theta \in [-1,1]$ and $\phi \in [0,2\pi]$.

B.1.1 Addition theorem

Spherical harmonics having two different directors $\hat{\boldsymbol{u}}$ and $\hat{\boldsymbol{u}}'$ can be related through the addition theorem, which is:

$$\sum_{\nu=0}^{\infty} Y^*_{\mu\nu}(\hat{\boldsymbol{u}}) \mathsf{Y}_{\mu\nu}(\hat{\boldsymbol{u}}') = \left(\frac{2\mu+1}{4\pi}\right) P_\mu(\hat{\boldsymbol{u}}\cdot\hat{\boldsymbol{u}}')\,, \tag{B.4}$$

where $\hat{\boldsymbol{u}}\cdot\hat{\boldsymbol{u}}' = cos\gamma$ and γ is the angle between $\hat{\boldsymbol{u}}$ and $\hat{\boldsymbol{u}}'$. Here $P_k(\hat{\boldsymbol{u}}\cdot\hat{\boldsymbol{u}}')$ is the k–th term of the Legendre polynomials.

B.1.2 Product rule

The multiplication of a pair of spherical harmonics results in

$$\mathsf{Y}_{\mu_1\nu_1}(\hat{\boldsymbol{u}})\mathsf{Y}_{\mu_2\nu_2}(\hat{\boldsymbol{u}}) = \sum_{\mu\nu}\left(\frac{(2\mu_1+1)(2\mu_2+1)}{4\pi(2\mu+1)}\right)^{\frac{1}{2}} C(\mu_1\mu_2\mu;000)\times C(\mu_1\mu_2\mu;\nu_1\nu_2\nu)\mathsf{Y}_{\mu\nu}(\hat{\boldsymbol{u}})\,, \tag{B.5}$$

where $C(\mu_1\mu_2\mu;\nu_1\nu_2\nu)$ is a Clebsch–Gordan coefficient (see Section B.2) . For a full definition of these coefficients and their use in mathematical physics we refer to Refs. [99, 113].

B.1.3 Integrals

Since the spherical harmonics are orthogonal functions [see Eq. (B.3)] the following integration rules are satisfied:

$$\int_{\mathbb{S}^2} \mathsf{Y}_{\mu\nu}(\hat{\boldsymbol{u}}) d\hat{\boldsymbol{u}} = (4\pi)^{1/2}\delta_{\mu 0}\delta_{\nu 0}\,, \tag{B.6}$$

$$\int_{\mathbb{S}^2} \mathsf{Y}_{\mu\nu}(\hat{\boldsymbol{u}}) Y^*_{\mu'\nu'}(\hat{\boldsymbol{u}}) d\hat{\boldsymbol{u}} = \delta_{\mu\mu'}\delta_{\nu\nu'}\,. \tag{B.7}$$

B.1.4 Series expansion

The spherical harmonics form a complete set of orthonormal functions and thus form an orthonormal basis of the field of quadratically integrable functions. Therefore an arbitrary

function $f(\hat{\boldsymbol{u}})$ on the unit sphere can be expanded in terms of a linear combination of spherical harmonics. Thus,

$$f(\hat{\boldsymbol{u}}) = \sum_{\mu=0}^{\infty} \sum_{\nu=-\mu}^{\mu} f_{\mu\nu} \mathsf{Y}_{\mu\nu}(\hat{\boldsymbol{u}}) \,, \tag{B.8}$$

where the $f_{\mu\nu}$ coefficients are given by

$$f(\hat{\boldsymbol{u}}) = \int_{\mathbb{S}^2} d\hat{\boldsymbol{u}} f_{\mu\nu} \mathsf{Y}^*_{\mu\nu}(\hat{\boldsymbol{u}}) \,. \tag{B.9}$$

The series in equation (B.8) is convergent if the μ coefficients decay sufficiently fast [122, 130].

B.2 Clebsch–Gordan coefficients

The spherical harmonics $\mathsf{Y}_{\mu\nu}(\hat{\boldsymbol{u}}')$ transform under rotations

$$\mathsf{Y}_{\mu\nu'}(\hat{\boldsymbol{u}}') = \sum_{\nu} \mathcal{D}^{\mu}_{\nu\nu'}(\Omega) \mathsf{Y}_{\mu\nu}(\hat{\boldsymbol{u}}) \,, \tag{B.10}$$

and the inverse transformation

$$\mathsf{Y}_{\mu\nu}(\hat{\boldsymbol{u}}) = \sum_{\nu'} \mathcal{D}^{\mu}_{\nu'\nu}(\Omega^{-1}) \mathsf{Y}_{\mu\nu'}(\hat{\boldsymbol{u}}') \,, \tag{B.11}$$

where $\hat{\boldsymbol{u}}$ and $\hat{\boldsymbol{u}}'$ are the orientation of $\mathbf{r}'$ with respect to XYZ and $X'Y'Z'$, respectively, and Ω denotes the rotation carrying XYZ into coincidence with $X'Y'Z'$ (see Ref. [99]). Equation (B.8) defines the rotation matrix $\mathcal{D}^{\mu}_{\nu\nu'}(\Omega^{-1})$ where $\mu = 1, 2, \cdots; \nu, \nu' = -\mu, \cdots, \mu$. The rotation matrices (also called the representation coefficients of the rotation group $SO(3)$) are functions of the rotation $\Omega = \{\phi, \theta, \psi\}$ (Euler angles) which carries the initial frame XYZ into coincidence with the final frame $X'Y'Z'$.

Equation (B.8) allows to write the product $\mathsf{Y}_{\mu_1\nu_1'}(\hat{\boldsymbol{u}}')\mathsf{Y}_{\mu_2\nu_2'}(\hat{\boldsymbol{u}}')$ [see (B.5)]:

$$\mathsf{Y}_{\mu_1\nu_1'}(\hat{\boldsymbol{u}}_1')\mathsf{Y}_{\mu_2\nu_2'}(\hat{\boldsymbol{u}}_2') = \sum_{\nu_1\nu_2} \mathcal{D}^{\mu_1}_{\nu_1\nu_1'}(\Omega)\mathcal{D}^{\mu_2}_{\nu_2\nu_2'}(\Omega)\, \mathsf{Y}_{\mu_1\nu_1}(\hat{\boldsymbol{u}}_1)\mathsf{Y}_{\mu_2\nu_2}(\hat{\boldsymbol{u}}_2) \,. \tag{B.12}$$

For fixed μ_1, μ_2, the interest is to find a linear combination $\mathsf{F}_{\mu\nu}(\hat{\boldsymbol{u}}_1, \hat{\boldsymbol{u}}_2)$ of products of spherical harmonics that transforms according to a single rotation matrix $\mathcal{D}^{\mu}$:

$$\mathsf{F}_{\mu\nu'}(\hat{\boldsymbol{u}}_1', \hat{\boldsymbol{u}}_2') = \sum_{\nu} \mathcal{D}^{\mu}_{\nu\nu'}(\Omega) \mathsf{F}_{\mu\nu}(\hat{\boldsymbol{u}}_1, \hat{\boldsymbol{u}}_2) \,. \tag{B.13}$$

In terms of the product of spherical harmonics $\mathsf{F}_{\mu\nu}(\hat{\boldsymbol{u}}_1, \hat{\boldsymbol{u}}_2)$ is defined as:

$$\mathsf{F}_{\mu\nu'}(\hat{\boldsymbol{u}}_1', \hat{\boldsymbol{u}}_2') = \sum_{\nu_1\nu_2} C(\mu_1\mu_2\mu; \nu_1\nu_2\nu)\mathsf{Y}_{\mu_1\nu_1}\mathsf{Y}_{\mu_2\nu_2}\,, \tag{B.14}$$

where $C(\mu_1\mu_2\mu; \nu_1\nu_2\nu)$ are the Clebsch–Gordan coefficients (see e.g. Ref. [99]). The linear combinations $\mathsf{F}_{\mu\nu}(\hat{\boldsymbol{u}}_1, \hat{\boldsymbol{u}}_2)$ are normalized to unity to ensure that $C(\mu_1\mu_2\mu; \nu_1\nu_2\nu)$ in Eq. (B.12) is a real valued unitary transformation. The above argument can also be extended to construct rotational invariants form triple products of spherical harmonics $\mathsf{Y}_{\mu_1\nu_1}\mathsf{Y}_{\mu_2\nu_2}\mathsf{Y}_{\mu_3\nu_3}$.

In the following we list a few properties of the Clebsch–Gordan coefficients:

Symmetry properties

$$C(\mu_1\mu_2\mu_3; \nu_1\nu_2\nu_3) = (-1)^{\mu_1+\mu_2+\mu_3} C(\mu_1\mu_2\mu_3; -\nu_1-\nu_2-\nu_3) \tag{B.15}$$

$$= (-1)^{\mu_1+\mu_2+\mu_3} C(\mu_2\mu_1\mu_3; \nu_2\nu_1\nu_3) \tag{B.16}$$

$$= (-1)^{\mu_1+\nu_1} \left(\frac{2\mu_3+1}{2\mu_2+1}\right)^{\frac{1}{2}} C(\mu_1\mu_3\mu_2; \nu_1-\nu_3-\nu_2) \tag{B.17}$$

$$= (-1)^{\mu_2+\nu_2} \left(\frac{2\mu_3+1}{2\mu_1+1}\right)^{\frac{1}{2}} C(\mu_3\mu_2\mu_1; -\nu_3\nu_2-\nu_1) \tag{B.18}$$

$$= (-1)^{\mu_1+\nu_1} \left(\frac{2\mu_3+1}{2\mu_2+1}\right)^{\frac{1}{2}} C(\mu_2\mu_3\mu_1; \nu_3-\nu_1\nu_2) \tag{B.19}$$

$$= (-1)^{\mu_2+\nu_2} \left(\frac{2\mu_3+1}{2\mu_1+1}\right)^{\frac{1}{2}} C(\mu_2\mu_3\mu_1; \nu_2\nu_3-\nu_1) \tag{B.20}$$

Orthogonality relations

$$\sum_{\mu_1\mu_2} C(\mu_1\mu_2\mu; \nu_1\nu_2\nu)\, C(\mu_1\mu_2\mu'; \nu_1\nu_2\nu') = \delta_{\mu\mu'}\delta_{\nu\nu'}\,, \tag{B.21}$$

$$\sum_{\mu_1\mu_2} C(\mu_1\mu_2\mu; \nu_1\nu_2\nu)\; C(\mu_1\mu_2\mu; \nu_1'\nu_2'\nu) = \delta_{\mu_1\mu_1'}\delta_{\mu_2\mu_2'}\,. \tag{B.22}$$

Series expansion (Rotational invariants)

Referred to an arbitrary space–fixed reference frame a two–molecule quantity $f(\mathbf{r}-\mathbf{r}', \hat{\boldsymbol{u}}, \hat{\boldsymbol{u}}')$ (e.g. pair potential, pair correlation function, etc.) may be represented as an infinite sum of spherical invariants.

$$f(\mathbf{r}-\mathbf{r}'; \hat{\boldsymbol{u}}, \hat{\boldsymbol{u}}') = \sum_{l_1l_2l} f(l_1l_2l; \mathbf{r}-\mathbf{r}')\Phi(l_1l_2l; \hat{\boldsymbol{u}}, \hat{\boldsymbol{u}}', \hat{\boldsymbol{u}}_x)\,, \tag{B.23}$$

where $f(l_i l_2 l; \mathbf{r}-\mathbf{r}')$ are the harmonic expansion coefficients given by

$$f(l_1 l_2 l; \mathbf{x}) = \frac{(2l_1+1)(2l_2+1)}{4\pi(2l+1)} \int_{\mathbb{S}^2} d\hat{\boldsymbol{u}} \int_{\mathbb{S}^2} d\hat{\boldsymbol{u}}' f(\mathbf{r}-\mathbf{r}'; \hat{\boldsymbol{u}}, \hat{\boldsymbol{u}}') \Phi(l_1 l_2 l; \hat{\boldsymbol{u}}, \hat{\boldsymbol{u}}', \hat{\boldsymbol{u}}_x)\,. \quad \text{(B.24)}$$

Here, the rotational invariants $\Phi(l_1 l_2 l; \hat{\boldsymbol{u}}, \hat{\boldsymbol{u}}', \hat{\boldsymbol{u}}_x)$ are given by

$$\Phi(l_1 l_2 l; \hat{\boldsymbol{u}}, \hat{\boldsymbol{u}}', \hat{\boldsymbol{u}}_x) = \sum_{m_1 m_2 m} C(l_1 l_2 l; m_1 m_2 m) \mathsf{Y}_{l_1 m_1}(\hat{\boldsymbol{u}}) \mathsf{Y}_{l_2 m_2}(\hat{\boldsymbol{u}}') \mathsf{Y}^*_{lm}(\hat{\boldsymbol{u}}_x)\,, \quad \text{(B.25)}$$

where Y_{lm} are the spherical harmonics and $C(l_1 l_2 l; m_1 m_2 m)$ are the Clebsch–Gordan coefficients. The notation in Eqs. (B.23) and (B.25) represents explicitly the following:

$$\sum_{l_1 l_2 l} \to \sum_{l_1=0}^{\infty} \sum_{l_2=0}^{\infty} \sum_{l=|l_1-l_2|}^{|l_1+l_2|} \quad \text{and} \quad \sum_{m_1 m_2 m} \to \sum_{m_1=-l_1}^{l_1} \sum_{m_2=-l_2}^{l_2} \sum_{m=-l}^{l} \delta_{m,m_1+m_2}\,. \quad \text{(B.26)}$$

B.3 Spherical components of symmetric traceless tensors

An arbitrary Cartesian vector $\mathbf{r} = (r_x, r_y, r_z)$ is written in terms of its spherical components r_μ with $\mu = 0, \pm 1$ in terms of the orthogonal basis

$$\mathbf{e}_0 = (0,0,1)\,, \qquad \mathbf{e}_{\pm 1} = \mp \frac{1}{\sqrt{2}} (1, \pm i, 0)\,, \quad \text{(B.27)}$$

where

$$\mathbf{e}^*_\mu \mathbf{e}_\nu = \delta_{\mu\nu} \quad \text{and} \quad \mathbf{e}^*_\mu = (-1)^\mu \mathbf{e}_{-\mu}\,. \quad \text{(B.28)}$$

Hence $\mathbf{r} = r_\mu \mathbf{e}_\mu$ where the r_μ coefficients are given by the relation $r_\mu = \mathbf{r} \cdot \mathbf{e}_\mu$.

B.3.1 Arbitrary rank tensors

A k rank tensor can be expressed in terms of the basis [113]:

$$\mathbf{e}^{(k)}_\mu = \left(\frac{k!(2\mu)!(2k-1)!!}{(k-\mu)!\mu!(k+\mu)!(2\mu-1)!!} \right)^{1/2} \overbrace{\mathbf{e}_0^{k-\mu} \mathbf{e}_1^{\mu}}\,, \quad \mu \geq 0\,. \quad \text{(B.29)}$$

$$\text{with} \quad \mathbf{e}^{(k)}_{-\mu} = (-1)^\mu \mathbf{e}^{(k)*}_\mu\,. \quad \text{(B.30)}$$

This tensor basis is orthogonal and complete, therefore:

$$\mathbf{e}^{(k)*}_\mu \odot \mathbf{e}^{(k)}_\nu = \delta_{\mu\nu} \quad \text{and} \quad \mathbf{e}^{(k)}_\mu \mathbf{e}^{(k)*}_\mu = \boldsymbol{\Delta}^{(k)}\,, \quad \text{(B.31)}$$

where $\mathbf{\Delta}^{(k)}$ is the $2k$ rank isotropic tensor addressed in App. A [1]

It follows directly from Eqs. (B.10), (B.12) and the orthogonality of the spherical harmonics that, in terms of the unit vector $\hat{\boldsymbol{u}} = (\sin\theta\cos\phi, \sin\theta\sin\phi, \cos\theta)$:

$$\mathsf{Y}_{k\mu}(\hat{\boldsymbol{u}}) = \left(\frac{(2k+1)!!}{4\pi k!}\right)^{1/2} (\overbrace{\hat{\boldsymbol{u}}^k})_\mu \,, \tag{B.32}$$

$$\overbrace{\hat{\boldsymbol{u}}^k} \odot \overbrace{\hat{\boldsymbol{u}}^k} = \frac{k!}{(2k-1)!!} \,, \tag{B.33}$$

$$\int_{\mathbb{S}^2} \overbrace{\hat{\boldsymbol{u}}^k}\, \overbrace{\hat{\boldsymbol{u}}^{k'}}\, d\hat{\boldsymbol{u}} = \frac{4\pi k!}{(2k+1)!!}\delta_{kk'}\mathbf{\Delta}^{(k)} \,. \tag{B.34}$$

Further identities and properties of the spherical harmonics and their tensor representation can be found in Refs. [99, 113].

[1] In the same manner as in the previous Appendix (App. A) Here the notation $^{(k)}$ refers to a $2k$ rank tensor.

Bibliography

[1] A. Mertelj, D. Lisjak, M. Drofenik, and M. Čopič, "Ferromagnetism in suspensions of magnetic platelets in liquid crystal," *Nature*, vol. 504, pp. 237–241, 2013.

[2] A. R. Morgan, A. B. Dawson, H. S. Mckenzie, T. S. Skelhon, R. Beanland, H. P. Franks, and S. A. Bon, "Chemotaxis of catalytic silica–manganese oxide matchstick particles," *Mater. Horiz.*, vol. 1, pp. 65–68, 2014.

[3] C. Su, J. Lien, and H. Lin, "Liquid crystal mixture and liquid crystal display panel," 2013. US Patent 8,558,973.

[4] C. Wang, W. Chu, R. Chiou, S. You, H. Zhang, and Y. Tan, "Liquid crystal compound and liquid crystal mixture," 2013. US Patent 8,388,861.

[5] R. Baetens, B. P. Jelle, and A. Gustavsen, "Properties, requirements and possibilities of smart windows for dynamic daylight and solar energy control in buildings: A state-of-the-art review," *Sol. Energ. Mat. Sol. Cells*, vol. 94, pp. 87–105, 2010.

[6] J. P. Lagerwall and G. Scalia, "A new era for liquid crystal research: Applications of liquid crystals in soft matter nano-, bio-and microtechnology," *Current Applied Physics*, vol. 12, pp. 1387–1412, 2012.

[7] S.-H. Sun, M.-J. Lee, Y.-H. Lee, W. Lee, X. Song, and C.-Y. Chen, "Immunoassays for the cancer biomarker ca125 based on a large-birefringence nematic liquid-crystal mixture," *Biomed. Opt. Express*, vol. 6, pp. 245–256, 2015.

[8] S. C. Glotzer and M. J. Solomon, "Anisotropy of building blocks and their assembly into complex structures," *Nat. Mater.*, vol. 6, pp. 557–562, 2007.

[9] J. Pelaez and M. Wilson, "Molecular orientational and dipolar correlation in the liquid crystal mixture e7: a molecular dynamics simulation study at a fully atomistic level," *Phys. Chem. Chem. Phys.*, vol. 9, pp. 2968–2975, 2007.

[10] C. L. Risi, A. F. Neto, P. R. Fernandes, A. R. Sampaio, E. Akpinar, and M. B. Santos, "Shear viscosity and rheology of ternary and quaternary lyotropic liquid crystals in discotic and calamitic nematic phases," *Rheol. Acta*, vol. 54, pp. 529–543, 2015.

[11] M. Shuai, A. Klittnick, Y. Shen, G. P. Smith, M. R. Tuchband, C. Zhu, R. G. Petschek, A. Mertelj, D. Lisjak, M. Čopič, *et al.*, "Spontaneous liquid crystal and ferromagnetic ordering of colloidal magnetic nanoplates," *Nat. Commun.*, vol. 7, p. 10394, 2016.

[12] P. Woolston and J. S. van Duijneveldt, "Isotropic-nematic phase transition of polydisperse clay rods,," *J. Chem. Phys*, vol. 142, 2015.

[13] R. M. van der Kooij and H. N. W. Lekkerkerker, "Liquid-crystalline phase behavior of a colloidal rod-plate mixture," *Phys. Rev. Lett.*, vol. 84, pp. 781–784, 2000.

[14] X. Zhou, H. Chen, and M. Iwamoto, "Orientational order in binary mixtures of hard gaussian overlap molecules," *J. Chem. Phys.*, vol. 120, p. 1832, 2004.

[15] S. Varga, K. Purdy, A. Galindo, S. Fraden, and G. Jackson, "Nematic-nematic phase separation in binary mixtures of thick and thin hard rods: Results from onsager-like theories," *Phys. Rev. E*, vol. 72, p. 051704, 2005.

[16] K. R. Purdy, S. Varga, A. Galindo, G. Jackson, and S. Fraden, "Nematic phase transitions in mixtures of thin and thick colloidal rods," *Phys. Rev. Lett.*, vol. 94, 2005.

[17] M. Dijkstra, "Entropy-driven demixing in a binary mixture of thick and thin spherocylinders." 2006.

[18] T. van Westen, T. J. H. Vlugt, and J. Gross, "The isotropic-nematic and nematic-nematic phase transition of binary mixtures of tangent hard-sphere chain fluids: An analytical equation of state," *J. Chem. Phys.*, vol. 140, p. 034504, 2014.

[19] P. G. de Gennes, *The physics of liquid crystals*. Clarendon Press, Oxford, 1993.

[20] C. Oseen, "The theory of liquid crystals," *J. Chem. Soc. Faraday Trans.*, vol. 29, pp. 883–899, 1933.

[21] F. C. Frank, "I. liquid crystals. on the theory of liquid crystals," *Discuss. Faraday Soc.*, vol. 25, pp. 19–28, 1958.

[22] S. Hess, *Tensors for Physics*. Springer Intl., Switzerland, 2015.

[23] I. Pardowitz and S. Hess, "Of the theory of irreversible processes in molecular liquids and liquid crystals, non-equilibrium phenomena associated with the second and forth rank alignment tensors," *Physica A*, vol. 100, 1980.

[24] L. Onsager, "The effects of shape on the interaction of colloidal particles," *Ann. N. Y. Acad. Sci.*, vol. 51, 1949.

[25] R. Evans, "The nature of the liquid-vapour interface and other topics in the statistical mechanics of non-uniform, classical fluids," *Adv. Phys.*, vol. 28, pp. 143–200, 1979.

[26] R. Evans, *Density functionals in the theory of nonuniform fluids*. Marcel Dekker, New York, 1992.

[27] P. Tarazona, "A density functional theory of melting," *Mol. Phys.*, vol. 52, pp. 81–96, 1984.

[28] P. Tarazona, J. A. Cuesta, and Y. Martínez-Ratón, *Density Functional of Hard Particle Systems*, vol. 753. Springer Verlag, 2008.

[29] A. Poniewierski and R. Holyst, "Density-functional theory for systems of hard rods," *Phys. Rev. A*, vol. 41, pp. 6871–6880, Jun 1990.

[30] Y. Singh and K. Singh, "Density-functional theory of curvature elasticity in nematic liquids. iii. numerical results for the berne-pechukas pair-potential model," *Phys. Rev. A*, vol. 33, p. 3481, 1985.

[31] K. Singh and Y. Singh, "Density-functional theory of curvature elasticity in nematic liquids. ii. effect of long-range dispersion interactions," *Phys. Rev. A*, vol. 34, p. 548, 1986.

[32] K. Singh and Y. Singh, "Density-functional theory of curvature elasticity in nematic liquids. i," *Phys. Rev. A*, vol. 35, p. 3535, 1987.

[33] M. Dennison, M. Dijkstra, and R. van Roij, "Phase diagram and effective shape of semiflexible colloidal rods and biopolymers," *Phys. Rev. Lett.*, vol. 106, 2011.

[34] M. Dennison, M. Dijkstra, and R. van Roij, "The effects of shape and flexibility on bio-engineered fd-virus suspensions," *The Journal of Chemical Physics*, vol. 135, no. 14, 2011.

[35] A. Malijevsky, G. Jackson, and S. Varga, "Many-fluid onsager density functional theories for orientational ordering in mixtures of anisotropic hard-body fluids," *J. Chem. Phys*, vol. 129, 2008.

[36] R. Wittkowski, H. Löwen, and H. R. Brand, "Derivation of a three-dimensional phase-field-crystal model for liquid crystals from density functional theory," *Phys. Rev. E*, vol. 82, p. 031708, Sep 2010.

[37] J. D. Parsons, "Nematic ordering in a system of rods," *Phys. Rev. A*, vol. 19, pp. 1225–1230, 1979.

[38] S.-D. Lee, "A numerical investigation of nematic ordering based on a simple hard-rod model," *J. Chem. Phys*, vol. 87, pp. 4972–4974, 1987.

[39] T. V. Ramakrishnan and M. Yussouff, "First-principles order-parameter theory of freezing," *Phys. Rev. B*, vol. 19, pp. 2775–2794, 1979.

[40] A. Poniewierski and J. Stecki, "Statistical theory of the elastic constants of nematic liquid crystals," *Mol. Phys.*, vol. 38, pp. 1931–1940, 1979.

[41] A. Poniewierski and J. Stecki, "Statistical theory of the frank elastic constants," *Phys. Rev. A*, vol. 25, pp. 2368–2370, Apr 1982.

[42] H. Löwen *J. Phys. Condens. Matter*, vol. 20, p. 404201, 2008.

[43] H. Löwen, "Colloidal dispersions in external fields," *J. Phys.: Condens. Matter*, vol. 24, p. 460201, 2012.

[44] D. Guu, J. Dhont, and M. Lettinga, "Dispersions and mixtures of particles with complex architectures in shear flow," *Eur. Phys. J. ST*, vol. 222, pp. 2739–2755, 2013.

[45] A. M. Menzel *Phys. Rep.*, vol. 554, pp. 1 – 45, 2015.

[46] P. D. Olmsted, *The effect of shear flow on the isotropic-nematic transition in liquid crystals*. PhD thesis, University of Illinois, Urbana-Champaign, 1991.

[47] Z. Dogic and S. Fraden, *Phase behavior of rod–like viruses and virus–sphere mixtures*. Wiley Verlag, 2007.

[48] G. Rienäcker and S. Hess, "Orientational dynamics of nematic liquid crystals under shear flow," *Physica A*, vol. 267, 1999.

[49] G. Rienäcker, *Orientational dynamics of nematic liquid crystals in a shear flow*. Shaker, Verlag, 2000.

[50] D. A. Strehober, H. Engel, and S. H. L. Klapp, "Oscillatory motion of sheared nanorods beyond the nematic phase," *Phys. Rev. E*, vol. 88, 2013.

[51] G. Rienäcker, M. Kröger, and S. Hess, "Chaotic orientational behavior of a nematic liquid crystal sybjected to a steady shear flow," *Phys. Rev. E*, vol. 66, 2002.

[52] B. Chakrabarti, M. Das, C. Dasgupta, S. Ramaswamy, and A. Sood, "Spatiotemporal rheochaos in nematic hydrodynamics," *Phys. Rev. Lett.*, vol. 92, p. 055501, 2004.

[53] S. M. Fielding and P. D. Olmsted, "Kinetics of the shear banding instability in startup flows," *Phys. Rev. E*, vol. 68, p. 036313, 2003.

[54] P. D. Olmsted *Rheol. Acta*, vol. 47, pp. 283–300, 2008.

[55] Y.-G. Tao, W. den Otter, and W. Briels, "Kayaking and wagging of rods in shear flow," *Phys. Rev. Lett.*, vol. 95, p. 237802, 2005.

[56] M. Ripoll, P. Holmqvist, R. G. Winkler, G. Gompper, J. K. G. Dhont, and M. P. Lettinga, "Attractive colloidal rods in shear flow," *Phys. Rev. Lett.*, vol. 101, p. 168302, 2008.

[57] S. Hess, "Pre– and post–transitional behavior of the flow alignment and flow–induced phase transition in liquid crystals," *Z. Naturforsch.*, vol. 30a, 1975.

[58] C. Pereira Borgmeyer and S. Hess, "Unified description of the flow alignment and viscosity in the isotropic and nematic phases of liquid crystals," *J. Non-Equilib. Thermodyn.*, vol. 20, pp. 359–384, 1995.

[59] P. D. Olmsted and C.-Y. D. Lu, "Phase separation of rigid-rod suspensions in shear flow," *Phys. Rev. E*, vol. 60, pp. 4397–4415, Oct 1999.

[60] M. Lettinga, Z. Dogic, H. Wang, and J. Vermant, "Flow behavior of colloidal rodlike viruses in the nematic phase," *Langmuir*, vol. 21, pp. 8048–8057, 2005.

[61] S. Heidenreich, P. Ilg, and S. Hess, "Robustness of the periodic and chaotic orientational behavior of tumbling nematic liquid crystals," *Phys. Rev. E*, vol. 73, p. 061710, Jun 2006.

[62] S. Heidenreich, S. Hess, S. Klapp, M. G. Forest, R. Zhou, and X. Yang, "Oscillating hydrodynamical jets in steady shear of nano-rod dispersions," in *THE XV INTERNATIONAL CONGRESS ON RHEOLOGY: The Society of Rheology 80th Annual Meeting*, vol. 1027, pp. 168–170, AIP Publishing, 2008.

[63] S. Heidenreich, *Orientational Dynamics and Flow Properties of Polar and Non-Polar Hard-Rod Fluids*. PhD thesis, 2009.

[64] H. Rehage and H. Hoffmann, "Rheological properties of viscoelastic surfactant systems," *The Journal of Physical Chemistry*, vol. 92, no. 16, pp. 4712–4719, 1988.

[65] H. Rehage and H. Hoffmann, "Viscoelastic surfactant solutions: model systems for rheological research," *Molecular Physics*, vol. 74, no. 5, pp. 933–973, 1991.

[66] S. M. Fielding and P. Olmsted, "Nonlinear dynamics of an interface between shear bands," *Phys. Rev. Lett.*, vol. 96, p. 104502, 2006.

[67] J. K. G. Dhont and W. J. Briels, *Rod-Like Brownian Particles in Shear Flow: Sections 3.1 3.9*, pp. 147–216. Wiley-VCH Verlag GmbH & Co. KGaA, 2007.

[68] J. K. Dhont and W. J. Briels, "Gradient and vorticity banding," *Rheol. Acta*, vol. 47, pp. 257–281, 2008.

[69] L. Chen, C. Zukoski, B. Ackerson, H. Hanley, G. Straty, J. Barker, and C. Glinka, "Structural changes and orientational order in a sheared colloidal suspension," *Phys. Rev. Lett.*, vol. 69, p. 688, 1992.

[70] J. Decruppe, R. Cressely, R. Makhloufi, and E. Cappelaere, "Flow birefringence experiments showing a shear-banding structure in a ctab solution," *Colloid Polym. Sci.*, vol. 273, pp. 346–351, 1995.

[71] H. Reinken, "Shear banding and constitutive instabilities in nematogenic fluids," 2016.

[72] J. Goveas and P. Olmsted, "A minimal model for vorticity and gradient banding in complex fluids," *Eur. Phys. J. E*, vol. 6, pp. 79–89, 2001.

[73] N. Spenley, X. Yuan, and M. Cates, "Nonmonotonic constitutive laws and the formation of shear-banded flows," *J. Phys. II*, vol. 6, pp. 551–571, 1996.

[74] P. Olmsted, O. Radulescu, and C.-Y. Lu, "Johnson–segalman model with a diffusion term in cylindrical couette flow," *J. Rheol.*, vol. 44, pp. 257–275, 2000.

[75] M. Das, B. Chakrabarti, C. Dasgupta, S. Ramaswamy, and A. K. Sood, "Routes to spatiotemporal chaos in the rheology of nematogenic fluids," *Phys. Rev. E*, vol. 71, p. 021707, 2005.

[76] E. F. Gramsbergen, L. Longa, and W. H. de Jeu, "Landau theory of the nematic-isotropic phase transition," *Phys. Rep.*, vol. 135, pp. 195–257, 1986.

[77] N. J. Mottram and C. J. Newton, "Introduction to q-tensor theory," *arXiv preprint arXiv:1409.3542*, 2014.

[78] W. Maier and A. Saupe, "Eine einfache molekular-statistische theorie der nematischen kristallinflüssigen phase. teil l1.," *Zeitschrift für Naturforschung A*, vol. 14, pp. 882–889, 1959.

[79] P. Kaiser, W. Wiese, and S. Hess, "Stability and instability of an uniaxial alignment against biaxial distortions in the isotropic and nematic phases of liquid crystals," *J. Non-Equilib. Thermodyn.*, vol. 17, pp. 153–170, 1992.

[80] S. Hess, "Fokker–planck equation approach to flow–alignment in liquid crystals," *Z. Naturforsch.*, vol. 31a, 1976.

[81] H. Mori, E. C. Gartland Jr, J. R. Kelly, and P. J. Bos, "Multidimensional director modeling using the q tensor representation in a liquid crystal cell and its application to the π cell with patterned electrodes," *Jpn. J. Appl. Phys.*, vol. 38, p. 135, 1999.

[82] D. Frenkel, *Statistical mechanics of liquid crystals*. Les Houches session LI, 1989.

[83] P. Sheng, "Boundary-layer phase transition in nematic liquid crystals," *Phys. Rev. A*, vol. 26, pp. 1610–1617, 1982.

[84] B. Jerome, "Surface effects and anchoring in liquid crystals," *Rep. Prog. Phys.*, vol. 54, p. 391, 1991.

[85] M. Ruths, S. Steinberg, and J. N. Israelachvili, "Effects of confinement and shear on the properties of thin films of thermotropic liquid crystal," *Langmuir*, vol. 12, pp. 6637–6650, 1996.

[86] O. Manyuhina, A.-M. Cazabat, and M. B. Amar, "Instability patterns in ultra-thin nematic films: Comparison between theory and experiment," *Europhys. Lett.*, vol. 92, p. 16005, 2010.

[87] R. Pathria and P. D. Beale, *Statistical Mechanics*. Academic Press, third edition ed., 2011.

[88] J.-P. Hansen and I. R. McDonald, *Theory of simple liquids*. Elsevier, 1990.

[89] P. Egelstaff, *An introduction to the liquid state*. Elsevier, 2012.

[90] J. E. Mayer, "Contribution to statistical mechanics," *J. Chem. Phys.*, vol. 10, pp. 629–643, 1942.

[91] J. R. Solana, *Perturbation Theories for the Thermodynamic Properties of Fluids and Solids*. CRC Press, 2013.

[92] D. J. Cleaver, C. M. Care, M. P. Allen, and M. P. Neal, "Extension and generalization of the gay-berne potential," *Phys. Rev. E*, vol. 54, pp. 559–567, Jul 1996.

[93] B. M. Mulder, "The excluded volume of hard sphero-zonotopes," *Mol. Phys.*, vol. 103, 2005.

[94] A. Isihara, "Theory of anisotropic colloidal solutions," *J. Chem. Phys.*, vol. 19, pp. 1142–1147, 1951.

[95] P. Hohenberg and W. Kohn, "Inhomogeneous electron gas," *Phys. Rev.*, vol. 136, pp. B864–B871, Nov 1964.

[96] N. D. Mermin, "Thermal properties of the inhomogeneous electron gas," *Phys. Rev.*, vol. 137, pp. A1441–A1443, Mar 1965.

[97] H. Löwen, "Density functional theory of inhomogeneous classical fluids: recent developments and new perspectives," *J. Phys.: Condens. Matter*, vol. 14, p. 11897, 2002.

[98] E. Keshavarzi and G. Parsafar, "The direct correlation function and its interpretation via the linear isotherm regularity," *J. Phys. Soc. Jpn.*, vol. 70, pp. 1979–1985, 2001.

[99] C. G. Gray and K. E. Gubbins, *Theory of molecular liquids*. Clarendon Press, Oxford, 1984.

[100] M. Rex, H. H. Wensink, and H. Löwen, "Dynamical density functional theory for anisotropic colloidal particles," *Phys. Rev. E*, vol. 76, p. 021403, Aug 2007.

[101] Y. Rosenfeld, "Free-energy model for the inhomogeneous hard-sphere fluid mixture and density-functional theory of freezing," *Phys. Rev. Lett.*, vol. 63, pp. 980–983, Aug 1989.

[102] H. Hansen-Goos and K. Mecke, "Fundamental measure theory for inhomogeneous fluids of nonspherical hard particles," *Phys. Rev. Lett.*, vol. 102, p. 018302, 2009.

[103] R. Wittmann, M. Marechal, and K. Meck, "Fundamental mixed measure theory for non-spherical colloids," *Europhys. Lett.*, vol. 109, p. 26003, 2015.

[104] W. Curtin, "Density-functional theory of the solid-liquid interface," *Phys. Rev. Lett.*, vol. 59, p. 1228, 1987.

[105] H. B. Callen, *Thermodynamics & an Intro. to Thermostatistics*. John Wiley & Sons, 2006.

[106] E. Velasco and L. Mederos, "A theory for the liquid-crystalline phase behavior of the gay–berne model," *J. Chem. Phys.*, vol. 109, pp. 2361–2370, 1998.

[107] S.-D. Lee, "The onsager-type theory for nematic ordering of finite-length hard ellipsoids," *J. Chem. Phys*, vol. 89, pp. 7036–7037, 1988.

[108] P. Bolhuis and D. Frenkel, "Tracing the phase boundaries of hard spherocylinders," *J. Chem. Phys.*, vol. 106, pp. 666–687, 1997.

[109] A. Cuetos, B. Martinez-Haya, S. Lago, and L. Rull, "Use of parsons-lee and onsager theories to predict nematic and demixing behavior in binary mixtures of hard rods and hard spheres," *Physical Review E*, vol. 75, 2007.

[110] H. Löwen, "A phase-field-crystal model for liquid crystals," *J. Phys.: Condens. Matter*, vol. 22, p. 364105, 2010.

[111] R. Lugo-Frías and S. H. L. Klapp, "Binary mixtures of rod-like colloids under shear: microscopically-based equilibrium theory and order-parameter dynamics," *J. Phys.: Condens. Matter*, vol. 28, p. 244022, 2016.

[112] S. Grandner, S. Heidenreich, S. Hess, and S. H. L. Klapp, "Polar nano-rods under shear: From equilibrium to chaos," *Eur. Phys. J. E*, vol. 24, 2007.

[113] F. McCourt, J. Beenakkeran, W. Koehler, and I. Kuscer, *Nonequilibrium phenomena in polyatomic gases*. Clarendon Press, Oxford, 1991.

[114] G. J. Vroege and H. N. W. Lekkerkerker, "Phase transitions in lyotropic colloidal and polymer liquid crystals," *Rep. Prog. Phys.*, vol. 55, p. 1241, 1992.

[115] M. Kröger, A. Ammar, and F. Chinesta, "Consistent closure schemes for statistical models of anisotropic fluids," *J. Non-Newtonian Fluid Mech.*, vol. 149, 2008.

[116] M. Kröger, "Simple models for complex nonquilibrium fluids," *Phys. Rep.*, vol. 390, 2003.

[117] J. Feng, C. V. Chaubal, and L. G. Leal, "Closure approximations for the doi theory: Which to use in simulating complex flows of liquid-crystalline polymers?," *J. Rheol.*, vol. 42, p. 1095, 1998.

[118] J. Han, Y. Luo, W. Wang, P. Zhang, and Z. Zhang, "From microscopic theory to macroscopic theory: a systematic study on modeling for liquid crystals," *Arch. Rational Mech. Anal.*, pp. 1–69, 2014.

[119] H. H. Wensink, "Spontaneous sense inversion in helical mesophases," *Europhys. Lett.*, vol. 3, 2014.

[120] L. Feigin and D. Svergun, *Structure Analysis by Small-Angle X-Ray and Neutron Scattering*. Plenum Press, New York, 1987.

[121] K. R. Elder, N. Provatas, J. Berry, P. Stefanovic, and M. Grant, "Phase–field crystal modeling and classical density functional theory of freezing," *Phys. Rev. B*, vol. 75, p. 064107, 2007.

[122] R. Courant and D. Hilbert, *Methods of Mathematical Physics*. Interscience, New York, 1989.

[123] C. V. Achim, R. Wittkowski, and H. Löwen, "Stability of liquid crystalline phases in the phase-field-crystal model," *Phys. Rev. E*, vol. 83, p. 061712, 2011.

[124] H. Emmerich, H. Löwen, R. Wittkowski, T. Gruhn, G. I. Tóth, G. Tegze, and L. Gránásy, "Phase-field-crystal models for condensed matter dynamics on atomic length and diffusive time scales: an overview," *Adv. Phys.*, vol. 61, pp. 665–743, 2012.

[125] N. F. Carnahan and K. E. Starling, "Equation of state for nonattracting rigid spheres," *J. Chem. Phys.*, vol. 51, pp. 635–636, 1969.

[126] P. J. Camp and M. P. Allen, "Hard ellipsoid rod-plate mixtures: Onsager theory and computer simulations," *Physica A*, vol. 229, pp. 410–427, 1996.

[127] T. Dingemans, L. Madsen, N. Zafiropoulos, L. Wenbin, and E. Samulski, "Uniaxial and biaxial nematic liquid crystals," *Phil. Trans. R. Soc. A*, vol. 364, pp. 2681–2696, 2006.

[128] M. J. Solomon and P. T. Spicer, "Microstructural regimes of colloidal rod suspensions, gels, and glasses," *Soft Matter*, vol. 6, 2010.

[129] J. Mewis and N. Wagner, *Colloidal Suspension Rheology*. Cambridge, 2012.

[130] G. B. Arfken, H. J. Weber, and F. E. Harris, *Mathematical methods for physicists: A comprehensive guide*. Academic press, 2011.

[131] S. Dussi and M. Dijkstra, "Entropy-driven formation of chiral nematic phases by computer simulations," *Nat. Commun.*, vol. 7, 2016.

[132] G. Taylor, "The motion of ellipsoidal particles in a viscous fluid," *Proc. R. Soc. A*, vol. 103, pp. 58–61, 1923.

[133] M. Fialkowski, "Viscous properties of binary mixtures of nematic liquid crystals," *Phys. Rev. E*, vol. 53, pp. 721–726, 1996.

[134] A. M. Menzel, A. Saha, C. Hoell, and H. Löwen, "Dynamical density functional theory for microswimmers," *The Journal of Chemical Physics*, vol. 144, no. 2, p. 024115, 2016.

[135] J. Ericksen, "Hydrostatic theory of liquid crystals," *Arch. Rational Mech. Anal.*, vol. 9, pp. 371–378, 1962.

[136] F. Leslie, "Some constitutive equations for liquid crystals," *Arch. Rational Mech. Anal.*, vol. 28, pp. 265–283, 1968.

[137] M. Doi and S. Edwards, "Dynamics of rod–like macromolecules in concentrated solution. pts. 1 and 2," *J. Chem. Soc.*, vol. 74, 1978.

[138] C. Eckart, "The thermodynamics of irreversible processes. i. the simple fluid," *Phys. Rev.*, vol. 58, p. 267, 1940.

[139] S. R. De Groot and P. Mazur, *Non-equilibrium thermodynamics*. Dover, 1983.

[140] R. Dong, "On the anisotropy of nuclear spin relaxation in a nematic liquid crystal," *Chem. Phys. Lett.*, vol. 9, pp. 600–602, 1971.

[141] L. Onsager, "Reciprocal relations in irreversible processes. i.," *Phys. Rev.*, vol. 37, pp. 405–426, Feb 1931.

[142] Z. Dogic, *Liquid crystalline phase transitions in virus and virus/polymer suspensions*. PhD thesis, Citeseer, 2000.

[143] K. R. Purdy, *Liquid Crystal Phase Transitions of Monodisperse and Bidisperse Suspensions of Rodlike Colloidal Virus*. PhD thesis, Brandeis University, 2004.

[144] D. Chakraborty, C. Dasgupta, and A. K. Sood, "Banded spatiotemporal chaos in sheared nematogenic fluids," *Phys. Rev. E*, vol. 82, p. 065301, 2010.

[145] R. Ganapathy, S. Majumdar, and A. K. Sood, "Spatiotemporal nematodynamics in wormlike micelles en route to rheochaos," *Phys. Rev. E*, vol. 78, p. 021504, Aug 2008.

[146] S. Hess and M. Kröger, "Regular and chaotic orientational and rheological behavior of liquid crystals," *J. Phys.: Condens. Matter*, vol. 16, 2004.

[147] S. Hess and M. Kröger, *in Computer Simulations of Liquid Crystals and Polymers*, pp. 295–333. Springer Verlag, 2005.

[148] R. Lugo-Frías, H. Reinken, and S. H. L. Klapp, "Shear banding in nematogenic fluids with oscillating orientational dynamics," *Eur. Phys. J. E Soft Matter*, p. submitted, 2016.

[149] O. Hess and S. Hess, "Nonlinear fluid behavior: from shear thinning to shear thickening," *Physica A*, vol. 207, 1994.

[150] M. E. Cates, D. A. Head, and A. Ajdari, "Rheological chaos in a scalar shear-thickening model," *Phys. Rev. E*, vol. 66, p. 025202, 2002.

[151] W. H. Press, S. A. Teukolsky, W. T. Vetterling, and B. P. Flannery, *Numerical recipes in C*. Cambridge university press Cambridge, 1996.

[152] O. Radulescu and P. Olmsted, "Matched asymptotic solutions for the steady banded flow of the diffusive johnson–segalman model in various geometries," *J. Non-Newton. Fluid*, vol. 91, pp. 143–164, 2000.

[153] J. Adams, S. Fielding, and P. Olmsted, "The interplay between boundary conditions and flow geometries in shear banding: Hysteresis, band configurations, and surface transitions," *J. Non-Newtonian Fluid Mech.*, vol. 151, pp. 101–118, 2008.

[154] T. Xu and V. A. Davis, "Rheology and shear-induced textures of silver nanowire lyotropic liquid crystals," *J. Nanomaterials*, vol. 2015, 2015.

[155] B. Saint-Michel, T. Gibaud, M. Leocmach, and S. Manneville, "Local oscillatory rheology from echography," *Phys. Rev. Applied*, vol. 5, p. 034014, Mar 2016.

[156] D. A. Strehober, E. Schöll, and S. H. L. Klapp, "Feedback control of flow alignment in sheared liquid crystals," *Phys. Rev. E*, vol. 88, 2013.

[157] J. L. Synge and A. Schild, *Tensor calculus*, vol. 5. Courier Corporation, 1969.

[158] H. Nguyen-Schäfer and J.-P. Schmidt, *Tensor Analysis*. Springer, 2014.

[159] K. B. Petersen, M. S. Pedersen, *et al.*, *The matrix cookbook*. PhD thesis, 2008.

[160] N. Herdegen and S. Hess, "Nonlinear flow behavior of the boltzmann gas," *Physica A*, vol. 115, pp. 281–299, 1982.

[161] W. Loose and S. Hess, "Nonequilibrium velocity distribution function of gases: Kinetic theory and molecular dynamics," *Phys. Rev. A*, vol. 37, p. 2099, 1988.

[162] R. Hornreich and S. Shtrikman, "Landau theory of blue phases," *Mol. Cryst. Liq. Cryst.*, vol. 165, pp. 183–211, 1988.

[163] R. Hornreich and S. Shtrikman, "Field-induced hexagonal blue phases in positive and negative dielectric anisotropy systems: Phase diagrams and topological properties," *Phys. Rev. A*, vol. 41, p. 1978, 1990.

[164] G. Burns, *Introduction to group theory with applications: materials science and technology*. Academic Press, 2014.

Acknowledgements

First of all I would like to thank my supervisor Prof. Dr. Sabine Klapp for giving me the chance to be park of her group. Thanks for all your help, advice and constant support. It was really challenging, I learned a lot and I had a lot of fun. Also, I would like to thank Dr. Andreas Menzel and Prof. Dr. Michael Lehmann for being part of my dissertation committee and taking the time to read my thesis.

Thanks a lot to all the past, present and future members of the AG Klapp: From day one you made me feel welcome and helped me a lot along the way. Specially I would like to thank Ken, Florian, Henning, Nicola, Robert, Arzu, David, Stavros, Alex, Sascha and Sarah with whom I probably spent more time discussing things that had nothing to do with physics.

I will also like to acknowledge financial support from the Research Training Group *1558*.

To my friends in Mexico, New Zealand, Germany, England, Spain and the US: I salute you, G.G.N.M.U!

Finally I would like to thank Kathrin; I find it difficult to express my appreciation because it is boundless. Thank you for your love, patience and support.

Este trabajo se lo dedico a mis padres.

De gente bien nacida es agradecer los beneficios que reciben
y uno de los pecados que más a Dios ofende es la ingratitud.
– El Quijote de la Mancha
Miguel de Cervantes Saavedra